

1227144

[00834844]

ENGINEERING CHANGE NOTICE

S
HMLM0351 105866/BA10

Page 1 of 2

1. ECN **198468**

Proj.
ECN

2. ECN Category (mark one) Supplemental <input type="radio"/> Direct Revision <input checked="" type="radio"/> Change ECN <input type="radio"/> Temporary <input type="radio"/> Standby <input type="radio"/> Supersedeure <input type="radio"/> Cancel/Void <input type="radio"/>	3. Originator's Name, Organization, MSIN, and Telephone No. R. Khaleel/FDNW/B4-43/376-6903		4. USQ Required? <input type="radio"/> Yes <input checked="" type="radio"/> No	5. Date December 2, 1999
	6. Project Title/No./Work Order No. ILAW PA/LMHC	7. Bldg./Sys./Fac. No. N/A		8. Approval Designator
	9. Document Numbers Changed by this ECN (includes sheet no. and rev.) HNF-4769, Rev. 0A	10. Related ECN No(s). N/A	11. Related PO No. N/A	

12a. Modification Work <input type="radio"/> Yes (fill out Bk. 12b) <input checked="" type="radio"/> No (NA Blks. 12b, 12c, 12d)	12b. Work Package No. N/A	12c. Modification Work Completed N/A Design Authority/Cog. Engineer Signature & Date	12d. Restored to Original Condition (Temp. or Standby ECNs only) N/A Design Authority/Cog. Engineer Signature & Date
---	-------------------------------------	---	---

13a. Description of Change
Complete revision of the document

13b. Design Baseline Document? Yes No

RECEIVED

OCT 20 2014

EDMC

14a. Justification (mark one) Criteria Change <input checked="" type="radio"/> Design Improvement <input type="radio"/> Environmental <input type="radio"/> Facility Deactivation <input type="radio"/> As-Found <input type="radio"/> Facilitate Const. <input type="radio"/> Const. Error/Omission <input type="radio"/> Design Error/Omission <input type="radio"/>	14b. Justification Details Revised to incorporate comments by an external peer reviewer.
---	--

15. Distribution (include name, MSIN, and no. of copies)
See distribution list

RELEASE STAMP

DEC 07 1999

DATE: _____

STA: 15

HANFORD
RELEASE

ID: _____

21

145

ENGINEERING CHANGE NOTICE

16. Design Verification Required

Yes
 No

17. Cost Impact

ENGINEERING

Additional \$ N/A
Savings \$ N/A

CONSTRUCTION

Additional \$ N/A
Savings \$ N/A

18. Schedule Impact (days)

Improvement N/A
Delay N/A

19. Change Impact Review: Indicate the related documents (other than the engineering documents identified on Side 1) that will be affected by the change described in Block 13. Enter the affected document number in Block 20.

SDD/DD	<input type="checkbox"/>	Seismic/Stress Analysis	<input type="checkbox"/>	Tank Calibration Manual	<input type="checkbox"/>
Functional Design Criteria	<input type="checkbox"/>	Stress/Design Report	<input type="checkbox"/>	Health Physics Procedure	<input type="checkbox"/>
Operating Specification	<input type="checkbox"/>	Interface Control Drawing	<input type="checkbox"/>	Spares Multiple Unit Listing	<input type="checkbox"/>
Criticality Specification	<input type="checkbox"/>	Calibration Procedure	<input type="checkbox"/>	Test Procedures/Specification	<input type="checkbox"/>
Conceptual Design Report	<input type="checkbox"/>	Installation Procedure	<input type="checkbox"/>	Component Index	<input type="checkbox"/>
Equipment Spec.	<input type="checkbox"/>	Maintenance Procedure	<input type="checkbox"/>	ASME Coded Item	<input type="checkbox"/>
Const. Spec.	<input type="checkbox"/>	Engineering Procedure	<input type="checkbox"/>	Human Factor Consideration	<input type="checkbox"/>
Procurement Spec.	<input type="checkbox"/>	Operating Instruction	<input type="checkbox"/>	Computer Software	<input type="checkbox"/>
Vendor Information	<input type="checkbox"/>	Operating Procedure	<input type="checkbox"/>	Electric Circuit Schedule	<input type="checkbox"/>
OM Manual	<input type="checkbox"/>	Operational Safety Requirement	<input type="checkbox"/>	ICRS Procedure	<input type="checkbox"/>
FSAR/SAR	<input type="checkbox"/>	IEFD Drawing	<input type="checkbox"/>	Process Control Manual/Plan	<input type="checkbox"/>
Safety Equipment List	<input type="checkbox"/>	Cell Arrangement Drawing	<input type="checkbox"/>	Process Flow Chart	<input type="checkbox"/>
Radiation Work Permit	<input type="checkbox"/>	Essential Material Specification	<input type="checkbox"/>	Purchase Requisition	<input type="checkbox"/>
Environmental Impact Statement	<input type="checkbox"/>	Fac. Proc. Samp. Schedule	<input type="checkbox"/>	Tickler File	<input type="checkbox"/>
Environmental Report	<input type="checkbox"/>	Inspection Plan	<input type="checkbox"/>	<u>N/A</u>	<input checked="" type="checkbox"/>
Environmental Permit	<input type="checkbox"/>	Inventory Adjustment Request	<input type="checkbox"/>		<input type="checkbox"/>

20. Other Affected Documents: (NOTE: Documents listed below will not be revised by this ECN.) Signatures below indicate that the signing organization has been notified of other affected documents listed below.

Document Number/Revision	Document Number/Revision	Document Number/Revision
N/A		

21. Approvals

Signature	Date	Signature	Date
Design Authority _____	_____	Design Agent _____	_____
Cog. Eng. R. Khaleel <i>R. Khaleel</i>	12/2/99	PE _____	_____
Cog. Mgr. R.J. Puigh <i>R.J. Puigh</i>	12/3/99	QA _____	_____
QA _____	_____	Safety _____	_____
Safety _____	_____	Design _____	_____
Environ. _____	_____	Environ. _____	_____
Other E.J. Freeman <i>E.J. Freeman</i>	12/2/99	Other _____	_____
F.M. Mann <i>F.M. Mann</i>	12/3/99		

DEPARTMENT OF ENERGY

Signature or a Control Number that tracks the Approval Signature

ADDITIONAL

FAR-FIELD HYDROLOGY DATA PACKAGE FOR IMMOBILIZED LOW-ACTIVITY TANK WASTE PERFORMANCE ASSESSMENT

Raz Khaleel

Fluor Daniel Northwest, Inc.

Richland, WA 99352

U.S. Department of Energy Contract DE-AC06-96RL13200

EDT/ECN: 198468

Org Code: 403

B&R Code:

UC:

Charge Code: 105866BA10 HMLM0351

Total Pages: 136/137 KN

Key Words: Low-level tank wastes, vadose zone, hydraulic properties, flow and transport parameters, stochastic theory

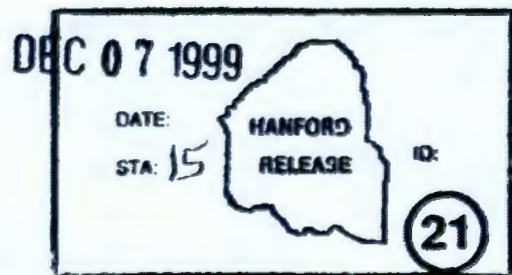
Abstract: A number of data packages are being assembled as part of 2001 Immobilized Low Activity Tank Waste (ILAW) Performance Assessment (PA). This data package deals with the far-field hydrology data needed to perform vadose zone flow and transport modeling for the ILAW PA. The report presents the laboratory measurements on physical and hydraulic properties for soil samples at the disposal sites, and results on application of stochastic theory to small-scale measurements.

TRADEMARK DISCLAIMER. Reference herein to any specific commercial product, process, or service by trade name, trademark, manufacturer, or otherwise, does not necessarily constitute or imply its endorsement, recommendation, or favoring by the United States Government or any agency thereof or its contractors or subcontractors.

Printed in the United States of America. To obtain copies of this document, contact: Document Control Services, P.O. Box 950, Mailstop H6-08, Richland WA 99352, Phone (509) 372-2420; Fax (509) 376-4969.

Brian H. Noland
Release Approval

12/7/99
Date



Release Stamp

Approved For Public Release

HNF-4769, Rev. 1

FAR-FIELD HYDROLOGY DATA PACKAGE

FOR

**IMMOBILIZED LOW-ACTIVITY TANK WASTE
PERFORMANCE ASSESSMENT**

**Raz Khaleel
Fluor Daniel Northwest, Inc.
P.O. Box 1050
Richland, WA 99352**

December, 1999

EXECUTIVE SUMMARY

A number of data packages are being assembled as part of 2001 Immobilized Low-Activity Tank Waste (ILAW) Performance Assessment (PA). This data package deals with the far-field hydrology data needed to perform vadose zone flow and transport modeling for the ILAW PA.

The ILAW PA shall be conducted for two sites; the new ILAW disposal site and the existing disposal site east of the new ILAW site in 200 East Area. Site characterization data are available for both sites. This report presents the laboratory measurements on physical and hydraulic properties for soil samples at the disposal sites, and results on application of stochastic theory to small-scale measurements. The effective (upscaled) parameter estimates are derived for saturated hydraulic conductivity, soil moisture retention and unsaturated hydraulic conductivity, bulk density, unretarded macrodispersivity and sorption-enhanced macrodispersivity. These parameters will serve as input to VAM3DF, a variably saturated vadose zone flow and transport code; VAM3DF will generate 'mean' solutions for the pressure head and contaminant concentration.

The stratigraphy at both disposal sites is dominated by two distinctly different sediment sequences. The upper part of the vadose zone is characterized by a sandy sequence, whereas the lower part is characterized primarily by a gravel sequence. At saturation, compared to the gravel-dominated sequence, the sand-dominated sequence is described by a smaller log-conductivity variance. However, compared to the gravel-dominated sequence, the log-unsaturated conductivity variance for the sand-dominated sequence is higher. Consequently, the macroscopic anisotropy relations for the sandy and gravelly sediments are different. The differences in the characteristics of the two sediment sequences also result in different macrodispersivity estimates. Overall, compared to sandy soils, gravelly soils are characterized by a much smaller saturated water content, higher bulk density, higher log-conductivity variance, smaller log-unsaturated conductivity variance, a much smaller macroscopic anisotropy and smaller macrodispersivities.

A methodology is presented to estimate uncertainties in model predictions. For far-field hydrology, three sources contribute to uncertainty estimates: (a) variations in model configurations, (b) uncertainties in the calculated mean solution for concentration, and (c) uncertainties around the calculated mean solution for concentration. The following approach will be used to evaluate these uncertainties. First, uncertainty will be defined for the 'mean' solutions for concentration distribution at the water table (as a function of position and time). The combined contribution to uncertainty in the mean solution due to model configuration and effective parameter (i.e., unsaturated hydraulic conductivity and macrodispersivity) variations will be investigated. A methodology developed by Kapoor and Gelhar (1994a,b) will then be used to estimate the uncertainty around the mean solution.

Model configurations will include variations in stratigraphy and clastic dike networks. Base case and uncertainty in stratigraphy and clastic dike network models will be provided in the geology data package. Selected VAM3DF runs will be performed to estimate the impact of these uncertainties on the resultant contaminant distribution at the water table. The uncertainty attributed to isotropy and sloped layering on calculated mean solutions will also be estimated.

Bounding estimates for concentrations at the water table will be provided through a choice of parameters and model configurations judged to provide a worst case representation of the system.

CONTENTS

1.0 Introduction..... 1

1.1 SCOPE OF THIS DATA PACKAGE..... 1

2.0 Laboratory Measurements for Soil Physical and Hydraulic Properties..... 4

2.1 NEW ILAW DISPOSAL SITE..... 4

2.1.1 100 Area Samples..... 5

2.2 EXISTING DISPOSAL SITE..... 9

3.0 Effective (Upscaled) Flow and Transport Properties..... 13

3.1 EFFECTIVE (UPSCALED) FLOW PARAMETERS..... 13

3.1.1 Stochastic Upscaling..... 14

3.1.2 Field Observations..... 14

3.1.3 Composite Macroscopic Relationships..... 14

3.1.3.1 Stochastic Model for Macroscopic Anisotropy..... 15

3.1.3.2 Macroscopic Anisotropy Relations..... 18

3.2 EFFECTIVE TRANSPORT PARAMETERS..... 20

3.2.1 Bulk Density..... 21

3.2.2 Diffusivity..... 21

3.2.3 Dispersivity..... 22

3.2.3.1 Saturated Media Dispersivities For Field Sites..... 22

3.2.3.2 Vadose Zone Dispersivities For Dry Desert Environment..... 24

3.2.3.3 Stochastic Models and Macrodispersivities for Large-Scale Media..... 25

3.2.3.4 Macrodispersivity Estimates For Non-Reactive Species..... 26

3.2.3.5 Heterogeneous Sorption Enhanced Macrodispersivities..... 27

3.2.3.6 Numerical Considerations..... 30

4.0 Uncertainties in Model Predictions..... 35

4.1 MODEL CONFIGURATIONS..... 35

4.1.1 Variations in Stratigraphy..... 35

4.1.2 Clastic dikes..... 36

4.1.3 Isotropy..... 38

4.1.4 Sloped Layering..... 38

4.2 UNCERTAINTIES IN THE MEAN SOLUTION DUE TO VARIATIONS OF EFFECTIVE PARAMETER ESTIMATES..... 38

4.3 UNCERTAINTIES AROUND THE MEAN SOLUTION..... 39

4.4 BOUNDING ESTIMATES..... 39

5.0 REFERENCES..... 41

6.0 PEER REVIEW..... 46

LIST OF TABLES

Table 1. Van Genuchten parameters (based on the multistep method), saturated hydraulic conductivity, and bulk density data for 20 ILAW borehole samples from the sandy sequence (after Fayer et al. 1998)..... 6

Table 2. Van Genuchten parameters, fitted saturated hydraulic conductivity, and measured bulk density data for 15 sandy gravel samples. 8

Table 3. Comparison of mean parameter estimates for the sandy sequence at the new ILAW and existing disposal sites..... 9

Table 4. Composite van Genuchten-Mualem parameters for the sand- and gravel-dominated sequences. 15

Table 5. Macroscopic anisotropy parameters for the sand- and gravel-dominated sequences. 19

Table 6. Effective parameter estimates, $E[\rho_b K_d]$, for the product of bulk density (g/cm^3) and K_d (cm^3/g) at the new ILAW and existing disposal sites. 21

Table 7. Non-reactive macrodispersivity estimates for soils at the new ILAW and existing disposal sites. 27

Table 8. Macrodispersivity enhancement for the sandy sequence at the new ILAW and existing disposal sites [ρ_b in g/cm^3 and K_d in cm^3/g]. 29

Table 9. Macrodispersivity enhancement for the gravelly sequence at the new ILAW and existing disposal sites [ρ_b in g/cm^3 and K_d in cm^3/g]. 30

Table 10. Van Genuchten parameters (based on the multistep method), saturated hydraulic conductivity, and bulk density for seven clastic dike samples (after Fayer and Ritter 1999). 37

LIST OF FIGURES

Figure 1. Modeling strategy for assessing ILAW disposal system impacts (after McGrail et al. 1998). 2

Figure 2. Geologic cross section of the new ILAW disposal site (after Reidel et al. 1998). 7

Figure 3. Particle-size distribution for 20 samples from the sand-dominated sequence at the new ILAW disposal site. 8

Figure 4. Fitted moisture retention and unsaturated conductivity curves for 20 samples for the sand-dominated sequence (the symbols represent various samples, not experimental data). 10

Figure 5. Fitted moisture retention and unsaturated conductivity curves for 15 samples for the gravel-dominated sequence (the symbols represent various samples, not experimental data). 11

Figure 6. Geologic cross section of the existing disposal site (after Kincaid et al. 1995). 12

Figure 7. Composite moisture retention and unsaturated conductivity curves for the sand-dominated sequence. 17

Figure 8. Composite moisture retention and unsaturated conductivity curves for the gravel-dominated sequence. 18

Figure 9. Experimental (triangles) and fitted theoretical (squares) variogram for LnKs. 19

Figure 10. Calculated macroscopic anisotropy (equation 3) as a function of mean pressure head for the sand-dominated sequence. 20

Figure 11. Calculated macroscopic anisotropy (equation 3) as a function of mean pressure head for the gravel-dominated sequence. 20

Figure 12. Longitudinal macrodispersivity in saturated media as a function of overall problem scale with data classified by reliability (after Gelhar et al. 1992). 23

Figure 13. Longitudinal macrodispersivity in unsaturated media as a function of overall problem scale (after Gelhar 1993). [Note that the triangles are data from Ward et al. 1998]..... 24

Figure 14. LnK versus R for (a) Cs-137, (b) Sr-90, (c) U, and (d) Se for the sand-dominated sequence. 32

Figure 15. LnK versus R for (a) Cs-137, (b) Sr-90, (c) U, and (d) Se for the gravel-dominated sequence. 34

Figure 16. Schematic of concentration (C) distribution at the water table. 36

APPENDICES

Appendix A. Physical and Hydraulic Measurements of FY1998 Borehole Cores A-i

Appendix B. Laboratory Data on Physical and Hydraulic Properties for 100 Area Samples (RETC Input File)..... B-i

Appendix C. Hydraulic Parameters of the Upper Hanford Formation C-i

Appendix D. Physical and Hydraulic Measurements of FY1998 Clastic Dike Samples D-i

Appendix E. Quality Assurance/Quality Control (QA/QC) ConsiderationsE-i

1.0 INTRODUCTION

The *Hanford Immobilized Low-Activity Tank Waste Performance Assessment* examines the long-term environmental and human health effects associated with the planned disposal of the vitrified low-level fraction of the waste presently contained in Hanford Site High-Level Waste Tanks. The objectives of the performance assessment are to provide a reasonable expectation that the disposal of the waste will be protective of the general public, groundwater resources, air resources, inadvertent intruder and surface water resources. A number of data packages are being assembled as part of 2001 Immobilized Low-Activity Tank Waste (ILAW) Performance Assessment (PA). This data package deals only with the far-field (Figure 1) hydrology data needed to perform vadose zone flow and transport modeling for the ILAW PA.

Figure 1 illustrates also the overall computational strategy for the ILAW PA. The near-field environment is defined as the domain through the vault to some distance below the floor of the disposal vault (Figure 1). A coupled unsaturated flow, chemical reactions, and contaminant transport simulator (STORM) will be used within the near-field (Bacon and McGrail 1997). The plume exiting the region near the vault is expected to be of high ionic strength and pH, and will migrate down into the near-field vadose zone for some distance. However, at some distance from the disposal vaults, geochemical conditions will approach those more typical of the Hanford vadose zone and for which simplifying assumptions (such as linear sorption, negligible precipitation/dissolution, no changes in hydraulic properties, and no density effects) can be used. This region is defined as the far-field environment and can be simulated using standard, nonreactive flow and transport codes. For the ILAW PA, computations in the far-field domain will be done by VAM3DF (Huyakorn and Panday 1995), a variably saturated flow and transport code. The primary reason for switching from the near-field simulator to VAM3DF is to apply a less complicated code for the far-field, and therefore a faster turnaround for the numerical simulations. The radionuclide flux exiting the far-field domain to the unconfined aquifer will be provided by VAM3DF and will be used as a boundary condition for the unconfined aquifer flow and transport simulator. The final step in the methodology is to compute the impacts, if any, from ingestion, inhalation, and external radiation to humans who become exposed to the contaminants by withdrawing water from the aquifer.

1.1 Scope of This Data Package

The scope for the far-field hydrology data package for the new ILAW disposal site and the existing disposal site include the following information:

- Stratigraphic cross-sectional models (Section 2.0). [Note that stratigraphic cross-sectional models are presented for context only; the scope of this data package does *not* include stratigraphic cross-sectional models. Such geologic models shall be provided as part of a separate data package (i.e., Reidel and Horton 1999)]

- Data on laboratory measurements for moisture retention, particle-size distribution, saturated and unsaturated hydraulic conductivity, and bulk density (Section 2.0).
- Effective (upscaled) moisture retention, saturated and unsaturated hydraulic conductivity, bulk density, diffusivity, and macrodispersivity estimates for geologic formations (Section 3.0).

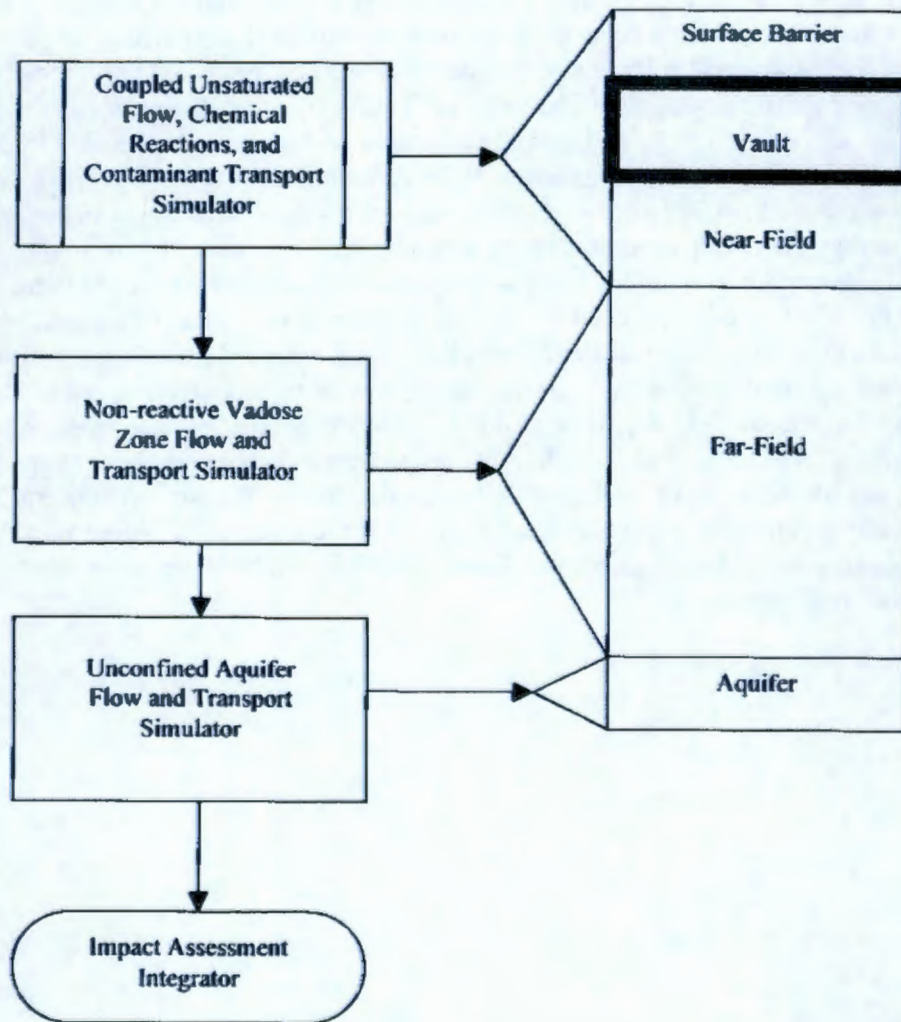


Figure 1. Modeling strategy for assessing ILAW disposal system impacts (after McGrail et al. 1998).

- Sorption-enhanced macrodispersivity estimates for selected radionuclide species (Section 3.0).
- Moisture retention, saturated and unsaturated hydraulic conductivity, bulk density, and macrodispersivity estimates for clastic dike infilling materials (Section 4.0).
- Bounding scenarios on model configurations and uncertainty estimates about the calculated mean concentration and around mean concentration (Section 4.0).

For the ILAW disposal facility with a capillary barrier and a surface barrier on top, the vadose zone water contents beneath the facility are expected to approach the natural moisture regime for arid soils. Field moisture contents are expected to be less than 10% (by volume); matric potentials of the order of -1000 cm and recharge rates of the order of 0.1 cm/yr. Under such arid conditions, the features and processes identified in the scope carry significant importance for the ILAW PA calculations. For example, the layered heterogeneous soils in 200 Areas are expected to show bulk anisotropic behavior, with the hydraulic conductivity parallel to the layers being larger than that normal to the layers. Furthermore, the degree of anisotropy increases rapidly with increasing tension or decreasing moisture content, becoming large in dry soils of the kind expected beneath the disposal facility. Also, the infiltrating water diverted around the vaults by the capillary barrier can potentially move beneath the vaults, creating moist conditions and enhancing contaminant movement to the water table. In addition, recent theoretical work and field experiments have shown that spreading of contaminants undergoing heterogeneous linear equilibrium sorption can be significantly larger than that of the non-sorbing tracer. Dispersivity enhancement can cause early arrival at the water table before they have had an opportunity to decay. Also, clastic dikes are of concern because they can potentially create preferred pathways.

2.0 LABORATORY MEASUREMENTS FOR SOIL PHYSICAL AND HYDRAULIC PROPERTIES

The purpose of this section is to summarize available data on laboratory measurements for moisture retention, particle-size distribution, saturated and unsaturated hydraulic conductivity, and bulk density for sediment samples from both new ILAW and existing disposal sites.

2.1 New ILAW Disposal Site

As part of site characterization activity for the new ILAW disposal site, sediment samples were obtained in fiscal year 1998 via a borehole drilling and sampling program (Reidel and Reynolds 1998). The borehole was drilled in the spring of 1998 (Reidel et al. 1998); Figure 2 shows the geologic cross section. The Hanford formation sandy sequence is about 200 ft thick and is the dominant facies at the site. The lower gravelly sequence is about 70 ft thick. For purposes of this data package, no distinction is made on gravel-dominated sequences of the lower Hanford formation and the upper Ringold Formation. The sediments from both of these formations have similar physical and hydraulic properties, and are characterized essentially as sandy gravel, with a significant gravel fraction (Khaleel and Freeman 1995a,b).

A work plan was prepared that provides details on the measurement and analysis of the hydraulic properties for the ILAW borehole sediment samples (Khaleel 1998)¹. Details on sampling, laboratory procedures, and analysis of samples are provided in Fayer et al. (1998)², and are included as Appendix A. The following summary is based on details provided in Appendix A.

A total of 45 cores were collected in liners, with core diameters ranging from 3.25- to 3.75- in. The total internal volume of the 3.25-in (8.26-cm) diameter cores was 803 cm³; it was 1,069 cm³ for the 3.75-in (9.53-cm) diameter core. It should be noted that, during drilling, sample recovery was less than 100% (Reidel et al. 1998), thereby biasing the recovered samples toward the finer fraction. Also, no vadose zone cores were collected below 242 ft because this zone was open framework gravel (i.e., gravel that supports itself with little to no finer grained material) and could not be sampled with the method used. Figure 2 shows the sampling locations relative to the geologic cross-section derived from the borehole data; twenty samples from these locations were used to obtain physical and hydraulic properties for the sandy sequence. As described later, for the gravel-dominated sequence, data on hydraulic properties from elsewhere on the Hanford Site were used as surrogates.

¹ Khaleel, R. 1998. Work plan for measurement and analysis of hydraulic properties for clastic dikes and ILAW Borehole No. 1 sediment samples. January, 1998. Fluor Daniel Northwest, Inc. Richland, WA.

² Fayer, M.J., A.L. Ward, J.S. Ritter, and R.E. Clayton. 1998. Physical and hydraulic measurements of FY 1998 borehole cores. Letter Report to Fluor Daniel Northwest, Inc. September, 1998. Pacific Northwest National Laboratory. Richland, WA.

The procedures used to analyze the twenty samples are listed in Appendix A. Because several tests were performed on the same core, the following test sequence was established: saturated conductivity, multistep outflow, and steady state unsaturated conductivity. The multistep and steady state methods were used to obtain moisture retention and unsaturated conductivity data. Both methods were performed on the same core using the same sensor locations (see Appendix A for details). In addition to cumulative outflow, the multistep method, which is an improvement over the one-step method of Kool et al. (1985a, b), provides water content-matric potential (θ - ψ) pairs. These data were used in conjunction with the MULSTP program (Eching and Hopmans 1993), a numerical inversion procedure, to determine the optimal set of van Genuchten model (Appendix A) parameters. The steady-state method, described by Klute and Dirksen (1986), provides water content-matric potential-unsaturated conductivity (θ - ψ - K) triplets; the method was primarily used as a check on the multistep method.

Table 1 shows the van Genuchten model (van Genuchten 1980) parameters determined using the MULSTP program and data from the multistep test. The pore-size distribution parameter l (Mualem 1976) was kept fixed at 0.5. Also listed in Table 1 are saturated conductivity and bulk density measurements for the 20 samples primarily from the sandy sequence. The particle-size distribution data are shown in Figure 3. The fitted moisture retention curves and unsaturated conductivity curves for the 20 samples from the sandy sequence are shown in Figure 4. Most of the borehole samples were fitted for α and n ; eight of the samples were also fitted for θ_s .

2.1.1 100 Area Samples

As discussed earlier, no site-specific data on soil moisture characteristics are available at the disposal sites for sediments in the gravel-dominated sequence. However, as part of the Environmental Restoration Project, moisture retention and unsaturated conductivity data for sandy gravel sediments are available elsewhere (100 Area along the Columbia River) on the Hanford Site. Fifteen samples having a large gravel fraction were chosen. These samples ranged in gravel content from 43 to 75 percent and were used as surrogate to represent the hydraulic properties for the gravel-dominated sequence.

Standard laboratory and Westinghouse Hanford Company quality assurance procedures were used to analyze these gravelly samples. The moisture retention data for the fine fraction (< 2 mm) and for the drainage cycle of up to -1,000 cm of pressure head were measured using "Tempe" pressure cells; the rest of the drainage data up to -15,000 cm was measured using the pressure plate extraction method (Klute 1986). Saturated hydraulic conductivities for the bulk samples (including gravels) were measured in the laboratory using constant-head permeameter. A variation of the unit gradient method (Klute and Dirksen 1986; Khaleel et al. 1995) was used to measure unsaturated hydraulic conductivities for the bulk samples. The laboratory measured data on < 2 mm size fraction were corrected for the gravel fraction (Gardner 1986; Khaleel and Relyea 1997).

No correction was needed for the saturated and unsaturated conductivities, since these were measured on the bulk sample.

The van Genuchten parameters were obtained via RETC (van Genuchten et al. 1991) and a simultaneous fit of both laboratory-measured moisture retention and unsaturated conductivity data; all five unknown parameters θ_r , θ_s , α , n , and K_s , with $m=1-1/n$ (van Genuchten 1980), were fitted to the data. The pore size distribution factor, ℓ (Mualem 1976) was kept fixed at 0.5 during the simultaneous fitting. The laboratory data, following gravel-correction of the moisture retention data, are included in Appendix B for the 15 samples. Appendix B serves as the input data file for RETC. The fitted moisture retention curves and unsaturated conductivity curves for the 15 samples for the gravel sequence are shown in Figure 5. Note that, unlike the borehole samples, the 100 Area samples were fitted for θ_r , θ_s , α , n , and K_s .

Table 1. Van Genuchten parameters (based on the multistep method), saturated hydraulic conductivity, and bulk density data for 20 ILAW borehole samples from the sandy sequence (after Fayer et al. 1998).

Sample	θ_r (cm ³ /cm ³)	θ_s (cm ³ /cm ³)	α (1/cm)	n (-)	Saturated Hydraulic Conductivity (cm/s)	Bulk Density (g/cm ³)
7A	0.377	0.0404	0.0290	1.825	1.04E-03	1.70
10A	0.413	0.0279	0.1161	1.784	2.95E-03	1.62
12A	0.363	0.0309	0.0650	1.755	2.15E-03	1.74
14A	0.416	0.0324	0.0445	1.728	1.99E-03	1.58
15A	0.380	0.0254	0.0487	1.844	2.09E-03	1.69
16A	0.420	0.0228	0.0682	1.710	9.57E-03	1.58
17A	0.423	0.0382	0.0689	1.899	1.99E-03	1.57
19A	0.444	0.0279	0.2010	1.542	4.31E-03	1.52
20A	0.419	0.0321	0.0305	2.081	2.54E-03	1.58
21A	0.403	0.0276	0.0545	1.926	2.94E-03	1.62
22A	0.352	0.0252	0.1078	1.585	5.06E-03	1.78
23A	0.371	0.0411	0.0079	1.553	2.65E-04	1.72
24A	0.321	0.0413	0.0130	1.684	5.69E-04	1.85
25A	0.345	0.0267	0.0842	2.158	5.40E-03	1.80
27A	0.377	0.0354	0.0830	1.532	8.14E-03	1.71
29A	0.359	0.0317	0.0784	1.732	3.75E-03	1.76
31A	0.418	0.0444	0.0058	2.012	8.21E-04	1.60
32A	0.359	0.0401	0.0931	1.703	6.71E-03	1.78
34A	0.316	0.0324	0.0819	2.398	1.32E-02	1.92
35A	0.299	0.0428	0.0897	2.160	1.06E-02	1.98

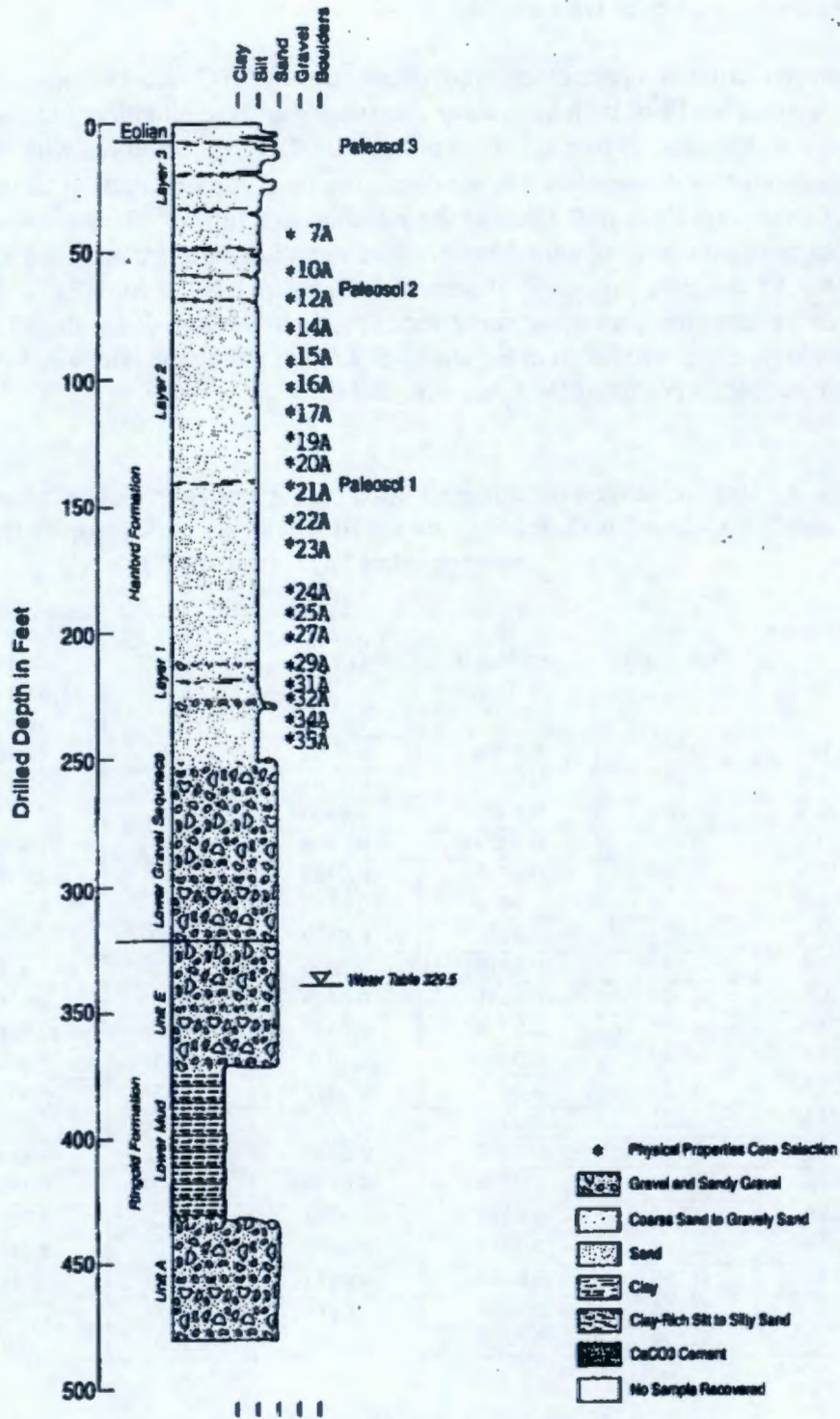


Figure 2. Geologic cross section of the new ILAW disposal site (after Reidel et al. 1998).

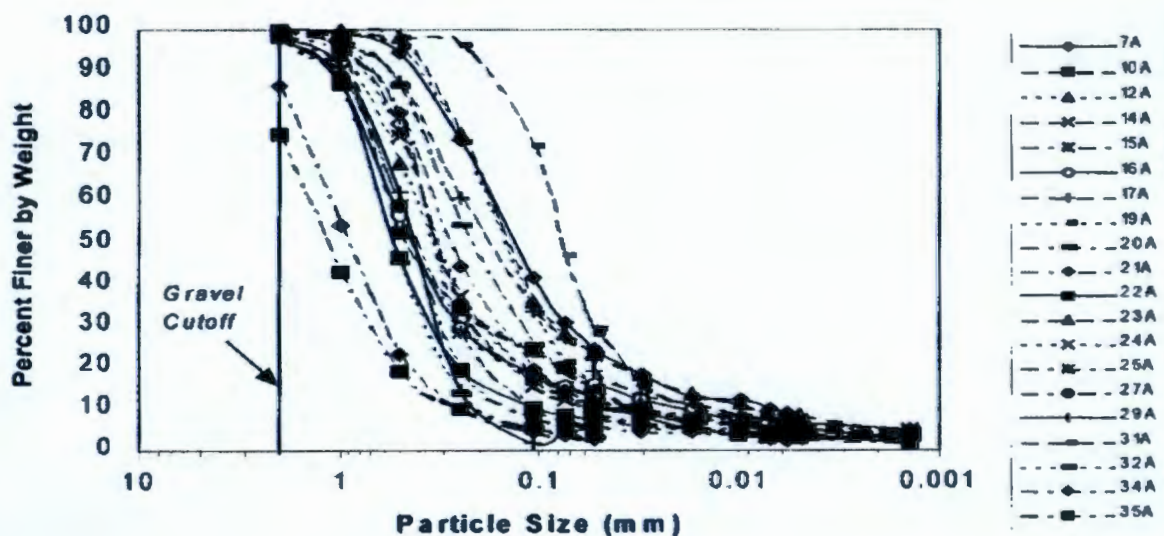


Figure 3. Particle-size distribution for 20 samples from the sand-dominated sequence at the new ILAW disposal site.

Table 2. Van Genuchten parameters, fitted saturated hydraulic conductivity, and measured bulk density data for 15 sandy gravel samples.

Sample	Operable Unit	Well Number	Depth (m)	Percent Gravel	θ_s (cm ³ /cm ³)	α (cm ³ /cm ³)	α (1/cm)	n (-)	Fitted K_s (cm/s)	Bulk Density (g/cm ³)
2-1307	100-HR-3	199-D5-14	18.90	43	0.236	0.0089	0.0130	1.447	1.29E-04	2.15
2-1308	100-HR-3	199-D5-14	30.64	58	0.120	0.0208	0.0126	1.628	6.97E-05	2.13
2-1318	100-HR-3	199-D8-54A	15.54	60	0.124	0.0108	0.0081	1.496	1.67E-04	2.16
2-2663	100-BC-5	199-B2-12	8.20	61	0.135	0.0179	0.0067	1.527	6.73E-05	2.38
2-2664	100-BC-5	199-B2-12	24.84	73	0.125	0.0136	0.0152	1.516	1.12E-04	2.25
2-2666	100-BC-5	199-B4-9	21.49	71	0.138	0.00	0.0087	1.284	1.02E-04	2.10
2-2667	100-BC-5	199-B4-9	23.93	75	0.094	0.00	0.0104	1.296	1.40E-04	2.16
3-0570	100-KR-1	116-KE-4A	3.50	60	0.141	0.00	0.0069	1.195	2.06E-02	2.12
3-0577	100-FR-3	199-4'S-43B	7.16	66	0.107	0.00	0.0166	1.359	2.49E-04	2.32
3-0686	100-FR-1	116-F-14	6.49	55	0.184	0.00	0.0123	1.600	5.93E-04	2.17
3-1702	100-DR-2	199-D5-30	9.78	68	0.103	0.00	0.0491	1.260	1.30E-03	2.33
4-1086	100-K	199-K-110A	12.77	65	0.137	0.00	0.1513	1.189	5.83E-02	2.26
4-1090	100-K	199-K-111A	8.20	50	0.152	0.0159	0.0159	1.619	4.05E-04	2.21
4-1118	100-K	199-K-109A	10.30	66	0.163	0.00	0.2481	1.183	3.89E-02	2.12
4-1120	100-K	199-K-109A	18.90	63	0.131	0.0070	0.0138	1.501	2.85E-04	2.06

2.2 Existing Disposal Site

The geologic cross-section in the vicinity of the existing disposal site is shown in Figure 6 (Kincaid et al. 1995). The cross-section appears to be very similar to that of the new ILAW disposal site. Again, for purposes of this data package, no distinction is made on gravel-dominated sequences of the lower Hanford formation and the Ringold Formation. Physical and hydraulic properties' information on sediments from borehole 299-E25-234 was obtained. Such information included particle-size distribution, bulk density, moisture retention, and saturated hydraulic conductivity. Unlike the new ILAW site, notably absent were any measurements of unsaturated hydraulic conductivity. It is, however, well recognized that estimated unsaturated conductivities, based on saturated conductivity and the van Genuchten retention model, can differ by up to several orders of magnitude with measured conductivities at the dry end (e.g., Khaleel et al. 1995). Therefore, it was decided to use, as much as possible, the new ILAW site sediment properties for the existing disposal site, since the geology for the two sites is not significantly different and measurements of both moisture retention and unsaturated conductivity are available for sediments at the new ILAW site. In fact, the average particle-size distribution for the sandy sequence sediments at the two sites is very similar: <1% gravel, 91% sand, 9% silt and clay for the existing disposal site and <2% gravel, 88% sand, 10% silt and clay for the new ILAW site. Similar to the new ILAW site, the gravel-dominated sequence at the existing disposal site is comprised primarily of sandy gravel. In summary, as indicated in Table 3, the soil physical and hydraulic properties at the new ILAW and existing disposal sites are similar.

Table 3. Comparison of mean parameter estimates for the sandy sequence at the new ILAW and existing disposal sites.

Parameter	New ILAW Disposal Site	Existing Disposal Site
θ_s	0.379	0.420
θ_r	0.033	0.023
K_s (geometric mean), cm/sec	0.0029	0.0016
Bulk Density, g/cm ³	1.71	1.58

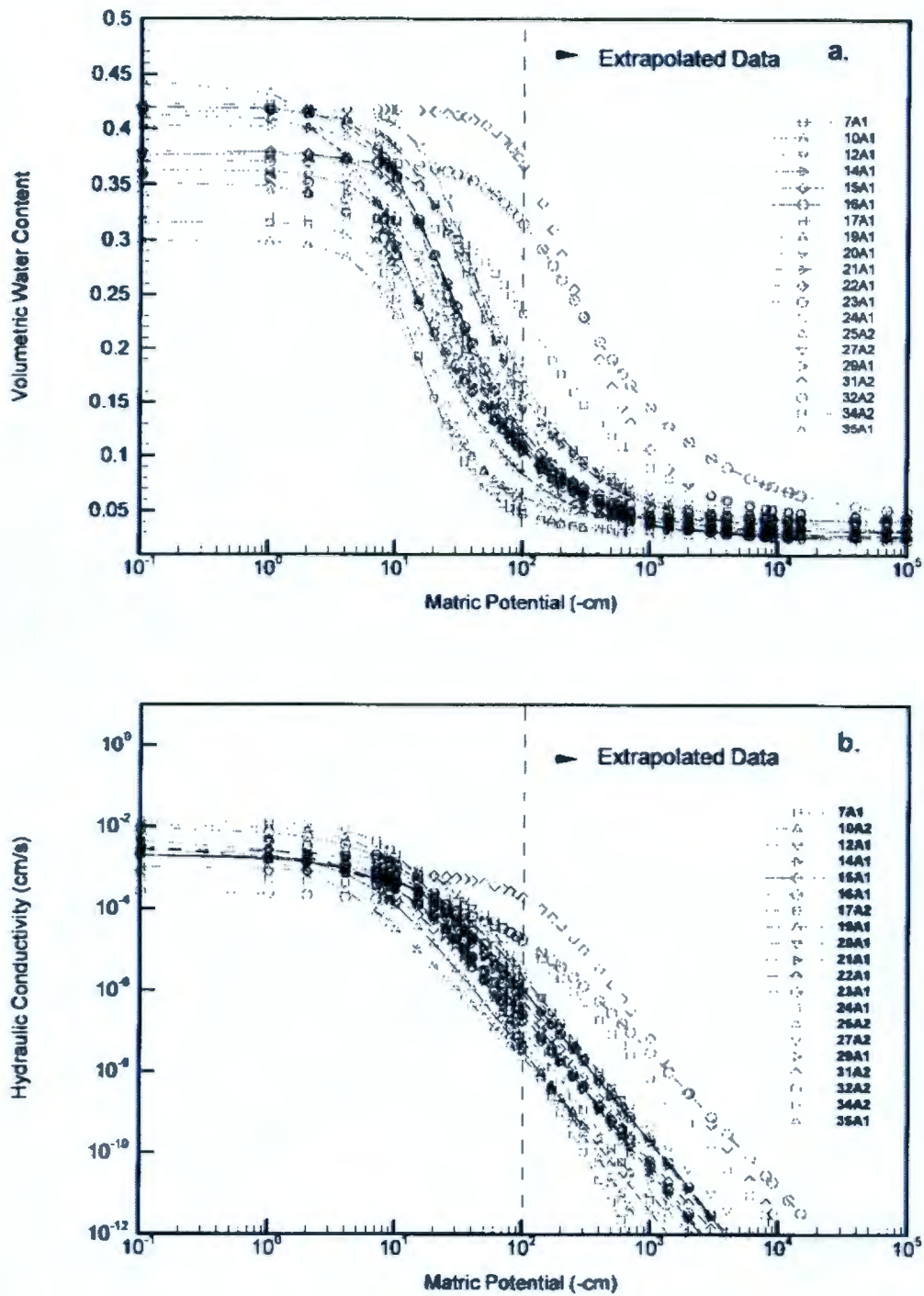


Figure 4. Fitted moisture retention and unsaturated conductivity curves for 20 samples for the sand-dominated sequence (the symbols represent various samples, not experimental data).

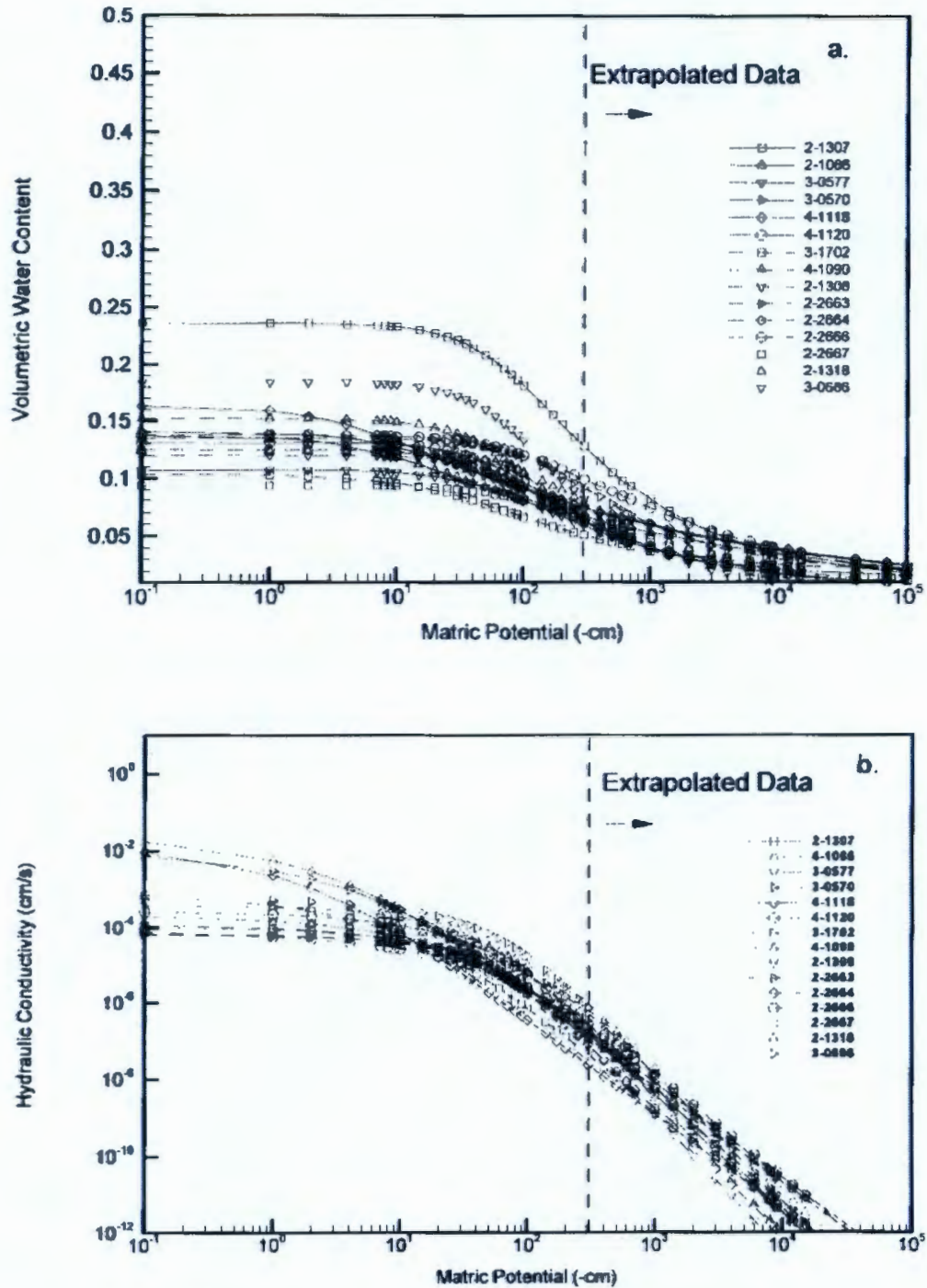


Figure 5. Fitted moisture retention and unsaturated conductivity curves for 15 samples for the gravel-dominated sequence (the symbols represent various samples, not experimental data).

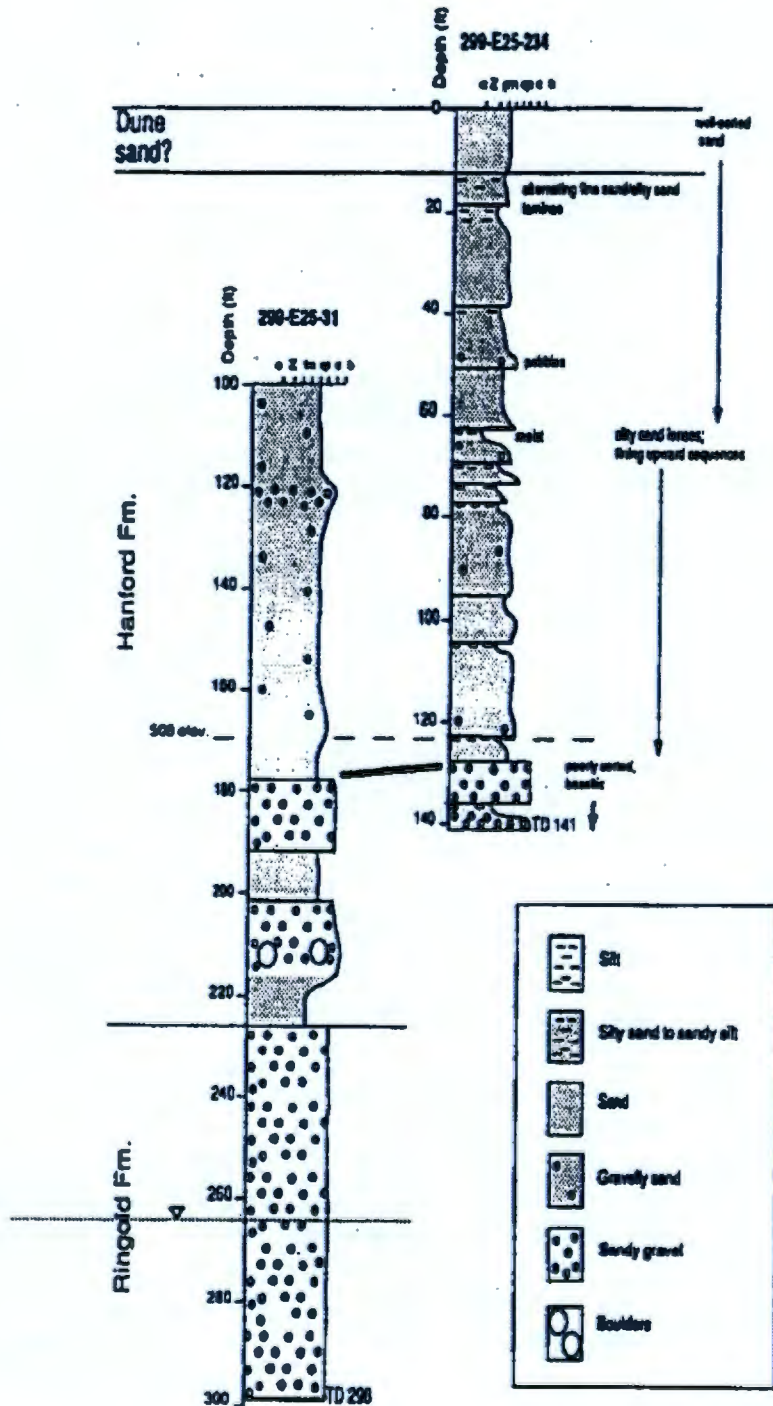


Figure 6. Geologic cross section of the existing disposal site (after Kincaid et al. 1995).

3.0 EFFECTIVE (UPSCALED) FLOW AND TRANSPORT PROPERTIES

Data on hydraulic properties, described in the preceding section, were obtained via laboratory tests on core samples (scales of the order of a few cm). However, numerical models of fluid flow and contaminant transport in the unsaturated zone require specifying hydraulic properties for each discretized grid block (scales of the order of meters). Therefore, the scale of the grid blocks is usually much larger than the scale at which the unsaturated properties were measured. The process of defining large-scale properties for the numerical grid blocks based on small, measurement-scale point measurements is called upscaling.

This section provides effective (upscaled) values of flow and transport parameters for the far-field vadose zone. Specific flow parameters include moisture retention, saturated and unsaturated hydraulic conductivity. Transport parameters include bulk density, diffusivity, and macrodispersivity. Sorption coefficients are included as part of another data package.

3.1 Effective (Upscaled) Flow Parameters

Any attempt at upscaling is confronted with the issue of spatial variability of hydraulic properties due to small-scale soil heterogeneities. The presence of spatial variability in hydraulic properties of Hanford soils has been well documented (e.g., Khaleel and Freeman 1995a). A fundamental issue is then how best to incorporate the effects of natural heterogeneity in modeling. A traditional approach is to use deterministic models and attempt to incorporate the overall heterogeneity of the system such as layering while neglecting the small-scale heterogeneity. The considerable spatial variability of Hanford soils makes complete characterization of the hydraulic properties at the field scale an almost impossible task, as an enormous amount of data is required for proper representation of the actual media heterogeneities.

An alternative approach is to define an equivalent homogeneous medium with average, effective (upscaled) hydraulic properties that are related to the local small-scale heterogeneities and thereby predict the mean flow and transport behavior of the field-scale, larger media. However, to represent a heterogeneous medium by its homogeneous equivalent, we need to estimate the effective hydraulic properties that represent this equivalent homogeneous medium. A straightforward approach would be to use statistical averages (arithmetic or geometric) of the local soil hydraulic properties, but such simple estimates may not always be able to properly describe the complicated nonlinear behavior in heterogeneous soils.

3.1.1 Stochastic Upscaling

For saturated media, an averaging of the heterogeneities in geologic media at a smaller scale leads to an effective hydraulic conductivity value, at the larger (macroscopic) scale, with the lateral hydraulic conductivity being much larger than the vertical conductivity (Freeze and Cherry 1979). For unsaturated media, theoretical (e.g., Mualem 1984, Yeh et al. 1985a, b; c, Bear et al. 1987; Mantoglou and Gelhar 1987; Green and Freyberg 1995) and experimental analyses (e.g., Stephens and Heerman 1988; Yeh and Harvey 1990; McCord et al. 1991) of field-scale unsaturated flow indicates that in stratified sediments, the effective hydraulic conductivity tensor is anisotropic with a tension-dependent (or moisture-dependent) degree of anisotropy. The anisotropy ratio of horizontal hydraulic conductivity to vertical hydraulic conductivity increases with decreasing moisture content. Variable, moisture-dependent anisotropy in unsaturated soils is therefore an effective, large-scale (macroscopic) flow property which results from media heterogeneities at a smaller scale, and provide a framework for upscaling laboratory-scale measurements to the effective (upscaled) properties for the large-scale vadose zone.

3.1.2 Field Observations

Field observations in the vicinity of the new ILAW and existing disposal sites do indeed provide evidence of saturation-dependent anisotropy and lateral migration. A test facility comprising an injection well at the center and a radial array of 32 monitoring wells was constructed in 1980 south of PUREX in 200 East Area. The facility was used in late 1980 and early 1981 to conduct an infiltration and multiple tracer (i.e., chloride, nitrate, barium, rubidium, Sr-85 and Cs-134) test, in which 45,000 L of liquid (in 11 increments) were injected at a depth of 4.7 m over a period of 133 days (Sisson and Lu 1984). Three-dimensional water content profiles in layered, coarse sediments were monitored to a depth of 18 m by down-hole neutron probe measurements. The initial water contents were measured at 30-cm increments over the 30- to 1800-cm depths in all 32 observation wells. In situ gamma energy analysis data were collected to determine the distribution of radioactive tracers. The unique three-dimensional nature of the experiment and the measured water content profiles provide evidence of tension-dependent anisotropy. The field data clearly show lateral spreading that occurred during injection. The horizontal wetting patterns dominated the experiment. In fact, numerical modeling results (Sisson and Lu 1984), based on the assumption of a uniform and isotropic model, showed a much deeper penetration of the moisture profile than occurring in the field (Sisson and Lu 1984). The degree of spreading was remarkable considering the apparent uniform lithology at the site.

3.1.3 Composite Macroscopic Relationships

Figures 4 and 5 show that moisture retention data show spatial variability, although the degree of variation at a given tension is more modest than that of hydraulic conductivity. Based on data in Tables 1 and 2, composite parameters for the moisture retention

relations were determined. For both sandy and gravelly soils, the composite van Genuchten parameters were obtained via RETC (van Genuchten et al. 1991) and a simultaneous fit of both moisture retention and unsaturated conductivity predictions; all four unknown parameters θ_r , θ_s , α , and n with $m=1-1/n$ (van Genuchten 1980), were fitted to the data. The pore size distribution factor ℓ was kept constant at 0.5 during the simultaneous fitting. The saturated conductivity, K_s , was also kept constant as geometric mean of the sample estimates.

The fitted composite moisture retention and unsaturated conductivity curves are shown as Figures 7 and 8, respectively, for the sandy and gravelly sequences. Table 3 shows the fitted parameters. Equivalent horizontal and vertical hydraulic conductivities are derived using macroscopic anisotropy relations.

Table 4. Composite van Genuchten-Mualem parameters for the sand- and gravel-dominated sequences.

Formation	Number of samples	θ_s	θ_r	α (1/cm)	n	ℓ	K_s (cm/s)
Sandy	20	0.375	0.041	0.057	1.768	0.5	2.88E-03
Gravelly	15	0.138	0.010	0.021	1.374	0.5	5.60E-04

3.1.3.1 Stochastic Model for Macroscopic Anisotropy

As discussed earlier, variable, tension-dependent anisotropy provides a framework for upscaling small-scale measurements to the effective (upscaled) properties for the large-scale vadose zone. A stochastic model is used to evaluate tension-dependent anisotropy for sediments at the new ILAW site.

Yeh et al. (1985b) analyzed steady unsaturated flow through heterogeneous porous media using a stochastic model; parameters such as hydraulic conductivity are treated as random variables rather than as deterministic quantities. The Gardner (1958) relationship was used by Yeh et al. to describe unsaturated hydraulic conductivity (K) as a function of saturated hydraulic conductivity (K_s) and tension (ψ), i.e.,

$$K(\psi) = K_s \exp(-\beta\psi) \quad (1)$$

where β is a fitting parameter. Equation (1) can be written as

$$\ln K(\psi) = \ln K_s - \beta\psi \quad (2)$$

Equation (2) is referred to as the log-linear model, since $\ln K$ is linearly related to ψ through the constant slope β . However, such a constant slope is often inadequate in describing $\ln K(\psi)$ over ranges of tension of practical interest for field applications. As an alternative, the slope β can be approximated locally by straight lines over a fixed range of tension. The " $\ln K_s$ " term in equation (2) can then be derived by extrapolating the local slopes back to zero tension.

Using a linear correlation model between the log-conductivity zero-tension intercept and β , Polmann (1990) presents a generalized model that accounts for the cross-correlation of the local soil property (i.e., $\ln K_s$ and β) residual fluctuations. Compared to uncorrelated $\ln K_s$ and β model, partial correlation of the properties is shown to have a significant impact on the magnitude of the effective parameters derived from the stochastic theory. The Polmann (1990) equations for deriving the effective parameters are as follows.

$$\begin{aligned} \langle \ln K \rangle &= \langle \ln K_s \rangle - A \langle \psi \rangle - \sigma_{\ln K_s}^2 \lambda [p - p^2 \langle \psi \rangle - \zeta^2 \langle \psi \rangle] / (1 + A\lambda) \\ \sigma_{\ln K}^2 &= \sigma_{\ln K_s}^2 [(1 - p \langle \psi \rangle)^2 + \zeta^2 \langle \psi \rangle^2] / (1 + A\lambda) \\ K_h^{eq} &= \exp[\langle \ln K \rangle + (\sigma_{\ln K}^2 / 2)] \\ K_v^{eq} &= \exp[\langle \ln K \rangle - (\sigma_{\ln K}^2 / 2)] \end{aligned} \quad (3)$$

where $\sigma_{\ln K}^2$ = variance of log unsaturated conductivity (which depends on mean tension),

$\langle \psi \rangle$ = mean tension,

$\sigma_{\ln K_s}^2$ = variance of $\ln K_s$,

$\langle \ln K_s \rangle$ = mean of $\ln K_s$,

p = slope of the β versus $\ln K_s$ regression line,

ζ = $\sigma_\beta / \sigma_{\ln K_s}$,

σ_β = standard deviation of the residuals in the β versus $\ln K_s$ regression,

A = mean slope, β , for $\ln K_s$ vs. ψ ,

λ = vertical correlation lengths for $\ln K_s$ (assumed to be same as that of β),

K_h^{eq} = equivalent unsaturated horizontal conductivity, and

K_v^{eq} = equivalent unsaturated vertical conductivity.

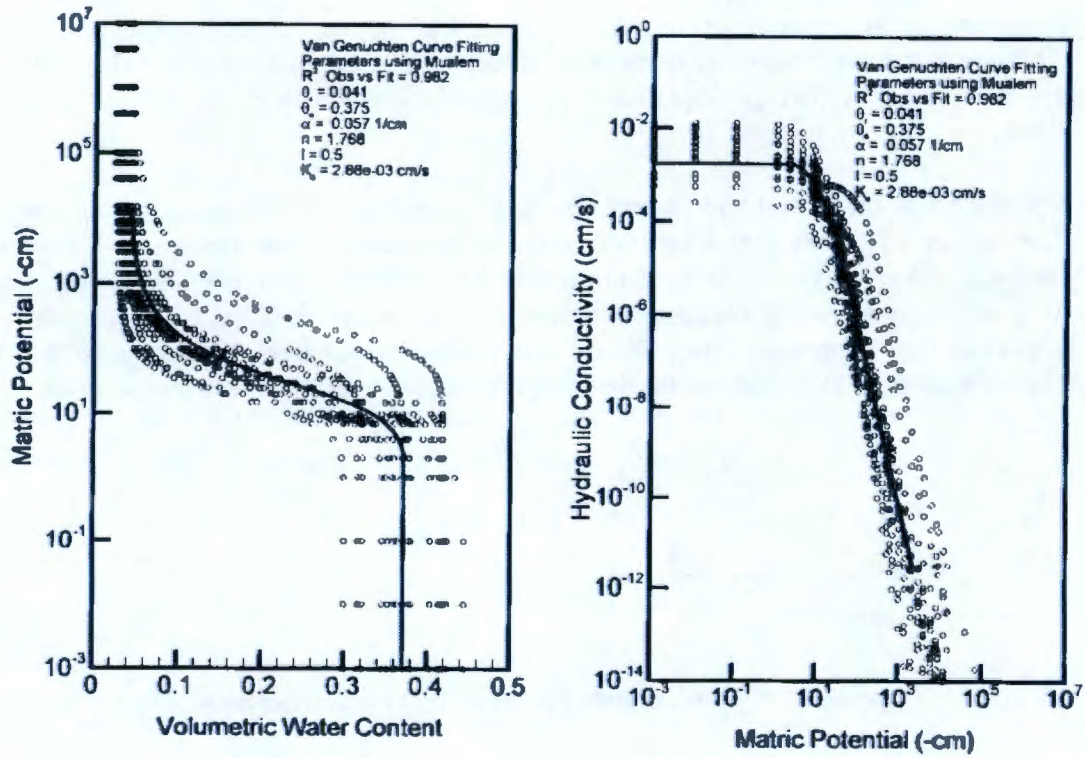


Figure 7. Composite moisture retention and unsaturated conductivity curves for the sand-dominated sequence.

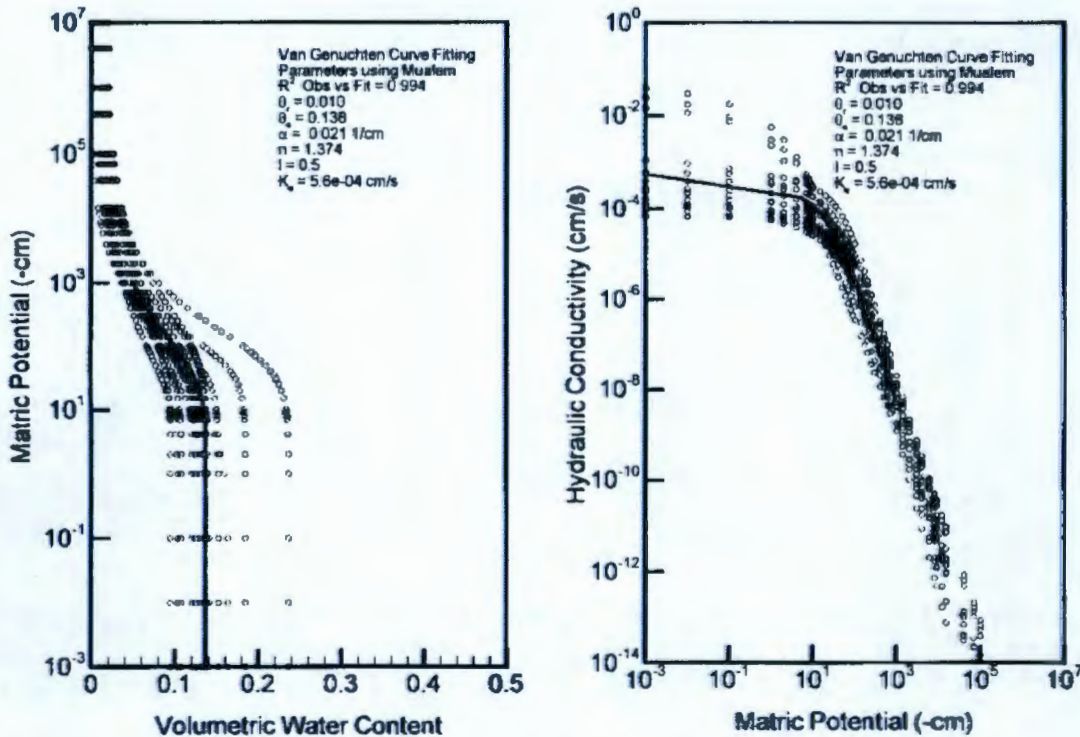


Figure 8. Composite moisture retention and unsaturated conductivity curves for the gravel-dominated sequence.

3.1.3.2 Macroscopic Anisotropy Relations

Results of application of equation (3) for variable anisotropy are presented below. The same 20 samples (Table 1) of the sandy sequence were used to obtain parameters $\langle \ln K_s \rangle$, $\sigma_{\ln K_s}^2$, ρ , ζ , and A . The slope and pseudo $\ln K_s$ estimates, discussed in the preceding section, were evaluated for the moisture regime of interest (i.e., tension range of 500 cm to 700 cm for the sandy sequence and 700 cm to 1000 cm for the gravelly sequence). It should be noted, however, that no experimental data are available for unsaturated conductivities in the tension range of interest; β and $\ln K_s$ estimates were based on the fitted van Genuchten-Mualem curves (Figures 7 and 8). The tension ranges are consistent with a base case recharge estimate of about 0.1 cm/yr (Figures 7 and 8).

An estimate of the correlation length, λ , is needed for anisotropy calculations. Most of the measurements in the vicinity of the ILAW site have been obtained at sampling intervals that are too coarse to yield a reasonable estimate for the correlation length. However, one data set is available that provides saturated conductivity estimates at about 30 cm intervals for a depth of 18 m within the Hanford formation; the site is located about 1/2 mile east of the ILAW site. Figure 9 shows the experimental variogram and the

fitted spherical variogram model for saturated conductivities. The fitted spherical variogram suggests a correlation length, λ , of about 50 cm; i.e., the distance at which the variogram drops to $[1-(1/e)]$ times the sill (Figure 9). The correlation length, λ , for both $\ln K_s$ and β were assumed to be equal.

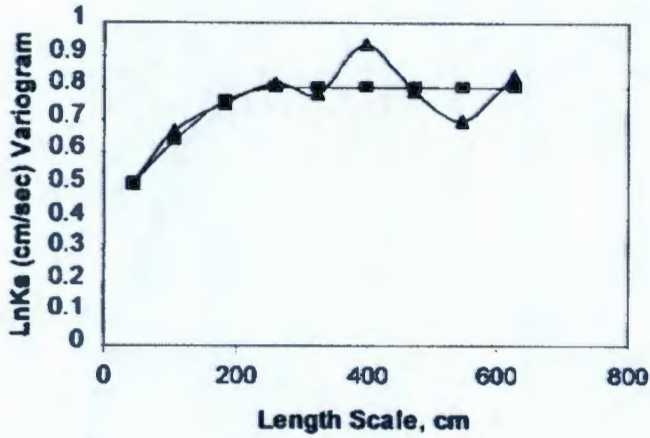


Figure 9. Experimental (triangles) and fitted theoretical (squares) variogram for $\ln K_s$.

The Polmann parameters for both sandy and gravel-dominated sequences are shown in Table 5. Note that, compared to the sandy soils, mean slope, A , $\langle \ln K_s \rangle$, $\sigma_{\ln K_s}^2$, and ζ values for the gravelly soils are significantly lower; σ_p^2 for the gravelly samples was also almost two orders of magnitude lower. Because of these different characteristics, the macroscopic anisotropy relations for the sandy and gravelly sediments are quite different. Figures 10 and 11 illustrate the macroscopic anisotropy relations for the two sediments. The anisotropy for the gravelly soils is much less compared to that for sandy soils. In fact, for the tension range of interest for ILAW PA modeling, anisotropy ratio is about two. Note that, for gravelly soils, no data were available for a variogram analysis. However, a smaller λ value (30 cm) is used (Table 5) because of a much higher variance of $\ln K_s$ for the gravelly soils than for the sandy soils.

Table 5. Macroscopic anisotropy parameters for the sand- and gravel-dominated sequences.

Formation	Number of samples	$\langle \ln K_s \rangle$	$\sigma_{\ln K_s}^2$	p	ζ	λ (cm)	A
Sandy	20	-17.3	2.89	-1.4E-4	3.18E-4	50	0.00680
Gravelly	15	-15.6	1.03	1.9E-4	4.24E-4	30	0.00354

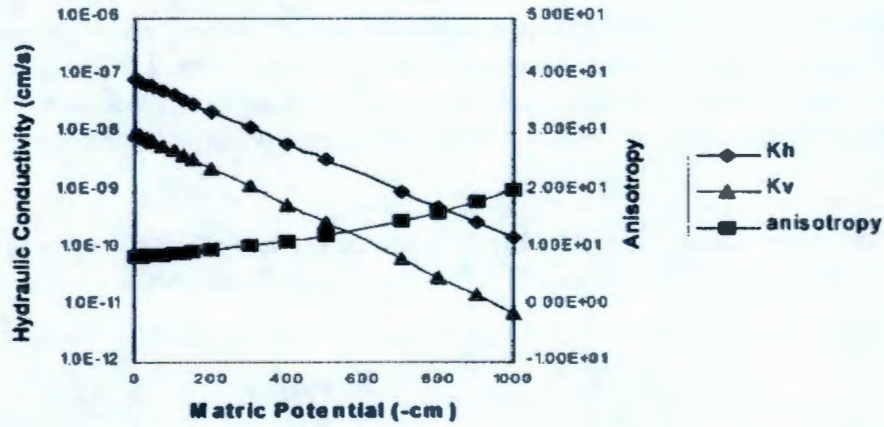


Figure 10. Calculated macroscopic anisotropy (equation 3) as a function of mean pressure head for the sand-dominated sequence.

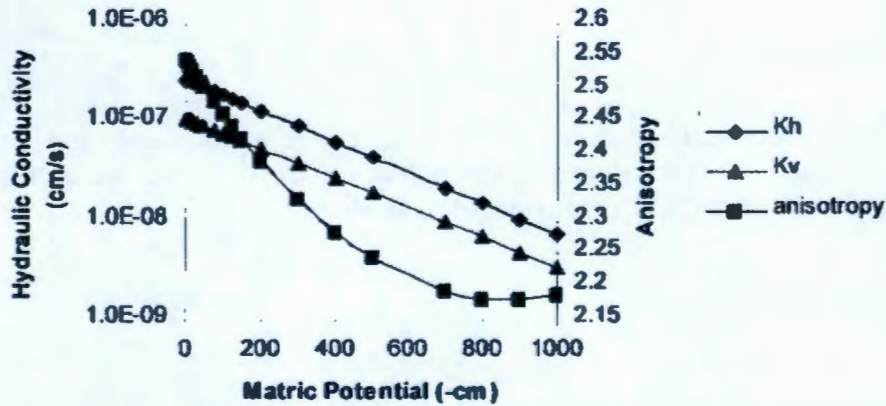


Figure 11. Calculated macroscopic anisotropy (equation 3) as a function of mean pressure head for the gravel-dominated sequence.

3.2 Effective Transport Parameters

Base case effective transport parameter (bulk density, diffusivity, and dispersivity) estimates are presented in this section. Because of natural variability, the transport parameters are all spatially variable. The purpose is again, similar to the flow parameters, to evaluate the effect of such variability on the large-scale transport process.

3.2.1 Bulk Density

Both bulk density (ρ_b) and K_d estimates are needed to calculate retardation factors for different species. The effective, large-scale estimate for the product $[\rho_b K_d]$ is the average of the product of small-scale laboratory measurements for bulk density and K_d (Gelhar 1993). The laboratory measurements for ρ_b are shown in Tables 1 and 2, respectively, for the sandy and the gravel-dominated sequences, whereas the K_d measurements are available in Kaplan et al. (1998). Table 6 provides the effective, large-scale estimates.

Table 6. Effective parameter estimates, $E[\rho_b K_d]$, for the product of bulk density (g/cm^3) and K_d (cm^3/g) at the new ILAW and existing disposal sites.

Species	$E[\rho_b K_d]$	
	Sandy	Gravelly
Cs	3473	1700
Sr	25.20	12.20
U	1.05	0.51
Se	11.32	5.56

3.2.2 Diffusivity

It is assumed that the effective, large-scale diffusion coefficients for both sandy and gravel-dominated sequences at both sites are a function of volumetric moisture content, θ . VAM3DF uses the Millington-Quirk (1961) empirical relation:

$$D_e(\theta) = D_0 \frac{\theta^{10/3}}{\theta_s^2} \quad (4)$$

where $D_e(\theta)$ is the effective diffusion coefficient of an ionic species, and D_0 is the effective diffusion coefficient for the same species in free water. The molecular diffusion coefficient for all species in pore water is assumed to be $2.5 \times 10^{-5} \text{ cm}^2/\text{sec}$ (Kincaid et al. 1995).

3.2.3 Dispersivity

An extended review is provided on the rationale of choice for vadose zone dispersivity estimates. Readers who are familiar with the state-of-the-art can proceed directly to Section 3.2.3.4.

A variety of factors such as the size of the flow domain, the flow regime (saturated versus unsaturated flow), field heterogeneities, and the contaminant species (retarded versus nonretarded) need to be recognized in estimating dispersivities. The objective of this section is to provide appropriate guidance on the choice of vadose zone dispersivity estimates for use in ILAW PA.

It should be noted that laboratory data would be of little use in estimating field-scale dispersivities. While well-designed, large-scale tracer experiments would provide useful information, limited field data are available at this time. Therefore, the dispersivity estimates needed for modeling are essentially based on literature values and the available stochastic equations.

Literature data suggest that much more information is available on dispersion in saturated media than in unsaturated media. Therefore, first the available data on dispersivities in saturated media are summarized (Gelhar et al. 1992). Second, available data on vadose zone dispersivities are presented, including results of small-scale tracer experiments in the vicinity of the new ILAW site in 200 East Arca. Third, the stochastic framework used in obtaining dispersivity estimates is reviewed, and estimates are provided for use in ILAW PA.

3.2.3.1 Saturated Media Dispersivities For Field Sites

A critical review of dispersivity observations from 59 different field sites was performed by Gelhar et al. (1992). Extensive tabulations of information were included by Gelhar et al. on aquifer type, hydraulic properties, flow configuration, type of monitoring network, tracer, method of data interpretation, overall scale of observation and longitudinal, horizontal transverse and vertical transverse dispersivities from original sources. The information was then used to classify the dispersivity data into three reliability classes: low, intermediate, and high. Overall, the data indicate a trend of systematic increase of the longitudinal dispersivity with observation scale but the trend is much less apparent when the reliability of data (Figure 12) is considered. The longitudinal dispersivity ranged from 10^{-1} to 10^5 m, but the largest scale for high reliability data was only 250 m. When the data are classified according to porous versus fractured media, no significant differences were apparent between these aquifer types. At a given scale, the longitudinal dispersivity values were found to range over 2 to 3 orders of magnitude and the higher reliability data approached the lower portion of this range. The high reliability dispersivity data ranged from a low of about 0.6 m at a scale of 15 m to about 1 m at a scale of 250 m; some data are on the order of 2 to 3.5 m at a scale of 30 m (Figure 12). It is not appropriate to represent the longitudinal dispersivity data by a single universal line.

The variations in dispersivity reflect the influence of differing degrees of aquifer heterogeneity at different sites. The data on transverse dispersivities are more limited but clearly indicate that vertical transverse dispersivities are typically an order of magnitude smaller than horizontal transverse dispersivities (Gelhar et al. 1992). Reanalysis of data from several of the field sites showed that improved interpretations most often lead to smaller dispersivities (Gelhar et al. 1992). Overall, Gelhar et al. concluded that longitudinal dispersivities in the lower part of the indicated range are more likely to be realistic for field situations. This suggests that, for conservative species, a longitudinal dispersivity of the order of a meter is a reasonable estimate for saturated media domains that are a couple of hundred meters in scale. Note that the estimates are for saturated media and conservative species. As discussed later, dispersivity estimates are enhanced due to heterogeneous sorption in both saturated and unsaturated media.

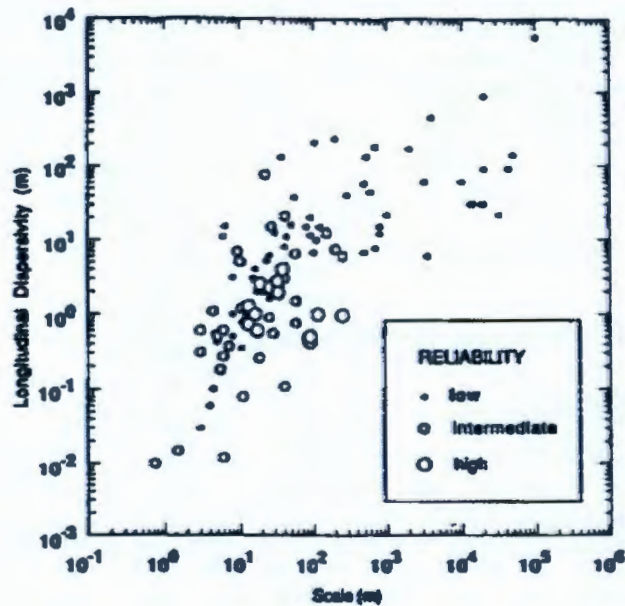


Figure 12. Longitudinal macrodispersivity in saturated media as a function of overall problem scale with data classified by reliability (after Gelhar et al. 1992).

3.2.3.2 Vadose Zone Dispersivities For Dry Desert Environment

As discussed earlier, for an engineered waste disposal facility with a capillary barrier and a surface barrier on top, the vadose zone water contents beneath the disposal facility are expected to approach the natural moisture regime for arid soils. Although exceptional precipitation events may cause transient high water contents near the soil surface, the source of the infiltration is not likely to be sustained at great depths within the vadose zone.

This inference is supported by the results of artificial tracer experiments on much shorter time scales. For example, two massively instrumented solute transport experiments were performed in desert soils near Las Cruces, New Mexico (Wierenga et al. 1991; Hills et al. 1991). Drip emitters were used to irrigate a plot adjoining a deep trench in a heterogeneous soil possessing well in excess of one order of magnitude standard deviation in saturated hydraulic conductivity. Monitoring of the trench face showed a spatially uniform progression of the wetting front and did not reveal indications of preferential flow (Wierenga et al. 1991). Hills et al. (1991) found that a dispersivity of 5 cm provided reasonably realistic simulations of ^3H and Br tracer distributions.

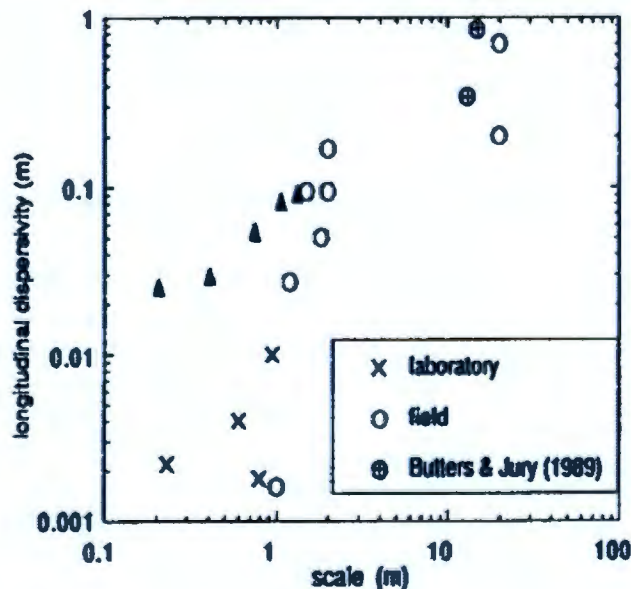


Figure 13. Longitudinal macrodispersivity in unsaturated media as a function of overall problem scale (after Gelhar 1993). [Note that the triangles are data from Ward et al. 1998]

For unsaturated flow, long-term environmental tracer studies at several arid southwestern sites indicate dispersivities of less than 10 cm. Phillips et al. (1988) assessed the degree of mixing in desert soils using the conventional advection-dispersion modeling, yielding

a dispersion coefficient of $50 \text{ cm}^2/\text{yr}$. This compares with the calculated effective diffusion coefficient of $25 \text{ cm}^2/\text{yr}$. A similar study by Scanlon (1992), at another southwestern arid site, obtained a dispersion coefficient of about $14 \text{ cm}^2/\text{yr}$. These, then, lead to effective dispersivities of about 7 and 4 cm, at the two arid sites, and Peclet numbers (displacement divided by dispersivity) of 23 and 17.

Ward et al. (1998)³ obtained dispersivity estimates via field measurements at a location close to the ILAW site, using KCl as a tracer. Analysis of the data provided dispersivities that ranged from 1.3 to 7.8 cm for travel distances ranging from 25 to 125 cm (Appendix C). Dispersivity increased with depth to about 0.75 m, after which it essentially became constant. Although these estimates are for the Hanford formation similar to the ILAW site, the transport distance within the vadose zone is indeed of limited extent. Nevertheless, results based on the limited data are consistent with the concept of a scale-dependent dispersivity. Thus, although no data exist on large-scale dispersivities near the ILAW site, it is expected that they will be larger than those based on the small-scale tracer experiment of Ward et al. (1998).

Based on a survey of literature, Gelhar (1993) presented, as shown in Figure 13, the longitudinal vadose zone dispersivities as a function of the scale of the experiment. The figure shows a lack of data for scales larger than 2 m. Nevertheless, similar to saturated flow, Figure 13 show an increase of dispersivity with an increase in scale. Also, shown in Figure 13 are results from the Ward et al. experiment; their data are in close agreement with others.

3.2.3.3 Stochastic Models and Macrodispersivities for Large-Scale Media

Field-scale dispersivities are referred to as macrodispersivities. The heterogeneities that exist at various length scales result in a scale dependence of macrodispersivities. Stochastic models have been developed which relate the macrodispersive spreading to the spatial variability of saturated hydraulic conductivity field in a saturated porous media (e.g., Gelhar and Axness 1983; Dagan 1984). The Gelhar and Axness (1983) model provides the asymptotic estimates of macrodispersivity, while the Dagan (1984) model describes the preasymptotic estimates of macrodispersivities for the near-source, early-time period. The Dagan (1984) model predicts that under steady state flow with a uniform mean hydraulic gradient, the ensemble longitudinal macrodispersivity increases with time and displacement distance as the solute first enters the flow domain. A constant, asymptotic value (i.e., Fickian behavior) is eventually reached after the solute travels a few tens of correlation scales of the hydraulic conductivity field.

For prediction of contaminant transport during early time or for short travel distances, simulating effects of scale-dependence on macrodispersion is a consideration. The dispersivities increase with time (or equivalently with distance) until they tend to

³ Ward, A.L., R.E. Clayton, and J.S. Ritter. 1998. Determination of in situ hydraulic parameters of the upper Hanford formation. Letter Report to Fluor Daniel Northwest, Inc. December, 1998. Pacific Northwest National Laboratory. Richland, WA.

converge on their unique asymptotic (large time) values. The second-moment evolution curve or the time-dependent, preasymptotic macrodispersivities are of particular interest, since it can take a long time (e.g., years or decades) for the asymptotic Fickian approximation to take hold. However, the early time scale dependence are of little consequence in simulations involving long times or large mean travel distances such as those for ILAW PA. For these predictions over large travel distances or large times, the use of a constant (asymptotic) dispersivity is considered to be adequate. An estimate of the maximum or asymptotic value of macrodispersivity for saturated media can be based on Gelhar and Axness' (1983) stochastic solution:

$$A_L = \sigma_{\ln K_s}^2 \lambda \quad (5)$$

where λ is the vertical correlation scale (i.e., average distance over which conductivities are correlated) for log saturated hydraulic conductivity.

In addition to the size of flow domain and vadose zone soil heterogeneities, dispersivities are expected to be a function of soil moisture content (or matric potential). Macrodispersivities are expected to increase with a decrease in saturation (e.g., Polmann 1990; Gelhar et al. 1994). Russo (1993) suggests that vadose zone macrodispersivities can be defined in a manner similar to saturated media estimates. This is based on his finding that the product of the variance and the correlation scale of log conductivity for both saturated and unsaturated media are of similar magnitude. In other words, an increase in the variance of log conductivity (and, concurrently, in the velocity variance) as moisture content decreases is compensated in part by a decrease in the correlation scale of log conductivity (and, concurrently, in the correlation scale of the longitudinal component of the velocity). Such an approximation (a) assumes use of Gardner's (1958) equation to describe unsaturated conductivity as a function of matric potential, and (b) holds as long as the correlation scale of β in Gardner's equation is relatively small compared with that of log saturated conductivity.

3.2.3.4 Macrodispersivity Estimates For Non-Reactive Species

The Gelhar and Axness equation can be used to estimate asymptotic values of macrodispersivity. However, to account for effects of unsaturated flow, a modified version is used for both disposal sites:

$$A_L(\langle \psi \rangle) = \sigma_{\ln K}^2 \lambda \quad (6)$$

where the longitudinal macrodispersivity depends on the mean tension $\langle \psi \rangle$. To apply equation (6), an estimate of the vertical correlation scale for unsaturated conductivity is needed. As discussed earlier, a correlation length of the order of about 50 cm was obtained for the sandy formation. However, compared to the saturated K's, an increase in the variance of log conductivity is expected to be compensated in part by a decrease in the correlation scale of log unsaturated conductivity. A correlation length of 30 cm is assumed for both sandy and gravelly formations. Table 6 provides the log unsaturated

conductivity variances (at a recharge rate of about 0.1 cm/yr) and the estimated longitudinal (A_L) and transverse (A_T) macrodispersivities for the two formations. The transverse dispersivities are estimated as $1/10^{\text{th}}$ of the longitudinal values (Gelhar et al. 1992). Gelhar (1993) presented results of stochastic analysis of macrodispersion in unsaturated media by Mantoglou and Gelhar (1985). The large-scale macrodispersivity estimates in Table 7 are of similar magnitude to those reported in Gelhar (1993) for Panoche and Maddock soil types.

Table 7. Non-reactive macrodispersivity estimates for soils at the new ILAW and existing disposal sites.

Formation	σ_{Tmk}^2	Correlation length, λ (cm)	A_L (cm)	A_T (cm)
Sandy	5.51	30	~200	20
Gravelly	0.96	30	~30	3

3.2.3.5 Heterogeneous Sorption Enhanced Macrodispersivities

As expected, the net effect of sorption is to retard the velocity of the contaminant in the soil. Because sorption for specific contaminants may be a function of soil properties, as the soil properties experience spatial variability, the sorption also varies (Gelhar 1993; Talbott and Gelhar 1994). The variation directly affects the velocity of the contaminant, which, in turn, enhances the spreading of the plume. The enhanced spreading is defined by a larger reactive longitudinal macrodispersivity, different from the non-reactive longitudinal macrodispersivity, as discussed in the preceding section. The increased plume spreading due to heterogeneous sorption (over and above the result for no sorption) is defined as the macrodispersivity enhancement. Stochastic theory and field data on contaminant plumes suggest that the effect of macrodispersivity enhancement only occurs in the longitudinal direction. The transverse macrodispersivity is unaffected by sorption variability (Garabedian et al. 1991). The results presented in this section will support the use of species-dependent enhanced longitudinal macrodispersivities in the ILAW PA modeling.

The radioisotopes considered are Cs-137, Sr-90, U, and Se. The objective is to evaluate differences in macrodispersivity enhancement due to a long-lived mobile radionuclide (e.g., U) and a short-lived relatively immobile radionuclide (e.g., Sr-90). During the laboratory analysis, measurements of K_d for each species have been obtained on the same soil samples, as are measurements of unsaturated hydraulic conductivity.

Based on laboratory measurements of unsaturated conductivity, K (Fayer et al. 1998; see footnote on p. 4) and K_d (Kaplan et al. 1998) for the same 20 samples for the Hanford

sandy sequence, a direct correlation of K and K_d was derived for Cs-137, Sr-90, U, and Se. Stochastic theory developed by Gelhar (1993) was evaluated to determine the importance of varying longitudinal macrodispersivity by contaminant species on the basis of sorption heterogeneity and correlation with hydraulic conductivity. An enhancement of macrodispersivity can have significant effects on the expected contaminant predictions for numerical models.

In order to understand clearly the importance of heterogeneous, spatially variable sorption, a number of parameters were defined. The variable K_d may be prescribed by a mean (\bar{K}_d) and a standard deviation (σ_{Kd}). Further, a retardation factor, R , was related to K_d by the following:

$$R = 1 + \frac{\rho_b K_d}{\theta} \quad (7)$$

where R may be described statistically by an effective retardation, $\bar{R} = E[R]$, and its standard deviation, σ_R .

By analyzing the mean and standard deviation of a sample data set of a measured soil property, and by showing a relationship between the soil property and R , \bar{R} and σ_R were calculated as a function of the soil property data set.

The net result of the variation in the retardation and the relationship between the retardation and $\ln K$ is to increase the longitudinal macrodispersivity of the sorbed species according to the following equation given by Talbott and Gelhar (1994):

$$A_{11} = A_0 \left\{ \left[1 + \gamma \frac{\sigma_R}{R \sigma_{\ln K}} \sqrt{\zeta} \right]^2 + (1 - \zeta) \frac{\sigma_R^2 \lambda_n}{R^2 \sigma_{\ln K}^2 \lambda_1} \gamma^2 \right\} \quad (8)$$

where A_0 is the non-reactive longitudinal macrodispersivity, λ_1 is the horizontal correlation scale, $\lambda_n \rightarrow \lambda_1$, and γ is defined as the ratio of harmonic to geometric mean for unsaturated K .

Equation (8) is identical to that in Talbott and Gelhar (1994), except that the appropriate variables are evaluated for unsaturated conditions. Equation (8) assumes random K_d but constant bulk density and moisture content. However, using the more general case (p. 256, Gelhar 1993) when all three (i.e., K_d , bulk density and moisture content) vary, it was found that the contribution to equation (8) from variations of bulk density and moisture content were negligibly small, compared to variations of K_d .

The $\ln K$ versus R relation for the four species for the sandy sequence are shown in Figure 14. The result of stochastic analysis for macrodispersivity enhancement for the Hanford sandy sequence is shown in Table 8. Note that the unsaturated K 's were

evaluated at -100 cm via the fitted van Genuchten-Mualem relation. As expected, the log conductivity variance, $\sigma_{\ln K}^2$ at a matric potential of -100 cm is much higher (~5.5) compared to the $\sigma_{\ln K_s}^2$ (~1.0) for the same 20 samples at saturation. The macrodispersivity enhancement, A_{11}/A_0 ranges from about 1.06 for Se to about 2.12 for U.

Table 8. Macrodispersivity enhancement for the sandy sequence at the new ILAW and existing disposal sites [ρ_b in g/cm³ and K_d in cm³/g].

Species	\bar{K}_d	σ_{K_d}/\bar{K}_d	\bar{R}	σ_r/\bar{R}	$\bar{\rho}_b$	$\bar{\theta}$	$\sigma_{\ln K}^2$	γ	ζ	λ_n/λ_1	A_{11}/A_0
Cs-137	2055	0.29	31002	0.50	1.71	0.138	5.51	0.22	0.52	1	1.07
Sr-90	14.7	0.11	241	0.62	1.71	0.138	5.51	0.22	0.45	1	1.08
U	0.62	0.20	11.1	0.52	1.71	0.138	5.51	0.22	0.53	1	2.12
Se	6.73	0.28	98.5	0.28	1.71	0.138	5.51	0.22	0.68	1	1.06

The LnK versus R relation for the four species for the gravelly sequence are shown in Figure 15. The result of stochastic analysis for macrodispersivity enhancement for the Hanford gravelly sequence is shown in Table 9. Again, the unsaturated K's were evaluated at -100 cm via the fitted van Genuchten-Mualem relation for the 15 gravelly samples. No data are available on the measurements of sorption coefficients for the gravel-dominated sequence. Based on the information for the sandy samples, all gravelly samples were first assigned the same average sorption coefficient for their respective species. This resulted in the coefficient of variation (i.e., Col. 3 in Table 9) to be identically zero for all four species. The bulk (gravel and fine fraction) retardation coefficients are then based on a correction of the actual surface area available for sorption, based on the individual gravel fraction for the 15 samples. Unlike for the sandy sequence, the log conductivity variance, $\sigma_{\ln K}^2$ at a matric potential of -100 cm is much lower (~0.96) compared to the $\sigma_{\ln K_s}^2$ (~5.31) for the same 15 samples at saturation. The macrodispersivity enhancement, A_{11}/A_0 varies over a very narrow range -- from about 1.05 for U to about 1.07 for Cs-137.

Table 9. Macrodispersivity enhancement for the gravelly sequence at the new ILAW and existing disposal sites [ρ_b in g/cm³ and K_d in cm³/g].

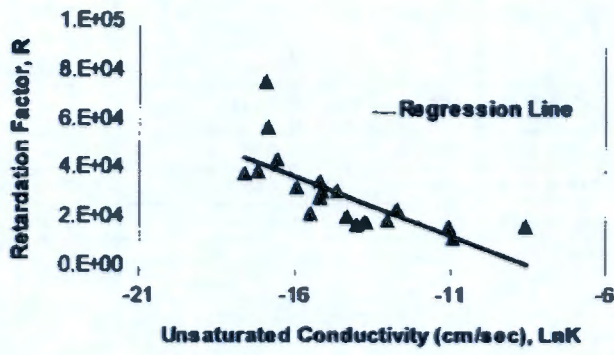
Species	\bar{K}_d	σ_{K_d}/\bar{K}_d	\bar{R}	σ_R/\bar{R}	$\bar{\rho}_b$	$\bar{\theta}$	σ^2_{LnK}	γ	ζ	λ_n/λ_1	A_{11}/A_0
Cs-137	2055	0	17148	0.21	2.19	0.10	0.96	0.62	0.033	1	1.07
Sr-90	14.7	0	124	0.20	2.19	0.10	0.96	0.62	0.033	1	1.06
U	0.62	0	6.13	0.17	2.19	0.10	0.96	0.62	0.033	1	1.05
Se	6.73	0	57.12	0.20	2.19	0.10	0.96	0.62	0.033	1	1.06

3.2.3.6 Numerical Considerations

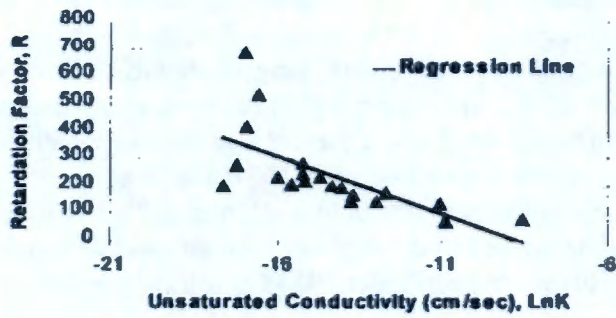
A complicating factor in numerical modeling of contaminant transport in porous media is that both finite-difference and finite-element solutions are affected by "numerical dispersion," which refers to artificial dispersion caused by errors associated with discretization of the flow domain. To minimize such errors, the grid should be designed so that the Peclet number ($P_e = \text{discretized distance}/\text{dispersivity}$) is less than or equal to one, although acceptable solutions can be obtained with P_e as high as 10 (Huyakorn and Pinder 1983). With low dispersivities within the vadose zone, the Peclet number criterion results in grid spacings that are not very practical to implement. This is why numerical modelers often resort to higher values of dispersivity. An alternative is to consider use of "upwinding" option (Huyakorn and Pinder 1983) to control numerical dispersion.

Another consideration is discretization of simulation time so that the Courant number ($C_r = \text{pore velocity} \cdot \text{time interval}/\text{grid spacing}$) is less than or equal to one. That is, the time step should be selected so that the chosen time interval is less than the value obtained by the ratio of grid spacing to pore velocity. Thus, the time step should be selected so that it is less than the time it takes for the solute to move one grid spacing. Note that, for a three-dimensional problem, the P_e and C_r criteria are applicable to transport in all three directions.

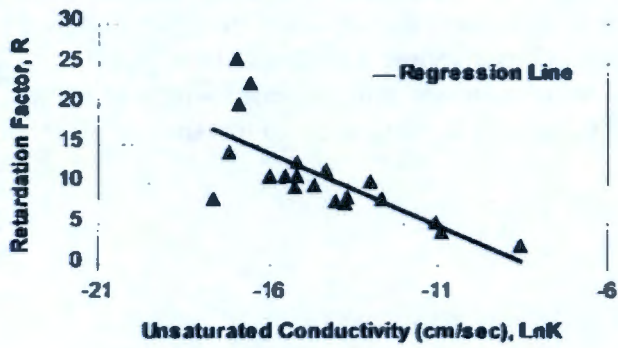
(a)



(b)



(c)



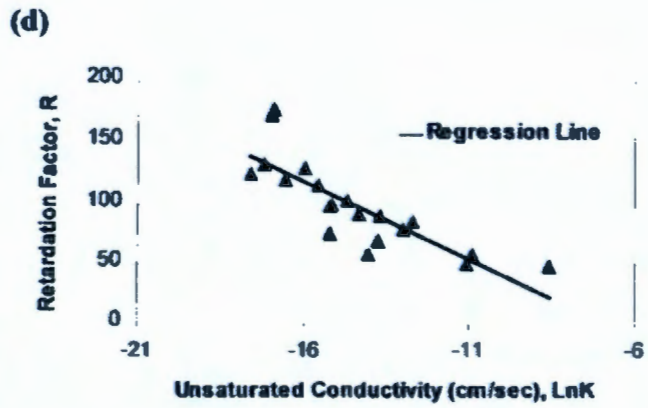
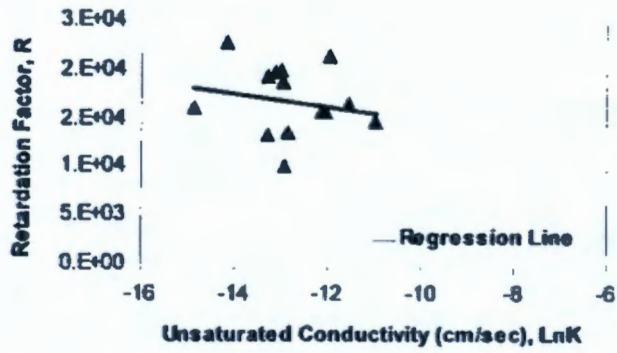
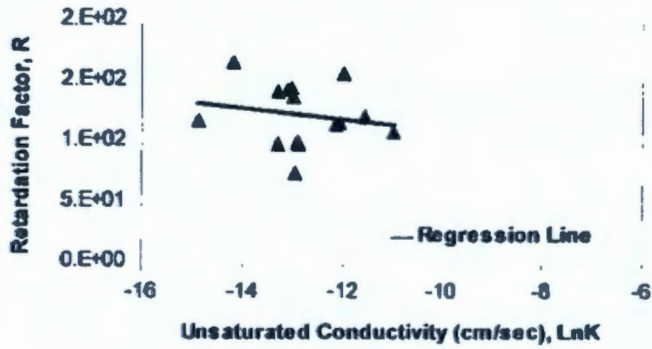


Figure 14. LnK versus R for (a) Cs-137, (b) Sr-90, (c) U, and (d) Se for the sand-dominated sequence.

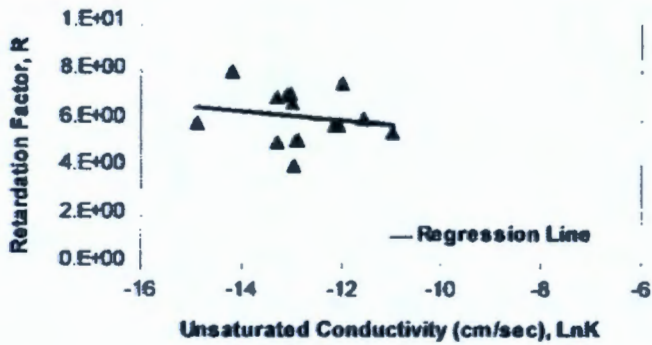
(a)



(b)



(c)



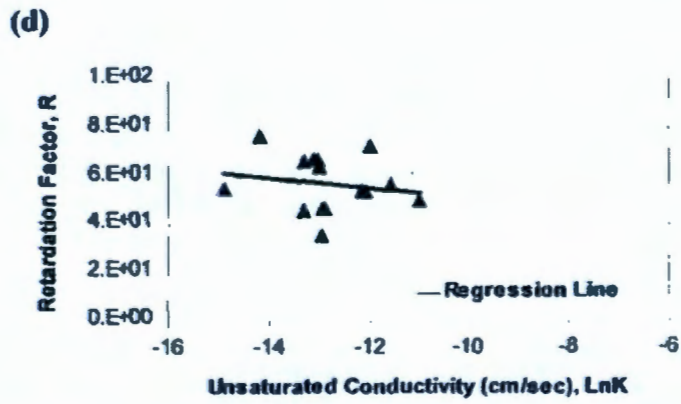


Figure 15. LnK versus R for (a) Cs-137, (b) Sr-90, (c) U, and (d) Se for the gravel-dominated sequence.

4.0 UNCERTAINTIES IN MODEL PREDICTIONS

As discussed in the preceding sections, the application of stochastic theory resulted in effective (upscaled) parameter estimates for saturated hydraulic conductivity, soil moisture retention and unsaturated hydraulic conductivity, bulk density, unretarded macrodispersivity and sorption-enhanced macrodispersivity. These parameters will serve as input to VAM3DF (Huyakorn and Panday 1995), a variably saturated flow and transport code; VAM3DF will generate 'mean' solutions for the pressure head and contaminant concentration.

The breakthrough curve due to contaminants released from the disposal facility is expected to appear as a "step" function at the water table, with the shape of the rise of the step function primarily governed by vadose zone heterogeneity, macrodispersivity, sorption, and radionuclide decay. Because of the long release time for the contaminants from the disposal facility, compared to the travel time through the vadose zone, it is reasonable to approximate the contaminant release as a step input function.

Three sources contribute to uncertainty calculations: (a) variations in model configurations, (b) uncertainties *in* the calculated mean concentration distribution at the water table, and (c) uncertainties *around* the calculated mean concentration distribution at the water table. Figure 16 illustrates the expected concentration distribution at the water table. The sigmoid-shaped mean concentration distribution (Figure 16) is calculated by VAM3DF, based on a particular conceptual model configuration and sensitivities to effective input parameters. However, the mean solution should be viewed as being an average of many 'realizations.' In other words, the expected peak concentration is not necessarily the calculated mean concentration (Figure 16). There is variation among different realizations, because of vadose zone heterogeneities. The variance (σ_c^2) about the mean characterizes such variation *around* a particular mean solution. While the uncertainties *in* the mean solution are calculated directly by VAM3DF, uncertainties *around* the calculated mean solution will be estimated based on available stochastic solutions, as described later.

4.1 Model Configurations

4.1.1 Variations in Stratigraphy

At this time, a basic layered geologic model is being postulated for VAM3DF base case calculations. Such a model is based on the most recent geologic information (Reidel et al. 1998; Kincaid et al. 1995) available on the stratigraphy at the two sites. Dips and inclines (as identified in the geology data package) of the various strata will be considered as part of variations of base case model configurations for both disposal sites. Such variations of the basic stratigraphic cross-sections at the two sites are part of the geology data package.

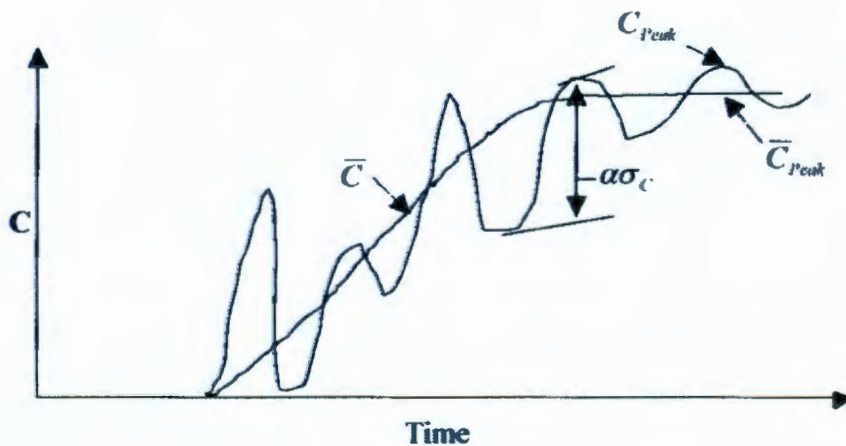


Figure 16. Schematic of concentration (C) distribution at the water table.

[\bar{C} = calculated mean concentration, \bar{C}_{peak} = calculated mean peak concentration, C_{peak} = peak concentration, σ_c = standard deviation of variation around the calculated mean solution, $\alpha\sigma_c$ = multiple of variation around the calculated mean solution for a particular model configuration and input effective parameters.]

4.1.2 Clastic dikes

Clastic dikes are ubiquitous sedimentary structures observed in outcrops and trenches that expose the Hanford formation in the 200 Areas. Their distribution, orientation, and other important characteristics are provided as part of the geology data package. The dikes are believed to represent dewatering structures that developed during compaction and settling of cataclysmic flood deposits during or soon after floodwaters drained from the Pasco Basin. The true nature and extent of clastic dikes are difficult to determine, because the dikes are rarely detected or observed in vertically oriented boreholes. Often they form a polygonal pattern where they intersect the ground surface.

An extensive atlas developed by Fecht et al. (1999)⁴ addresses a subset of dikes (i.e., clastic injection dikes) that have been formed as a result of sediments in fissures. Clastic injection dikes are fissures which may total a meter or more in thickness. These dikes are typically filled with poor to well-sorted sand, but may also contain silt, clay, and gravel.

⁴ Fecht, K.R., K.A. Lindsey, B.N. Bjornstad, D.G. Horton, G.V. Last, and S.P. Reidel. 1999. Clastic Injection Dikes of the Pasco Basin and Vicinity. BIII-01103 Rev. 0. July, 1999. Bechtel Hanford Inc. Richland, WA.

These dikes are of particular interest to the ILAW PA because they occur as near-vertical tabular bodies filled with multiple layers of unconsolidated sediments. Thin clay/silt linings separate the margins of most dikes and internal layers within dikes.

It is important to develop an understanding of the potential presence of these discrete structures in the vicinity of disposal sites such that uncertainties in flow and transport calculations can be adequately accounted for. Such an understanding on the presence of clastic dike networks in the vicinity of disposal sites will be provided as part of the geology data package. The potential for clastic injection dikes to provide preferential pathways will be examined as part of variations of model configurations at both disposal sites.

One particular scenario will be considered to provide a bounding estimate: presence of a near-vertical (or otherwise as characterized in geology data package) clastic dike directly below a vault and extending through the Hanford formation (or as identified in the geology data package). The width of the dike will be based on information in the geology data package.

Data on physical and hydraulic parameters are needed for clastic dike infilling materials to model their effects on flow and contaminant transport. Such physical and hydrologic properties (e.g., bulk density, particle-size distribution, moisture retention, saturated and unsaturated hydraulic conductivities) for clastic dike infilling materials are included in Fayer and Ritter (1999)⁵. A summary of the physical and hydraulic parameters is given in Table 10. As suggested in Table 10, the measured properties represent fine material. Other database (e.g., Fecht et al. 1998) will be consulted for possible presence of coarse infilling materials in a clastic dike.

Table 10. Van Genuchten parameters (based on the multistep method), saturated hydraulic conductivity, and bulk density for seven clastic dike samples (after Fayer and Ritter 1999).

Sample	θ_s (cm ³ /cm ³)	θ_r (cm ³ /cm ³)	α (1/cm)	n (-)	Saturated Hydraulic Conductivity (cm/s)	Bulk Density (g/cm ³)
1	0.424	0.063	0.0839	1.33	5.97E-04	1.57
2A	0.446	0.019	0.0762	1.98	4.70E-03	1.50
2B	0.443	0.023	0.0741	1.84	3.14E-03	1.51
3A	0.424	0.025	0.0143	2.49	3.41E-03	1.46
3B	0.448	0.050	0.0593	1.54	1.14E-03	1.52
4A	0.454	0.030	0.0092	1.97	1.84E-03	1.49
4B	0.425	0.021	0.0823	2.09	5.43E-03	1.57

⁵ Fayer M.J. and J.S. Ritter. 1999. Physical and hydraulic measurements of FY 1998 clastic dike samples. Letter Report to Fluor Daniel Northwest, Inc. March, 1999. Pacific Northwest National Laboratory. Richland, WA.

4.1.3 Isotropy

The base case simulations will consider a layer-cake stratigraphy and tension-dependent anisotropy. This is expected to result in more of lateral than vertical migration of contaminants. A variation of the base case will consider an isotropic case. This is expected to result in enhanced vertical migration, compared to the base case.

4.1.4 Sloped Layering

Another case that will be considered has to do with the combined effects of variation in stratigraphy and anisotropy. For unsaturated flow, the degree of anisotropy depends not only on the variability of soil hydraulic properties, but also on the orientation of the soil layers relative to the mean hydraulic gradient. The tension-dependent anisotropy relationships will be reevaluated for dips and inclines identified (in geology data package) for variations in base case stratigraphy, and their effects examined via VAM3DF simulations.

4.2 Uncertainties in the Mean Solution due to Variations of Effective Parameter Estimates

As mentioned earlier, uncertainties in the mean solution are due to variations in conceptual model configuration and sensitivities to effective input parameters. Variations in conceptual model configuration have been discussed in the preceding section. Sensitivities to effective input parameter variations are discussed in this section.

The sensitivity of the model predictions to uncertainties in the effective parameters will be considered for two important parameters, i.e., unsaturated conductivity and macrodispersivity. Sensitivity of these two effective parameters and their estimated effects on the mean solution are discussed below. Note that variations in saturated conductivity will not be considered, since the moisture regime within the far-field vadose zone for the disposal sites is not expected to be at or near saturation. It should also be noted that recharge and variations in recharge estimates are another source of uncertainty. However, sensitivities to recharge estimates will be propagated via changes in effective parameter estimates for unsaturated conductivity and macrodispersivity.

The stratigraphy at both disposal sites is dominated by two distinctly different sediment sequences. The upper part of the vadose zone is characterized by a sandy sequence, whereas the lower part is characterized primarily by a gravel sequence. At saturation, compared to the gravel-dominated sequence, the sand-dominated sequence is described by a smaller log-conductivity variance. However, compared to the gravel-dominated sequence, the log-unsaturated conductivity variance for the sand-dominated sequence is higher. The variations in unsaturated conductivities for both sandy and gravelly sequences are discussed in detail earlier. Variabilities in unsaturated conductivities lead to macroscopic anisotropy relations for the sandy and gravelly

sediments that are quite different. Consequently, VAM3DF simulations incorporating variations in macroscopic anisotropy relations will produce different mean concentration distributions at the water table.

A much more important parameter that will affect mean concentration distribution, for a given model configuration, is macrodispersivity. Typically, in modeling transport, the same unretarded dispersivity value is assumed for all transported (retarded and unretarded) species. VAM3DF simulations will consider, for the transported species, comparisons of enhanced longitudinal macrodispersivity with that of a nonretarded macrodispersivity. The variability in these estimates, along with professional judgement (e.g., an increase or decrease of 25% of estimated macrodispersivities), will be used to quantify uncertainties in the mean solution.

Note that each VAM3DF-calculated mean solution incorporates effects due to model configuration variations and sensitivities to effective input parameter variations. The goal will be to limit the number of VAM3DF runs. Nevertheless, once the mean solutions are obtained for various VAM3DF runs, they can be used to obtain variance estimates for the mean solutions, and therefore characterize the uncertainty in the mean solutions.

4.3 Uncertainties Around the Mean Solution

As described earlier, since the effective concentration predictions represent a mean solution, fluctuations about this mean, due to heterogeneity, are another source of uncertainty. The variations in concentrations around the mean concentration can be characterized through a stochastic evaluation of the concentration variance. It will be assumed that the developed theory for the nonretarded species is applicable to the case with spatially variable sorption, provided that the enhanced macrodispersivity is used for the sorbing species. The concentration variance tends to be large in regions close to the source where concentration gradients are large. Using stochastic approaches described by Kapoor and Gelhar (1994a,b), the coefficient of variation of concentration will be estimated at the water table. Detailed equations are presented in Kapoor and Gelhar, but briefly the concentration variance is directly proportional to the mean concentration gradient for the VAM3DF-calculated mean concentration distribution at the water table and the longitudinal macrodispersivity, and inversely proportional to the local dispersivity values.

4.4 Bounding Estimates

Note that the cumulative effect of uncertainties is not additive. Rather, bounding scenarios will be based on combinations of various worst case conditions. For example, a bounding scenario may be postulated as the one having isotropic material properties for both sand- and gravel-dominated sequences, high recharge, clastic dike, and minimum values of macrodispersivity. In other words, bounding estimates will be dictated by

selected model configuration and effective parameter estimates that produce a higher mean concentration at the water table.

5.0 REFERENCES

- Bacon, D. J. and B. P. McGrail. 1997. Source Term Analysis for Hanford Low-Activity Tank Waste Using the STORM Code: A Coupled Unsaturated Flow and Transport Model, in *Symposium on Science and Technology for Disposal of Radioactive Tank Wastes*, ed. N.J. Lombardo and W.W. Schulz. Plenum Publishing. Las Vegas, NV.
- Bear, J., C. Braester and P. C. Menier. 1987. Effective and relative permeabilities of anisotropic porous media. *Transport in Porous Media* 2: 301-316.
- Dagan, G. 1984. Solute transport in heterogeneous porous formations. *J. Fluid Mech.* 145:151-157.
- Eching S. O, and J. W. Hopmans. 1993. Optimization of hydraulic functions from transient outflow and soil water pressure data. *Soil Sci. Soc. Am. J.* 57:1167-1175.
- Freeze, R. A. and J. A. Cherry. 1979. *Groundwater*. Prentice-Hall, Inc., Englewood Cliffs, NJ.
- Garabedian, S. P., D. R. LeBlanc, L. W. Gelhar, and M. A. Celia, Large-scale Natural-gradient Tracer Test in Sand and Gravel, Cape Cod, Massachusetts: 2, Analysis of Tracer Moments for a Nonreactive Tracer, *Water Resources Research*, 27(5), 911-924, 1991.
- Gardner, W. H. 1986. Water Content, in *Methods of Soils Analysis, Part I*, edited by A. Klute, pp. 493-544. Amer. Soc. of Agron. Madison, Wisc.
- Gardner, W. R. 1958. Some steady-state solutions of the unsaturated moisture flow equation with applications to evaporation from a water table. *Soil Sci.* 85:228-232.
- Gelhar, L. W., M. A. Celia and D. McLaughlin. 1994. *Modeling Field Scale Unsaturated Flow and Transport Processes*. NUREG/CR-5965. Nuclear Regulatory Commission, Washington, D.C.
- Gelhar, L. W., C. Welty, and K. R. Rehfeldt. 1992. A critical review of data on field-scale dispersion in aquifers. *Water Resour. Res.* 28:1955-1974.
- Gelhar, L. W. 1993. *Stochastic Subsurface Hydrology*, Prentice Hall, New York.
- Gelhar, L. W. and C. L. Axness. 1983. Three-dimensional analysis of macrodispersion in a stratified aquifer. *Water Resour. Res.* 19:161-180.

- Green, T. R. and D. L. Freyberg. 1995. State-dependent anisotropy: comparisons of quasi-analytical solutions with stochastic results for steady gravity drainage. *Water Resour. Res.* 31:2201-2212.
- Hills, R. G., P. J. Wierenga, D. B. Hudson, and M. R. Kirkland. 1991. The second Las Cruces Trench experiment: experimental results and two-dimensional flow predictions. *Water Resour. Res.* 27:2707-2718.
- Huyakorn, P. S. and S. Panday. 1995. VAM3DF - A Variably Saturated Analysis Model in Three Dimensions for the Data Fusion System. HydroGeoLogic, Inc. Herndon, VA.
- Huyakorn, P. S. and G. F. Pinder. 1983. *Computational Methods in Subsurface Flow*. Academic Press, NY.
- Kaplan, D. I., K. E. Parker and I. V. Kutynakov. 1998. Radionuclide Distribution Coefficients for Sediments Collected from Borehole 299-E17-21: Final Report for Subtask 1a. PNNL-11966. Pacific Northwest National Laboratory. Richland, WA.
- Kapoor, V. and L. W. Gelhar. 1994a. Transport in three-dimensionally heterogeneous aquifers 1. Dynamics of concentration fluctuations. *Water Resour. Res.* 30:1775-1788.
- Kapoor, V. and L. W. Gelhar. 1994b. Transport in three-dimensionally heterogeneous aquifers 2. Predictions and observations of concentration fluctuations. *Water Resour. Res.* 30:1789-1801.
- Khaleel, R. and J. F. Relyea. 1997. Correcting laboratory-measured moisture retention data for gravels. *Water Resour. Res.* 33:1875-1878.
- Khaleel, R., J. F. Relyea and J. L. Conca. 1995. Evaluation of van Genuchten-Mualem relationships to estimate unsaturated conductivity at low water contents. *Water Resour. Res.* 31:2659-2668.
- Khaleel, R. and E. J. Freeman. 1995a. *Variability and Scaling of Hydraulic Properties for 200 Area Soils, Hanford Site*. WHC-EP-0883. Westinghouse Hanford Company. Richland, Washington.
- Khaleel, R. and E. J. Freeman. 1995b. *A Compilation of Hydrologic Properties for Low-Level Tank Waste Disposal Facility Performance Assessment*. WHC-SD-WM-RPT-165, Rev. 0. Westinghouse Hanford Company. Richland, Washington.
- Kincaid, C. T., J. W. Shade, G. A. Whyatt, M. G. Piepho, K. Rhoads, J. A. Voogd, J. H. Westsik, Jr., M. D. Freshley, K. A. Blanchard, B. G. Lauzon. 1995. Performance

Assessment of Grouted Double-Shell Tank Waste Disposal at Hanford, WHC-SD-WM-EE-004, Rev. 1, Westinghouse Hanford Company. Richland, WA.

- Klute, A. 1986. Water Retention: Laboratory Methods, in *Methods of Soils Analysis, Part I*, edited by A. Klute, pp. 635-660. Amer. Soc. of Agron. Madison, Wisc.
- Klute, A. and C. Dirksen. 1986. Hydraulic Conductivity and Diffusivity: Laboratory methods, in *Methods of Soils Analysis, Part I*, edited by A. Klute, pp. 687-734. Amer. Soc. of Agron. Madison, WI.
- Kool, J. B., J. C. Parker, and M. T. van Genuchten. 1985a. Determining soil hydraulic properties from one-step outflow experiments by parameter estimation, I, Theory and numerical studies. *Soil Sci. Soc. Am. J.* 49:1348-1354.
- Kool, J. B., J. C. Parker, and M. T. van Genuchten. 1985b. Determining soil hydraulic properties from one-step outflow experiments by parameter estimation, II, Experimental studies. *Soil Sci. Soc. Am. J.* 49:1354-1359.
- Mann, F. M., R. P. Puigh, II, P.D. Rittmann, N. W. Kline, J. A. Voogd, , Y. Chen, C. R. Eiholzer, C. T. Kincaid, B. P. McGrail, A. H. Lu, G. F. Williamson, N. R. Brown and P. E. LaMont. 1998. *Hanford Immobilized Low-Activity Tank Waste Performance Assessment*. DOE/RL-97-69, Rev.0, U.S. Department of Energy, Richland, WA.
- Mantoglou, A. and L. W. Gelhar. 1987. Stochastic modeling of large-scale transient unsaturated flow. *Water Resour. Res.* 23:37-46.
- Mantoglou, A. and L. W. Gelhar. 1985. Large scale models of transient unsaturated flow and contaminant transport using stochastic methods. Ralph M. Parsons Laboratory Tech. Rpt. 299. Massachusetts Institute of Technology. Cambridge, MA.
- McCord, J. T., D. B. Stephens and J. L. Wilson. 1991. Hysteresis and state-dependent anisotropy in modelling unsaturated hillslope hydrologic processes. *Water Resour. Res.* 27:1501-1518.
- McGrail, B. P., W.L. Ebert, D.H. Bacon, and D. M. Strachan. 1998. A Strategy to Conduct an Analysis of the long-term Performance of Low-Activity Waste Glass in a Shallow Subsurface Disposal System at Hanford. PNNL-11834. Pacific Northwest National Laboratory. Richland, WA.
- Millington, R. J. and J. P. Quirk. 1961. Permeability of Porous Solids. *Trans. Faraday Soc.* 57:1200-1207.
- Mualem, Y. 1984. Anisotropy of unsaturated soils. *Soil Sci. Soc. Am. J.* 48:505-509.

- Mualem, Y. 1976. A new model for predicting the hydraulic conductivity of unsaturated porous media. *Water Resour. Res.* 12:513-522.
- Phillips, F., J. Mattick, T. Duval, D. Elmore, and P. Kubik. 1988. Chlorine 36 and tritium from nuclear weapons fallout as tracers for long-term liquid and vapor movement in desert soils. *Water Resour. Res.* 24:1877-1891.
- Polmann, D. J. 1990. Application of Stochastic Methods to Transient Flow and Transport in Heterogeneous Unsaturated Soils. Ph.D. Thesis. Massachusetts Institute of Technology. Cambridge, MA.
- Reidel, S. P. and D. G. Horton. 1999. Geologic Data Package for 2001 Immobilized Low-Activity Waste Performance Assessment. PNNL-12257, Rev. 1. Pacific Northwest National Laboratory. Richland, WA.
- Reidel, S. P., K. D. Reynolds and D. G. Horton. 1998. Immobilized Low-Activity Waste Borehole 299-E17-21. PNNL-11957. Pacific Northwest National Laboratory. Richland, WA.
- Russo, D. 1993. Stochastic modeling of macrodispersion for solute transport in a heterogeneous unsaturated porous formation. *Water Resour. Res.* 29:383-397.
- Scanlon, B. R. 1992. Evaluation of liquid and vapor water flow in desert soils based on chlorine 36 and tritium tracers and nonisothermal flow simulations. *Water Resour. Res.* 28:285-297.
- Sisson, J. B. and A. H. Lu. 1984. *Field Calibration of Computer Models for Application to Buried Liquid Discharges: A Status Report*. RHO-ST-46P. Rockwell Hanford Operations, Richland, WA.
- Stephens, D. B. and S. Heermann. 1988. Dependence of anisotropy on saturation in a stratified sand. *Water Resour. Res.* 24:770-778.
- Talbott, M. E. and L. W. Gelhar, *Performance Assessment of a Hypothetical Low-Level Waste Facility: Groundwater Flow and Transport Simulation*, NUREG/CR-6114 Vol. 3, U.S. Nuclear Regulatory Commission, Washington, D.C., 1994.
- van Genuchten, M. Th. 1980. A closed-form solution for predicting the conductivity of unsaturated soils. *Soil Sci. Soc. Am. J.* 44:892-898.
- van Genuchten, M. Th., F. J. Leij, and S. R. Yates. 1991. *The RETC code for quantifying the hydraulic functions of unsaturated soils*. U.S. E.P.A., EPA/600/2-91/065.
- Wierenga, P. J., R. G. Hills, and D. B. Hudson. 1991. The Las Cruces Trench site: Characterization, experimental results, and one-dimensional flow predictions. *Water Resour. Res.* 27:2695-2706.

- Yeh, T.-C. J. and D. J. Harvey. 1990. Effective unsaturated hydraulic conductivity of layered sands. *Water Resour. Res.* 26:1271-1279.
- Yeh, T.-C. J., L. W. Gelhar and A. L. Gutjahr. 1985a. Stochastic analysis of unsaturated flow in heterogeneous soils, 1. statistically isotropic media. *Water Resour. Res.* 21:447-456.
- Yeh, T.-C. J., L. W. Gelhar and A. L. Gutjahr. 1985b. Stochastic analysis of unsaturated flow in heterogeneous soils, 2. statistically anisotropic media with variable α . *Water Resour. Res.* 21:457-464.
- Yeh, T.-C. J., L. W. Gelhar and A. L. Gutjahr. 1985c. Stochastic analysis of unsaturated flow in heterogeneous media, 3. observations and applications. *Water Resour. Res.* 21:465-471.

6.0 PEER REVIEW

Practice 134 298 1112
 Publication Date 22Nov99
 Attachment 02 - Sheet 1 of 1

FLUOR DANIEL NORTHWEST

TECHNICAL PEER REVIEWS

CHECKLIST FOR TECHNICAL PEER REVIEW

Document Reviewed: FAR-FIELD HYDROLOGY DATA PACKAGE FOR IMMOBILIZED
 Title: LOW-ACTIVITY TANK WASTE PERFORMANCE ASSESSMENT
 Author: RAZ KHALEEL
 Date: DECEMBER 3, 1999
 Scope of Review:

Yes No NA

- ** Previous reviews complete and cover analysis, up to scope of this review, with no gaps.
- Problem completely defined.
- Accident scenarios developed in a clear and logical manner.
- Necessary assumptions explicitly stated and supported.
- Computer codes and data files documented.
- Data used in calculations explicitly stated in document.
- Data checked for consistency with original source information as applicable.
- Mathematical derivations checked including dimensional consistency of results.
- Models appropriate and used within range of validity, or use outside range of established validity justified.
- Hand calculations checked for errors. Spreadsheet results should be treated exactly the same as hand calculations.
- Software input correct and consistent with document reviewed.
- Software output consistent with input and with results reported in document reviewed.
- Limits/criteria/guidelines applied to analysis results are appropriate and referenced.
- Limits/criteria/guidelines checked against references.
- Safety margins consistent with good engineering practices.
- Conclusions consistent with analytical results and applicable limits.
- Results and conclusions address all points required in the problem statement.
- Format consistent with applicable guides or other standards.
- ** Review calculations, comments, and/or notes are attached.
- Document approved (for example, the reviewer affirms the technical accuracy of the document).

Eugene Freeman 
 Reviewer (printed name and signature)

December 3, 1999
 Date

- * All "no" responses must be explained below or on an additional sheet.
- ** Any calculations, comments, or notes generated as part of this review should be signed, dated, and attached to this checklist. The material should be labeled and recorded in such a manner as to be intelligible to a technically qualified third party.

APPENDIX A

**Physical and Hydraulic Measurements of FY1998 Borehole
Cores**

Physical and Hydraulic Measurements of FY 1998 Borehole Cores

MJ Fayer, AL Ward, JS Ritter, and RE Clayton
10 September 1998

Introduction

Pacific Northwest National Laboratory (PNNL) assists the Lockheed Martin Hanford Company (LMHC) in designing and assessing the performance of disposal facilities for radioactive wastes stored in single and double shell tanks at the Hanford Site. The preferred method of disposing of the portion that is classified as immobilized low-activity waste (ILAW) is to vitrify the waste and place the product in a near-surface, shallow-land burial facility. The current plans are that some of the ILAW will be placed in the existing vaults (built by the former Grout Project); the majority will be placed in the ILAW Disposal Site, to be located southwest of the PUREX Plant. The LMHC project to assess the performance of these two disposal facilities is known as the Hanford ILAW Performance Assessment (PA) Activity, hereafter called the ILAW PA.

Regulatory and public acceptance of ILAW disposal at Hanford depends on demonstrating that public health and the environment are adequately protected. This goal is achieved by predicting contaminant migration from the facility and using the predictions to calculate the impacts to public health and the environment. To predict contaminant migration requires estimates of the physical and hydraulic properties of sediments within the vadose zone beneath and around the disposal facility. These properties include water retention and hydraulic conductivity of the major sediment types as well as descriptions of their spatial variability. In addition to supporting the PA, these data and parameters can be used to support remediation and closure activities at sites such as tank farms and specific retention basins that have similar geology.

As part of site characterization activity for the ILAW disposal facility, sediment samples were obtained in fiscal year 1998 via a borehole drilling and sampling program (Reidel and Reynolds 1998). A work plan was also prepared that provides details on the measurement and analysis of the hydraulic properties for the ILAW borehole sediment samples (Khaleel 1998)¹.

As part of the work plan, a PNNL task was initiated, entitled "Hydraulic Property Lab Tests for ILAW Samples." The objective of this task is to provide the measured data for various geologic formations and soil types at the disposal sites (LMHC 1997; Reidel and Reynolds 1998). These data will provide the basis for upscaling of laboratory data to field estimates (Khaleel 1998), which will be used to predict the movement of contaminants from the disposal

¹ Khaleel R, January 1998. "Work plan for measurement and analysis of hydraulic properties for clastic dikes and the ILAW Borehole No. 1 sediment samples," Fluor Daniel Northwest, Inc., P.O. Box 1050, Richland, Washington.

facility to the groundwater. The objective of this letter report is to document the physical and hydraulic properties for the first characterization borehole.

Properties

Physical and hydraulic properties are required for each of the major geologic materials identified by Reidel and Reynolds (1998), namely, the Hanford sandy sequence, the Hanford lower gravel, and the Ringold Unit E. Multiple measurements of these properties are required to give some estimate of the degree of variability within each geologic material. The properties, which are required (directly or indirectly) by the models used for the ILAW PA, are:

Particle Size Distribution. Particle size distribution (PSD) refers to the fractions of the various particle-size classes (e.g., the fraction of particles with diameters between 1 and 2 mm).

Particle Density (ρ_p). Particle density is the mass of the sediment or construction material particles per unit volume of the same sediment or material. This property is used to relate the bulk density to the porosity.

Bulk Density (ρ_b). Bulk density is the mass of oven-dry material per unit bulk volume. The unit bulk volume is the combined volume of material, water, and air prior to oven drying.

Porosity (ϕ). Porosity is the volume of voids per unit bulk volume.

Water Retention. Water retention refers to the retention of water by the sediment at various matric potentials. Mathematical functions are fit to the retention data and the resulting parameters are used directly in computer models for predicting water and contaminant movement. Numerous functions are available, but the van Genuchten function is most commonly used:

$$\theta = \theta_r + (\theta_s - \theta_r) \left[1 + (\alpha h)^n \right]^{-m}$$

where θ_s = saturated water content (cm^3/cm^3)

θ_r = residual water content (cm^3/cm^3)

h = matric potential (-cm)

α, n, m = empirical fitting parameters (α units are $1/\text{cm}$; n and m are dimensionless)

Typically, m is approximated as $m = 1 - 1/n$

Saturated Hydraulic Conductivity (K_s). Saturated hydraulic conductivity is the proportionality constant in the Darcy equation that relates the flux density to a unit potential gradient.

Unsaturated Hydraulic Conductivity [$K = f(\theta, \psi)$]. Unsaturated hydraulic conductivity is the proportionality factor in the Richards equation that relates the flux density to a unit potential gradient at a specific water content. Because the water content varies in the unsaturated zone, the unsaturated conductivity varies also.

Mathematical functions are used to represent the unsaturated conductivity data; these functions are typically estimated using the water retention functions and saturated conductivity. When measured unsaturated conductivity values are available, the conductivity and retention data can be fit to optimize both the retention and conductivity functions. Several functions are available, but the Mualem conductivity function is most commonly used (in conjunction with the van Genuchten retention function, assuming $m = 1 - 1/n$):

$$K = K_s \frac{\left\{ 1 - (\alpha h)^{n-1} [1 + (\alpha h)^n]^{-m} \right\}^2}{[1 + (\alpha h)^n]^{2m}}$$

The K_s value and the pore interaction term (ℓ) are the only requirements for this model. The parameter ℓ is typically assigned a value of 0.5.

Borehole Cores

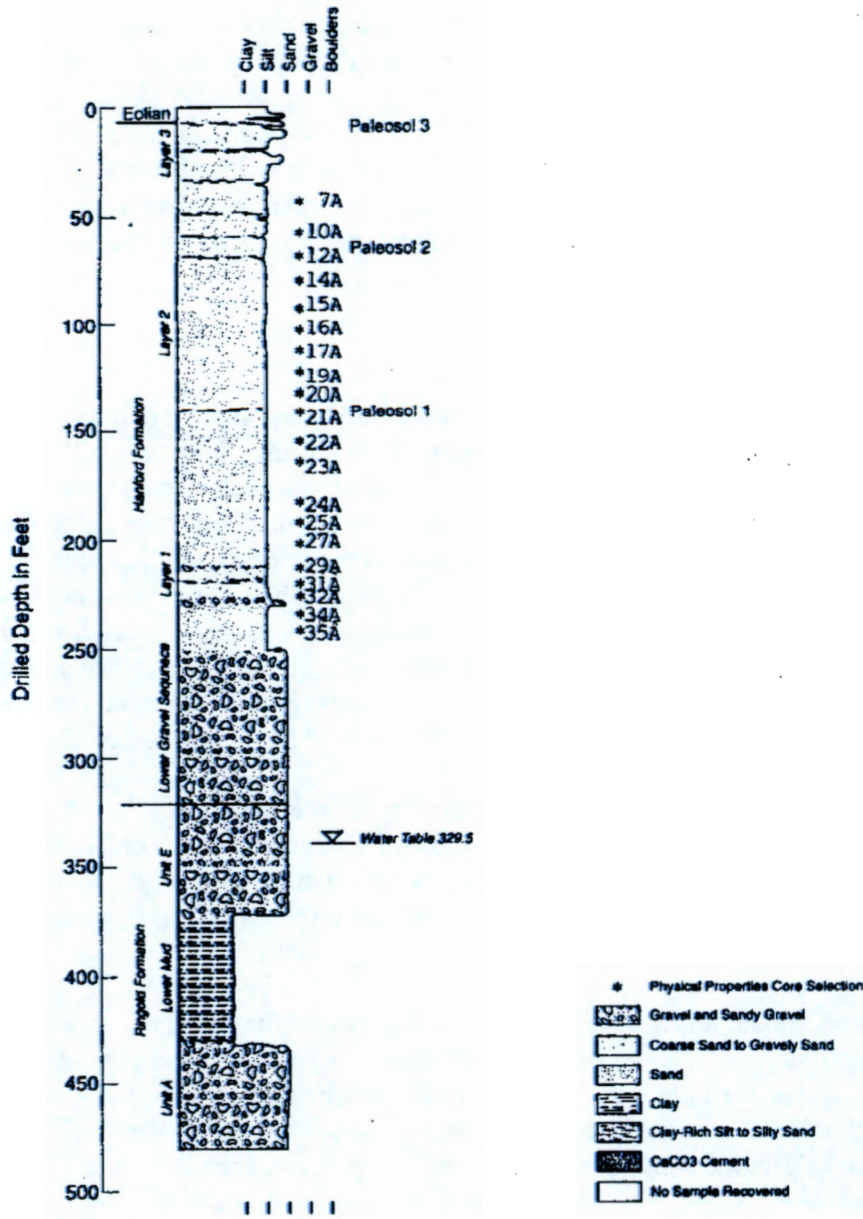
The FY 1998 borehole was drilled in the spring of 1998 (Reidel et al. 1998). A total of 45 cores were collected in liners. Thirty of the 45 liners had a 8.26-cm (3.25-inch) internal diameter and came from depths between 45 and 175 ft. The remaining fifteen liners had a 9.53-cm (3.75-inch) internal diameter and came from depths between 175 and 242 ft. All of the sediment from the depth interval from 0 to 45 ft went to the tracer task for tracer-specific analyses. The decision was made that undisturbed cores from this interval were not necessary for hydraulic property measurements because these sediments will not exist in their current state once the disposal facility is built. No vadose zone cores were collected below 242 ft. because this zone was open framework gravel (i.e., gravel that supports itself with little to no finer grained material) and could not be sampled with the method used.

PNNL was requested to analyze twenty of the FY 98 borehole cores for hydraulic and physical properties. Each of the 45 liners was inspected to verify whether a 15-cm (6-inch) long undisturbed section could be obtained. Thirteen liners did not meet this requirement because they were either incompletely filled, the sediments were disturbed, or the liner material was damaged. These liners will be stored for possible future testing. Of the remaining 32 acceptable liners, twenty liners were chosen for testing by the FDNW principal investigator for the ILAW PA far-field hydrology task, in consultation with the PNNL principal investigator. These twenty liners were chosen on the basis of providing somewhat evenly spaced coverage of the sampled vadose zone. Table 1 lists the sample numbers, depths, and diameters. Figure 1 shows the location of the liners relative to the geologic cross-section derived from the borehole data.

Table 1. Liner samples analyzed for the first characterization borehole

Sample ID	Total Depth Interval ft	Internal Diameter in.	Depth Interval of Intact Core ft
B8500-07A	45.9 to 47.9	3.25	46.3 to 46.8
B8500-10A	57.8 to 59.8	3.25	58.0 to 58.5
B8500-12A	69.4 to 70.95	3.25	69.8 to 70.3
B8500-14A	80.3 to 82.8	3.25	80.8 to 81.3
B8500-15A	90.5 to 93.0	3.25	90.8 to 91.3
B8500-16A	100.5 to 103.0	3.25	102.0 to 102.5
B8500-17A	109.8 to 112.2	3.25	111.3 to 111.8
B8500-19A	121.0 to 123.5	3.25	122.6 to 123.1
B8500-20A	129.7 to 132.0	3.25	131.1 to 131.6
B8500-21A	141.5 to 144.0	3.25	141.8 to 142.3
B8500-22A	151.9 to 154.4	3.25	153.7 to 154.2
B8500-23A	160.4 to 162.9	3.25	162.1 to 162.6
B8500-24A	180.7 to 182.7	3.75	181.9 to 182.4
B8500-25A	189.7 to 191.7	3.75	190.9 to 191.4
B8500-27A	199.3 to 201.3	3.75	200.5 to 200.9
B8500-29A	209.4 to 211.4	3.75	210.6 to 211.1
B8500-31A	219.6 to 221.6	3.75	220.9 to 221.3
B8500-32A	226.1 to 228.1	3.75	227.4 to 227.9
B8500-34A	236.1 to 238.1	3.75	237.2 to 237.7
B8500-35A	239.5 to 241.5	3.75	240.7 to 241.2

Figure 1. Geologic cross section of the disposal site based on the borehole samples (after Reidel et al. 1998).



Methods

Two types of subsamples were removed from each liner. One subsample was an intact portion of the liner that retained its undisturbed nature. This intact core was used for the unsaturated conductivity tests and for determining bulk density and porosity. The depth intervals of these intact cores are listed in Table 1. A second subsample was taken from a 4 to 5 inch portion of the liner next to the intact core. This loose material, which ranged from 850 to 1200 g, was placed in a sealed bag and mixed thoroughly. It was used for the tests of particle size distribution, particle density, initial water content, and water retention using pressure plates and vapor adsorption, as well as the sorption tests that were conducted by another task under this project.

Intact Core Preparation

Each 0.6-m-long liner was inspected to identify portions that displayed no visible disturbance such as cracking or mixing. Within the undisturbed portion, a 15-cm length was chosen for the unsaturated conductivity test. The liner was marked where the base plate would go. A band saw was used to cut most of the way through the liner, then a thin metal plate was advanced into the cut as the blade proceeded around the liner for the final cut. This technique kept sediment loss to a minimum. When completely cut, the sample was placed vertically upside down and the bottom end cap was attached². The sample was then placed horizontally, marked, and cut in the same manner as before. The sample was then placed vertically upright and the upper end cap was attached. The entire assembly was weighed. The total internal volume of the 3.25-in diameter cores was 803 cm³; it was 1,069 cm³ for the 3.75-in diameter core.

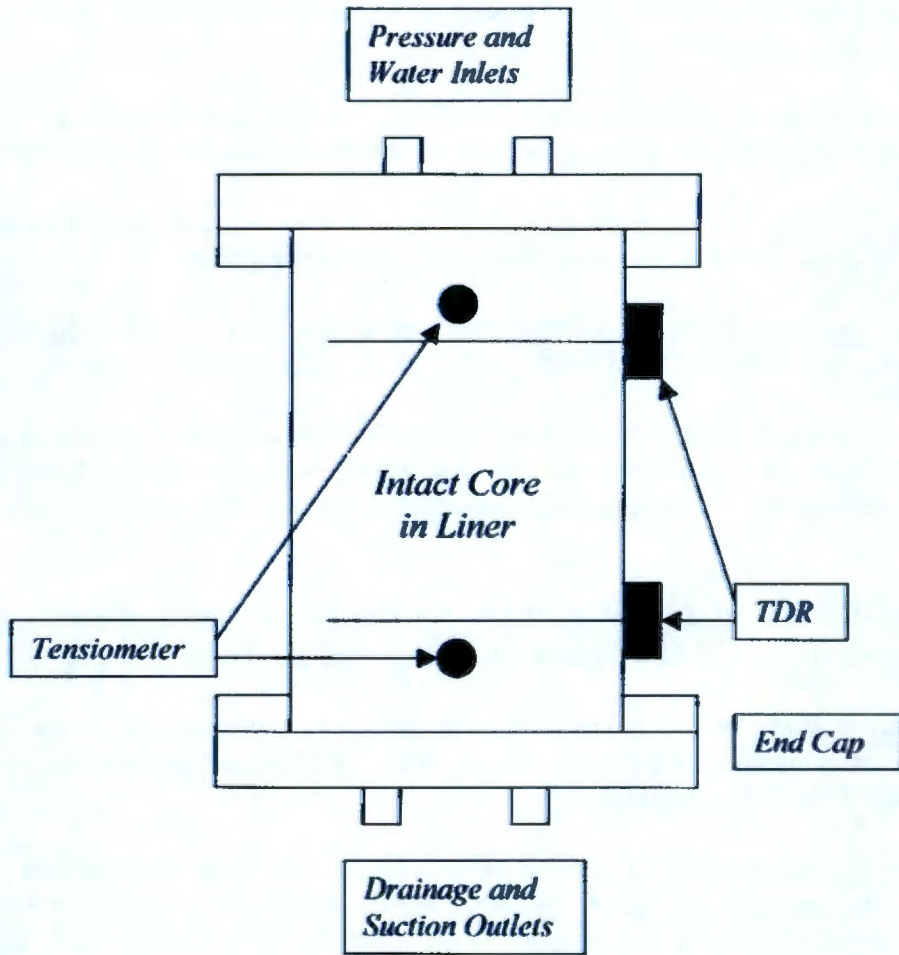
Two holes were drilled horizontally into the liner and tapped to yield threads for the tensiometer assemblies. The holes were positioned 1.5 cm from each end plate. Each tensiometer was 0.62 cm in diameter and 6.4 cm long, which allowed the tensiometers to penetrate about 75% of the core diameter. The sediment was fairly soft so each tensiometer was pushed directly into the sample without removing any material.

Two additional holes were drilled horizontally into the liners to accommodate the time-domain reflectometry (TDR) probes. The holes were offset 90 degrees laterally from the tensiometers and about 1 cm from the plane of the tensiometers and towards the core center. Because of the thinness of the liner, plexiglass blocks were glued to the outside of the liner in the TDR location to provide enough material to tap and provide threads for the TDR assemblies. The TDR rods were 0.23 cm in diameter and 8 cm long, which allowed the TDR rods to penetrate about 95% of the core diameter. Like the tensiometers, the TDR rods were pushed directly into the samples without removing material.

Figure 2 shows the final assembly with tensiometers, TDR rods, end plates, and two ports on either end plates to facility liquid and gas addition or removal from the core. Each assembly was tested at 0.5 bar positive pressure to identify leaks prior to conducting the conductivity tests.

² End caps were purchased from Soil Measurements Systems of Tucson, Arizona. Each end cap contained a rubber gasket and rubber O-ring to ensure a tight seal with the core liner.

Figure 2. Conductivity testing cell



Leaks were eliminated using Teflon™ tape, vacuum grease, and Silly Putty™. After leak testing, a vacuum was applied to one of the upper ports of each assembly. The entire assembly was then wetted from below using a solution comprising tap water and 5 g thymol per 20 L of water for control of bacterial growth. Wetting in this manner placed the samples on the primary drainage path.

Procedures

Table 2 lists the procedures used to analyze the samples. Additional details for each procedure are discussed below.

Particle Density. Two replicates of the particle density test were performed using 30 g of the loose subsample for each test using the pycnometer method (Blake and Hartge 1986a).

Initial Water Content. Two replicate measurements of the initial water content were made using the loose subsample for each test using the method of Gardner (1986).

Particle Size Distribution. The PSD test was performed using 40 g of the loose subsample for each test using the methods ASTM 1985 and Gee and Bauder (1986).

Bulk Density. A single measurement of bulk density was made using the intact core. Following the conductivity test, the sediment in the core was oven dried and weighed. Dividing this weight by the volume of the core yielded the bulk density, as per the method of Blake and Hartge (1986b).

Porosity. A single estimate of porosity was made using the bulk density of intact core and the average particle density. The formula used was $\phi = 1 - \rho_s / \rho_r$ (Freeze and Cherry 1979).

Water Retention. Water retention data were obtained using the pressure-plate extraction and vapor equilibrium methods described by Klute (1986). Additional measurements were obtained during the unsaturated conductivity tests.

Saturated Hydraulic Conductivity. Saturated hydraulic conductivity was measured on the intact core prior to the unsaturated conductivity tests using the method of Klute and Dirksen (1986). The measurement of saturated conductivity was conducted several times to verify that a steady value of conductivity was achieved.

Unsaturated Hydraulic Conductivity. The multistep and steady state methods were used to measure unsaturated conductivity. Both methods were performed on the same core using the same sensor locations. The multistep method, which is an improvement of the one-step method of Kool et al. (1985 a,b), provides $\theta-\psi$ pairs and cumulative outflow. These data were used in conjunction with the MULSTP program (Eching and Hopmans 1993) to determine the optimal set of hydraulic parameters. MULSTP employs a numerical inversion procedure to find the set

Teflon is a trademark of E.I. du Pont de Nemours and Company, Wilmington, DE.
Silly Putty is a trademark of Binney & Smith Inc., Corporation, DE.

Table 2. Procedures for measuring physical and hydraulic properties.

Number	Title	Comment
PNL-MA-567, SA-2	Sieve Procedure	For materials > 50 μm effective diameter
PNL-MA-567, SA-3	Particle-Size Analysis	Hydrometer method for materials < 50 μm effective diameter
PNL-MA-567, SA-4	Constant Head Hydraulic Conductivity (HC)	Laboratory measurement for materials with $\text{HC} > 10^{-6}$ cm/s
PNL-MA-567, SA-5	Falling Head--Saturated Hydraulic Conductivity (HC)	Laboratory measurement for materials with $\text{HC} < 10^{-6}$ cm/s
PNL-MA-567, SA-6	Water Retention Procedure	Laboratory method for core or bulk sample (saturation to air dry)
PNL-MA-567, SA-7	Water Content	Necessary for constant head hydraulic conductivity
PNL-MA-567, SA-8	Clod Density/Bulk Density	Necessary for constant head hydraulic Conductivity
PNL-MA-567, SA-9	Determining Particle Density	Necessary for constant head hydraulic conductivity
Klute (1986)	Water Retention: Laboratory Methods	Pressure plate and vapor adsorption methods
Klute and Dirksen (1986)	Hydraulic Conductivity and Diffusivity: Laboratory Methods	Steady-state flux control method for unsaturated conductivity
Eching and Hopmans (1993)	Unsaturated Hydraulic Properties	Multistep outflow method for unsaturated conductivity and water retention estimation

of parameters that minimizes the differences between simulated variables and those test variables contained in the objective function. For these tests, the objective function contained the cumulative outflow data and the matric potential data. Eching and Hopmans (1993) found that this objective function yielded excellent results when compared to independently measured data. Although this method relies on specific retention and conductivity functions and it does not yield specific values of conductivity, it promises to be quicker than the steady-state method and could represent a cost savings for future sample analyses.

The steady-state method, described by Klute and Dirksen (1986), provides θ - ψ - K triplets, which can be fitted with retention and conductivity functions. The value of this method is that it provides simultaneous triplets that are independent of retention and conductivity models. If the resulting parameter set for these functions is equivalent to the set derived by the multistep method, then the multistep method could be employed more frequently to achieve the same result.

Because several tests must be performed on the same core, the following test sequence was established: saturated conductivity, multistep unsaturated conductivity, and steady state unsaturated conductivity. Following the saturated conductivity test, the cores were re-wetted to saturation and analyzed using the multistep method. Two pressure changes were used: 0.06 and 0.3 bars. Changes in water content and matric potential were monitored with a datalogger every 0.1-h following each pressure change. Outflow was monitored manually at time intervals ranging from 3 minutes to 24 hours. The next change in pressure was initiated only after the most recent change outflow was less than 1% of the cumulative outflow since the last pressure change.

Following the multistep test, the cores were re-wetted to saturation and analyzed using the steady-state method. A Mariotte-type reservoir was used to provide a source of water at a pre-defined matric potential at the upper surface of the samples. Fluxes into each sample were unique and dependent on the unsaturated conductivity of the sample at the imposed matric potential. Concurrent with establishing the matric potential at the top of the sample, the matric potential at the bottom of the sample was set to the same value by lowering the outflow tube. Water content and matric potential were measured continuously. Once the matric potential values within the sample ceased changing, indicating steady flow conditions had been achieved, the matric potential at the top of the sample was lowered to the next value and the outflow tube was lowered a similar amount. After equilibrating with the final and lowest potential, the cores were opened and the bulk density values were determined.

Results

Table 3 shows that particle density varies between 2.71 and 2.82 g/cm³ for this section of the Hanford formation. The average and median values are both 2.74 g/cm³, which would indicate a normal distribution. However, the two deepest values are the highest. These two samples, as shown below, have a higher gravel content. Subsequent tests could be used to determine whether the gravel has a particle density that is higher than the finer sediment.

Table 3 also shows that the initial water contents of the loose subsample material ranged from 0.0119 to 0.0382 g/g. The average and median values were similar: 0.020 and 0.0196 g/g, respectively. These water content values are low but not atypical of the Hanford formation. They were measured two to three months after drilling and, during that interval, the liners were stored in a refrigerated container where they could have experienced some evaporative losses. However, the water content values in Table 3 are very similar to values measured by Ellyn Murphy, another ILAW project researcher. Dr. Murphy measured water contents on a small sample from the end of each core immediately after the cores were drilled. Her average water contents were about 10% less than what is shown in Table 3.

Table 4 shows the results for both the sieve and hydrometer methods. In all but two samples, the gravel content was less than 2%. In contrast, samples 34A and 35A had 13 and 25% gravel, respectively. These were the deepest samples that were analyzed (between 236 and 242 ft). As shown in Figure 1, this depth range corresponds to the lower gravel sequence of the Hanford formation. Figure 3 shows all of the data combined to highlight the degree of variability in particle size distribution.

Table 5 shows that the bulk density ranged from 1.52 to 1.98 g/cm³. The mean and median were identical: 1.70 g/cm³. The highest densities were associated with the two samples (34A and 35A) that had significant gravel contents. Khaleel and Relyea (1997) found a similar effect from high gravel contents. Table 5 also shows the porosity data, which ranged from 0.299 to 0.444 and had nearly identical mean and median values of 0.377 and 0.374, respectively.

When opened for the bulk density measurements, most of the cores appeared homogenous. However, several cores had noticeable layering. The most dramatic layering

occurred in sample 7A, which had about 7 cm of sand in the upper part of the core and 8 cm of finer-textured sand in the lower part of the sample. It appeared that the upper set of sensors penetrated the coarser material and the lower set penetrated the finer material. Sample 19A had a 1-mm thick, silty-looking layer located about 1 cm from the top of the sample. Layers in two other samples were less distinct and not recorded.

Another feature that we observed when the cores were opened was the presence of a layer of finer and denser material along the walls of roughly half of the liners. We had observed this effect when we were preparing the cores, but it was more obvious when the cores were wet. One possible explanation is that the drilling technique caused migration of fines to the wall, where the heat from drilling caused water to move towards the interior of the sample, thus allowing the fines to consolidate more densely. We estimated the thickness of this zone as no more than 2 mm, which accounts for less than 5% of the sample area. Because of the small area, we expect that this phenomenon did not have a major impact on the measurements reported here, but it should be looked at more closely if another borehole is drilled for samples.

Table 6 shows the pressure plate data for four pressures. As expected, samples that were finer-textured (e.g., 31A) had higher water contents at any given pressure. The mean values at each pressure are all greater than the mean value of the initial water contents reported in Table 3. This result suggests that the *in situ* matric potential values were less than -4,080 cm (4 bar), the lowest pressure tested.

Table 7 shows that the vapor adsorption data covered a significant range of matric potential, from -4,170 cm to as dry as -1,110,000 cm. The associated water contents ranged from 0.056 to 0.0 g/g. This range of water content encompasses the initial water contents reported in Table 4.

Table 8 shows the saturated hydraulic conductivity values for the intact cores. The values range from 2.65E-4 to 1.32E-2 cm/s, with average and median values of 4.30E-3 and 2.94E-3 cm/s, respectively. The two highest values were for the two deepest cores (34A and 35A), which contained the highest gravel content.

Table 9 shows the parameter estimates determined using the MULSTP program and data from the multistep test. Parameters α and n were fitted to matric potential data, drainage data, and a single retention point using a weighting scheme to adjust the importance of each; typical weightings were 1, 1, and 1, respectively. Some samples had weightings of 0.5 and 0 for tension data; these are identified in Table 9. During parameter estimation, θ_s and saturated K were fixed at measured values; θ_r was estimated for tension value of 15,300 cm using linear interpolation between pressure plate reading of 4,080 cm and wettest vapor adsorption value that was still drier than 15,300 cm.

Figure 3 shows how the predictive model, based on MULSTP-derived parameters, simulates the experimental data for matric potential and drainage for the 20 samples. In general, the comparison is good.

Table 10 shows the θ - ψ - K triplets that were generated using the steady state method. The measurements are all at matric potentials above -40 cm. Even so, unsaturated conductivity values were 1 to 2 orders of magnitude less than the saturated values. Because the potentials were so high, the water contents were also relatively high. Water contents were much lower at the end of the multistep test.

Summary

Twenty intact cores from the FY 98 ILAW PA borehole were analyzed for physical and hydraulic properties. These data and parameters will be used to predict the movement of contaminants from the disposal facility to the groundwater. Health and environmental impacts from the contamination will be calculated and the results used to ascertain the suitability of the disposal facility to protect the public and the environment. In addition to supporting the ILAW PA, these data and parameters can be used to support remediation and closure activities at sites such as tank farms and specific retention basins that have similar geology.

The twenty cores reported here were from the geologic unit known as the Hanford formation sandy sequence. The cores showed a fairly uniform set of properties deriving from the high percentage of medium to fine sand in nearly all of the cores. The variability among the twenty cores is within the range reported by Khaleel and Freeman (1995) for the 200 Areas. What is significant and valuable is that the data reported here give a true indication of the parameters and their variability *beneath the ILAW disposal site*. These data are also significant to the ILAW analysis for other reasons. First, a complete set of physical and hydraulic properties was measured on undisturbed cores. The tests included measurements of unsaturated conductivity and water retention in dry sediments. Secondly, a set of geochemical measurements was performed on the core material. Having a complete set of physical, chemical, and hydraulic data on site-specific cores is rare and should facilitate the PA calculations and enhance their credibility.

Two zones in the borehole were finer in texture and had lower saturated conductivity values than the other zones. These zones, or layers, could impact flow and transport calculations and increase lateral spreading. The results in this report will be considered in forming the conceptual model of the site. Additional boreholes planned for FY 1999 and FY 2000 will help to verify whether these and other particular layers are continuous across the disposal site.

A unexpected feature of the ILAW borehole site was the presence of a relatively thick open-framework gravel sequence below 250 ft. No data are available at present on the physical and hydraulic properties of this sequence. However, plans are in place to collect the necessary data for the gravelly sequence as part of the ILAW site characterization via boreholes No. 2 and 3.

Regarding parameter estimation of vadose zone hydraulic properties, several issues were raised by the 1997 external peer-review panel for the ILAW PA (Mann et al. 1998). These include a) use of the standard van Genuchten-Mualem approach with the saturated conductivity as a match point, b) correction for the presence of gravel in sediments, and c) upscaling of laboratory-measured data to block scale values in numerical models. Issues (a) and (b) are being

addressed as part of the analysis and parameter estimation of hydraulic properties for the borehole samples. The upscaling issue is being addressed as part of other FY98 tasks.

Table 3. Particle density and initial water content of material adjacent to the cores

Sample	Particle Density rep 1 (g/cm ³)	Particle Density rep 2 (g/cm ³)	Average Particle Density, g/cm ³	Initial Water Content, rep 1, g/g	Initial Water Content, rep 2, g/g	Average Initial Water Content, g/g
B8500-07A	2.718	2.717	2.72	0.0157	0.0176	0.0166
B8500-10A	2.747	2.745	2.75	0.0153	0.0152	0.0152
B8500-12A	2.740	2.737	2.74	0.0164	0.0174	0.0169
B8500-14A	2.716	2.711	2.71	0.0166	0.0163	0.0165
B8500-15A	2.720	2.722	2.72	0.0119	0.0120	0.0119
B8500-16A	2.728	2.727	2.73	0.0149	0.0148	0.0149
B8500-17A	2.720	2.721	2.72	0.0285	0.0268	0.0276
B8500-19A	2.728	2.731	2.73	0.0196	0.0199	0.0197
B8500-20A	2.720	2.722	2.72	0.0194	0.0203	0.0199
B8500-21A	2.721	2.723	2.72	0.0228	0.0213	0.0220
B8500-22A	2.751	2.750	2.75	0.0139	0.0146	0.0142
B8500-23A	2.731	2.736	2.73	0.0163	0.0162	0.0163
B8500-24A	2.731	2.731	2.73	0.0258	0.0236	0.0247
B8500-25A	2.748	2.745	2.75	0.0199	0.0197	0.0198
B8500-27A	2.747	2.745	2.75	0.0199	0.0189	0.0194
B8500-29A	2.733	2.736	2.74	0.0201	0.0204	0.0203
B8500-31A	2.756	2.750	2.75	0.0395	0.0370	0.0382
B8500-32A	2.753	2.752	2.75	0.0272	0.0275	0.0273
B8500-34A	2.793	2.797	2.80	0.0175	0.0178	0.0176
B8500-35A	2.822	2.822	2.82	0.0189	0.0217	0.0203

Table 4. Particle size distribution of material adjacent to the cores

Sample 7A		Sample 10A		Sample 12A		Sample 14A	
Particle Diameter (μm)	% Less Than Diameter	Particle Diameter (μm)	% Less Than Diameter	Particle Diameter (μm)	% Less Than Diameter	Particle Diameter (μm)	% Less Than Diameter
2000	99.8	2000	100.0	2000	99.3	2000	99.8
1000	99.3	1000	95.6	1000	93.9	1000	96.5
500	94.7	500	52.3	500	68.6	500	76.5
250	74.2	250	33.8	250	36.1	250	34.1
106	41.5	106	24.1	106	17.3	106	15.2
75	30.7	75	19.8	75	13.8	75	12.2
53	24.3	53	14.4	53	11.5	53	10.4
52.0	23.4	53.4	13.7	53.2	11.4	53.7	11.1
30.4	18.0	31.1	10.0	30.9	9.3	31.1	9.1
16.9	12.7	17.1	7.2	17.0	8.1	17.1	6.6
9.8	12.1	9.9	6.5	9.8	8.1	9.9	6.3
6.9	9.8	7.0	5.5	6.9	7.0	7.0	6.3
5.7	8.9	5.7	5.2	5.7	5.8	5.7	5.2
4.9	6.8	5.0	5.0	4.9	5.1	5.0	5.0
1.4	5.2	1.4	2.7	1.4	4.4	1.4	4.5

Sample 15A		Sample 16A		Sample 17A		Sample 19A	
Particle Diameter (μm)	% Less Than Diameter	Particle Diameter (μm)	% Less Than Diameter	Particle Diameter (μm)	% Less Than Diameter	Particle Diameter (μm)	% Less Than Diameter
2000	99.5	2000	98.5	2000	99.7	2000	100.0
1000	90.7	1000	87.5	1000	97.3	1000	99.1
500	58.6	500	56.7	500	87.9	500	95.8
250	29.7	250	29.3	250	60.8	250	73.6
106	17.9	106	18.0	106	33.5	106	33.1
75	14.9	75	15.4	75	27.0	75	21.4
53	13.0	53	13.3	53	22.0	53	15.4
53.4	12.4	53.4	15.9	52.4	19.1	52.6	15.1
31.0	10.0	31.1	12.3	30.7	13.8	30.8	10.2
17.1	7.2	17.2	9.6	16.9	11.3	16.9	8.3
9.9	6.0	10.0	7.2	9.8	8.8	9.8	6.2
7.0	4.8	7.1	6.2	7.0	7.4	7.0	4.9
5.7	4.8	5.8	6.5	5.7	6.4	5.7	4.5
5.0	4.5	5.0	5.3	5.0	5.5	4.9	4.5
1.4	4.8	1.4	2.9	1.4	5.1	1.4	3.2

Table 4. Particle size distribution of material adjacent to the cores (cont.)

Sample 20A		Sample 21A		Sample 22A		Sample 23A	
Particle Diameter (μm)	% Less Than Diameter	Particle Diameter (μm)	% Less Than Diameter	Particle Diameter (μm)	% Less Than Diameter	Particle Diameter (μm)	% Less Than Diameter
2000	99.8	2000	99.6	2000	98.4	2000	100.0
1000	98.3	1000	96.6	1000	88.2	1000	99.9
500	87.1	500	80.7	500	46.5	500	98.2
250	54.2	250	44.5	250	19.3	250	75.5
106	25.3	106	19.5	106	10.6	106	35.6
75	19.0	75	14.7	75	8.7	75	28.1
53	14.8	53	11.6	53	7.3	53	23.5
53.1	14.0	53.4	11.2	54.2	10.5	53.0	23.2
31.0	10.2	30.9	10.8	31.3	9.2	31.0	18.2
17.1	7.6	17.1	7.1	17.3	5.9	17.1	13.4
9.9	6.4	9.9	6.0	10.0	3.6	9.9	11.5
7.0	4.7	7.0	4.3	7.1	3.3	7.1	8.9
5.7	4.0	5.7	3.0	5.8	3.6	5.8	8.4
5.0	4.5	5.0	3.2	5.0	3.3	5.0	8.4
1.4	4.3	1.4	4.1	1.4	1.6	1.4	3.6

Sample 24A		Sample 25A		Sample 27A		Sample 29A	
Particle Diameter (μm)	% Less Than Diameter	Particle Diameter (μm)	% Less Than Diameter	Particle Diameter (μm)	% Less Than Diameter	Particle Diameter (μm)	% Less Than Diameter
2000	99.8	2000	99.7	2000	98.3	2000	98.8
1000	95.8	1000	96.5	1000	89.3	1000	93.7
500	75.0	500	79.5	500	58.9	500	68.5
250	37.3	250	28.6	250	18.9	250	27.8
106	17.0	106	10.1	106	8.3	106	12.5
75	13.4	75	7.5	75	6.6	75	10.1
53	11.0	53	5.9	53	5.5	53	8.9
54.2	13.2	54.2	7.8	54.1	8.4	56.3	5.9
31.5	9.7	31.4	6.4	31.4	6.4	32.7	4.5
17.3	8.5	17.2	5.4	17.2	5.7	18.0	2.6
10.0	7.9	10.0	4.2	10.0	4.4	10.4	1.6
7.1	8.2	7.1	4.7	7.1	4.7	7.4	1.4
5.8	7.3	5.8	4.7	5.8	4.9	6.1	0.5
5.0	7.3	5.0	4.0	5.0	4.9	5.3	0.3
1.4	2.9	1.4	2.6	1.4	3.7	1.5	0.1

Table 4. Particle size distribution of material adjacent to the cores (cont.)

Sample 31A		Sample 32A		Sample 34A		Sample 35A	
Particle Diameter (μm)	% Less Than Diameter	Particle Diameter (μm)	% Less Than Diameter	Particle Diameter (μm)	% Less Than Diameter	Particle Diameter (μm)	% Less Than Diameter
2000	99.8	2000	98.2	2000	87.0	2000	75.7
1000	99.4	1000	86.3	1000	54.4	1000	42.8
500	98.4	500	45.4	500	23.1	500	18.8
250	96.4	250	13.7	250	10.1	250	9.8
106	72.9	106	5.5	106	4.6	106	5.5
75	46.9	75	4.1	75	3.5	75	4.5
53	28.2	53	3.2	53	2.9	53	3.8
51.7	29.2	54.3	7.6	53.6	5.9	53.2	8.5
30.8	15.8	31.5	5.9	31.1	4.5	30.8	6.7
17.0	10.8	17.3	4.8	17.0	4.5	16.9	5.7
9.9	8.3	10.0	3.8	9.8	4.1	9.8	5.0
7.0	7.2	7.1	3.8	7.0	2.7	6.9	4.5
5.7	7.0	5.8	3.8	5.7	2.3	5.7	4.7
5.0	6.2	5.0	3.3	4.9	2.5	4.9	4.5
1.4	5.2	1.4	2.5	1.4	1.8	1.4	2.0

Table 5. Core volume, bulk density, and porosity of the cores

Sample	Core Volume (cm ³)	Bulk Density (g/cm ³)	Porosity (cm ³ /cm ³)
B8500-07A	803	1.70	0.377
B8500-10A	803	1.62	0.413
B8500-12A	803	1.74	0.363
B8500-14A	803	1.58	0.416
B8500-15A	803	1.69	0.380
B8500-16A	803	1.58	0.420
B8500-17A	803	1.57	0.423
B8500-19A	803	1.52	0.444
B8500-20A	803	1.58	0.419
B8500-21A	803	1.62	0.403
B8500-22A	1,069	1.78	0.352
B8500-23A	1,069	1.72	0.371
B8500-24A	1,069	1.85	0.321
B8500-25A	1,069	1.80	0.345
B8500-27A	1,069	1.71	0.377
B8500-29A	1,069	1.76	0.359
B8500-31A	1,069	1.60	0.418
B8500-32A	1,069	1.78	0.359
B8500-34A	1,069	1.92	0.316
B8500-35A	1,069	1.98	0.299

Table 6. Water retention data from the pressure plate technique

7A		10A		12A		14A	
Matric Potential -cm	Water Content g/g						
561	0.0503	561	0.0400	561	0.0374	561	0.0357
1020	0.0484	1020	0.0344	1020	0.0324	1020	0.0342
2040	0.0415	2040	0.0320	2040	0.0255	2040	0.0372
4080	0.0395	4080	0.0255	4080	0.0255	4080	0.0303

15A		16A		17A		19A	
Matric Potential -cm	Water Content g/g						
561	0.0368	561	0.0403	561	0.0595	561	0.0421
1020	0.0316	1020	0.0338	1020	0.0475	1020	0.0336
2040	0.0307	2040	0.0287	2040	0.0400	2040	0.0265
4080	0.0241	4080	0.0232	4080	0.0366	4080	0.0260

Table 6. Water retention data from the pressure plate technique (cont.)

20A		21A		22A		23A	
Matric Potential -cm	Water Content g/g						
561	0.0470	561	0.0334	561	0.0296	561	0.0669
1020	0.0378	1020	0.0284	1020	0.0223	1020	0.0525
2040	0.0351	2040	0.0257	2040	0.0209	2040	0.0421
4080	0.0281	4080	0.0234	4080	0.0191	4080	0.0342

24A		25A		27A		29A	
Matric Potential -cm	Water Content g/g						
561	0.0425	561	0.0304	561	0.0291	561	0.0346
1020	0.0364	1020	0.0261	1020	0.0254	1020	0.0272
2040	0.0318	2040	0.0247	2040	0.0232	2040	0.0242
4080	0.0290	4080	0.0199	4080	0.0218	4080	0.0222

31A		32A		34A		35A	
Matric Potential -cm	Water Content g/g						
561	0.0603	561	0.0357	561	0.0328	561	0.0329
1020	0.0472	1020	0.0333	1020	0.0290	1020	0.0309
2040	0.0402	2040	0.0342	2040	0.0268	2040	0.0281
4080	0.0375	4080	0.0284	4080	0.0204	4080	0.0214

Table 7. Water retention data from the vapor adsorption technique

7A		10A		12A		14A	
Matric Potential -cm	Water Content g/g						
24145	0.0152	8781	0.0170	7396	0.0222	28908	0.0116
21945	0.0206	16766	0.0167	45690	0.0112	16298	0.0200
78701	0.0077	113305	0.0048	152030	0.0043	138301	0.0052
129149	0.0045	137994	0.0034	140282	0.0037	188749	0.0036
207546	0.0027	161833	0.0029	121521	0.0042	392007	0.0023
1075921	0.0000	1082660	0.0003	1087258	0.0006	1054326	0.0009

15A		16A		17A		19A	
Matric Potential -cm	Water Content g/g						
10683	0.0405	32690	0.0093	7873	0.0230	4628	0.0375
22817	0.0124	39451	0.0107	33754	0.0170	4632	0.0291
364967	0.0023	182999	0.0038	203274	0.0048	238015	0.0038
168294	0.0034	188513	0.0019	221937	0.0038	186010	0.0039
1082928	0.0008	181075	0.0034	252444	0.0035	349726	0.0027
		1063482	0.0009	1070939	0.0009	1042683	0.0011

Table 7. Water retention data from the vapor adsorption technique (cont.)

20A		21A		22A		23A	
Matric Potential -cm	Water Content g/g						
6485	0.0258	8349	0.0276	4633	0.0562	10211	0.0289
8341	0.0216	6021	0.0237	11175	0.0460	142403	0.0078
235350	0.0045	234127	0.0039	215747	0.0059	134462	0.0071
232477	0.0043	277628	0.0033	197216	0.0045	225253	0.0054
322711	0.0034	278460	0.0030	1090154	0.0015	223222	0.0048
1105338	0.0014	1092187	0.0008			1075491	0.0024

24A		25A		27A		29A	
Matric Potential -cm	Water Content g/g						
4171	0.0392	18992	0.0140	17232	0.0206	5566	0.0268
120958	0.0118	245392	0.0064	55936	0.0148	32360	0.0156
135542	0.0112	316708	0.0061	248841	0.0099	226565	0.0068
257943	0.0088	258559	0.0051	277107	0.0083	250807	0.0068
251919	0.0078	285889	0.0052	252086	0.0085	247094	0.0059
1072363	0.0051	1062967	0.0034	1061386	0.0058	1054101	0.0037

31A		32A		34A		35A	
Matric Potential -cm	Water Content g/g						
7894	0.0329	6033	0.0236	7432	0.0197	32783	0.0218
46384	0.0196	73280	0.0161	12568	0.0214	7432	0.0457
226164	0.0076	270140	0.0096	252391	0.0095	43717	0.0135
282406	0.0058	255850	0.0093	283862	0.0083	343812	0.0155
261127	0.0063	268249	0.0090	306591	0.0083	335749	0.0082
1047364	0.0030	1036466	0.0060	1023601	0.0047	1029646	0.0058

Table 8. Saturated hydraulic conductivity of the cores

Sample	Saturated Hydraulic Conductivity (cm/s)			Average Saturated Hydraulic Conductivity (cm/s)	Method
	Rep 1	Rep 2	Rep 3		
B8500-07A	7.81E-04	9.78E-04	1.35E-03	1.04E-03	Falling head
B8500-10A	1.96E-03	2.22E-03	4.68E-03	2.95E-03	Falling head
B8500-12A	2.27E-03	2.35E-03	1.82E-03	2.15E-03	Falling head
B8500-14A	1.47E-03	2.08E-03	2.41E-03	1.99E-03	Falling head
B8500-15A	1.50E-03	1.90E-03	2.87E-03	2.09E-03	Falling head
B8500-16A	8.37E-03	1.05E-02	9.87E-03	9.57E-03	Falling head
B8500-17A	1.88E-03	1.96E-03	2.12E-03	1.99E-03	Falling head
B8500-19A	3.74E-03	4.30E-03	4.88E-03	4.31E-03	Falling head
B8500-20A	2.24E-03	2.54E-03	2.83E-03	2.54E-03	Falling head
B8500-21A	2.84E-03	2.89E-03	3.09E-03	2.94E-03	Falling head
B8500-22A	4.89E-03	5.23E-03	5.05E-03	5.06E-03	Constant head
B8500-23A	2.57E-04	2.76E-04	2.61E-04	2.65E-04	Constant head
B8500-24A	5.88E-04	5.61E-04	5.58E-04	5.69E-04	Constant head
B8500-25A	5.37E-03	5.42E-03	5.43E-03	5.41E-03	Constant head
B8500-27A	8.22E-03	8.10E-03	8.09E-03	8.14E-03	Constant head
B8500-29A	3.77E-03	3.75E-03	3.73E-03	3.75E-03	Constant head
B8500-31A	8.49E-04	8.14E-04	8.01E-04	8.21E-04	Constant head
B8500-32A	6.68E-03	6.71E-03	6.74E-03	6.71E-03	Constant head
B8500-34A	1.32E-02	1.31E-02	1.32E-02	1.32E-02	Constant head
B8500-35A	1.07E-02	1.06E-02	1.06E-02	1.06E-02	Constant head

Table 9. Van Genuchten parameters (based on the multistep method) for 20 ILAW borehole samples from the sandy sequence. Parameters α and n were fitted to matric potential data, drainage data, and a single retention point using a weighting scheme to adjust the importance of each. The typical weightings were 1, 1, and 1, respectively. The superscript a indicates the weightings were 0.5, 1, and 1. The superscript b indicates the weightings were 0, 1, and 1. In these special cases, the matric potential weighting was reduced until the R^2 exceeded 0.6.

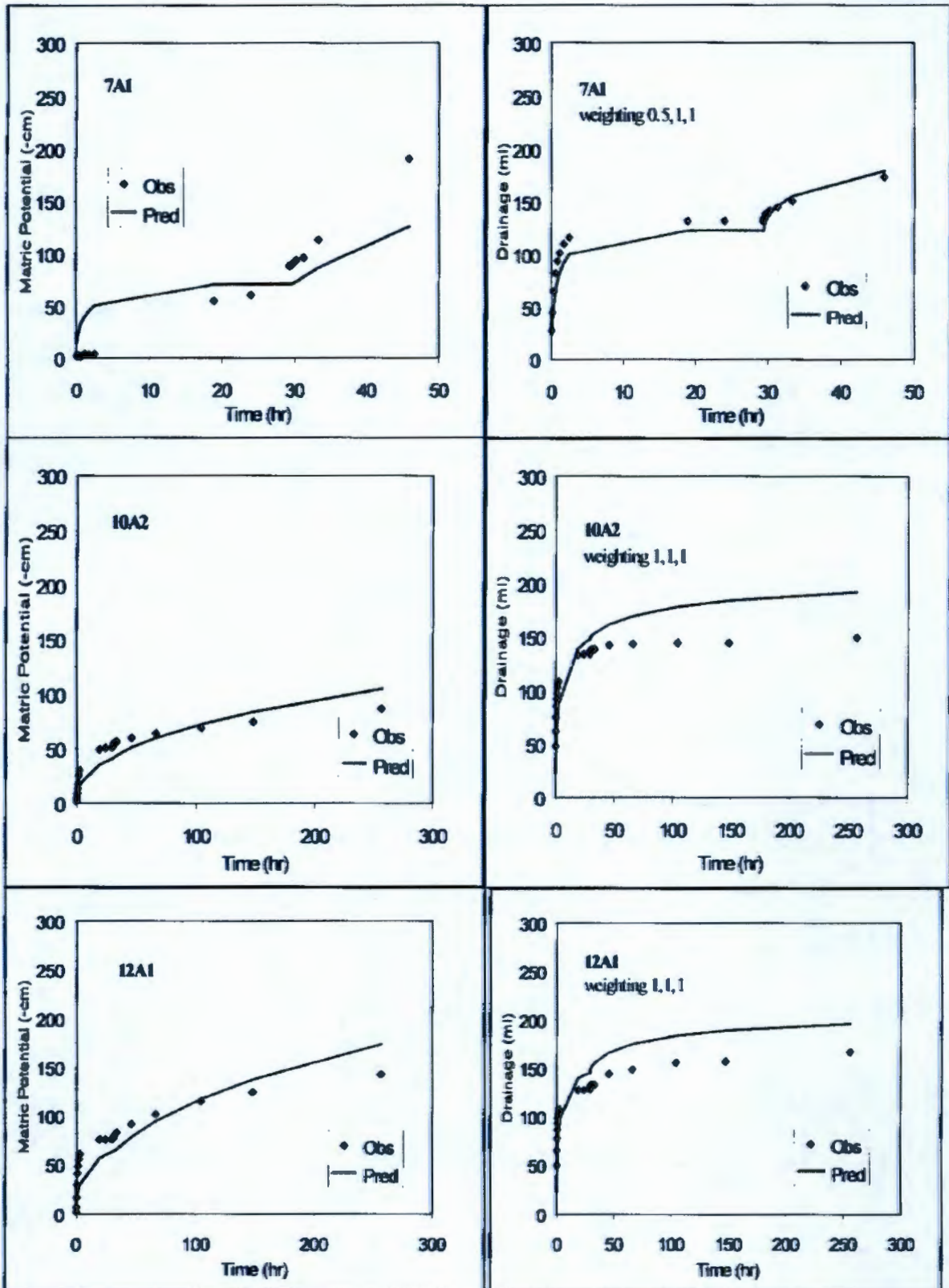
Sample	θ_r (cm ³ /cm ³)	θ_s (cm ³ /cm ³)	Fitted α (1/cm)	Fitted n (-)	R^2
7A1 [#]	0.377	0.0404	0.0290 ^a	1.825 ^a	0.816
10A2 [#]	0.413	0.0279	0.1161	1.784	0.687
12A1	0.363	0.0309	0.0650	1.755	0.621
14A1	0.416	0.0324	0.0445 ^b	1.728 ^b	0.966
15A1	0.380	0.0254	0.0487	1.844	0.744
16A1	0.420	0.0228	0.0682	1.710	0.862
17A2	0.423	0.0382	0.0689	1.899	0.741
19A1	0.444	0.0279	0.2010 ^a	1.542 ^a	0.715
20A1	0.419	0.0321	0.0305	2.081	0.942
21A1	0.403	0.0276	0.0545	1.926	0.813
22A1	0.352	0.0252	0.1078	1.585	0.879
23A1	0.371	0.0411	0.0079	1.553	0.900
24A1	0.321	0.0413	0.0130	1.684	0.983
25A2	0.345	0.0267	0.0842	2.158	0.930
27A2	0.377	0.0354	0.0830	1.532	0.884
29A1	0.359	0.0317	0.0784	1.732	0.777
31A2	0.418	0.0444	0.0058 ^a	2.012 ^a	0.915
32A2	0.359	0.0401	0.0931	1.703	0.826
34A2	0.316	0.0324	0.0819	2.398	0.854
35A1	0.299	0.0428	0.0897	2.160	0.945

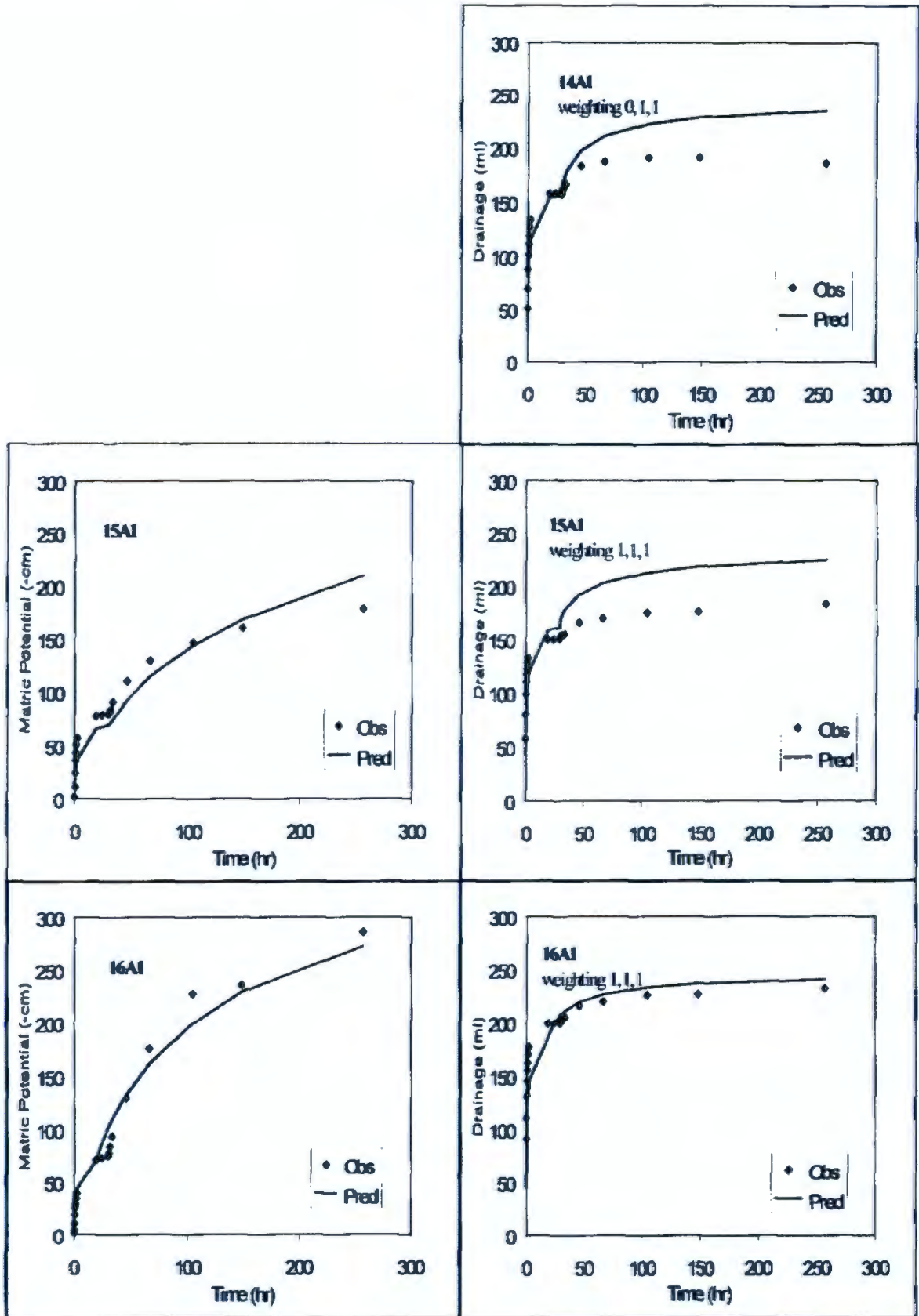
1 and 2 following A indicate tensiometer locations near the top and bottom, respectively (Fig. 2)

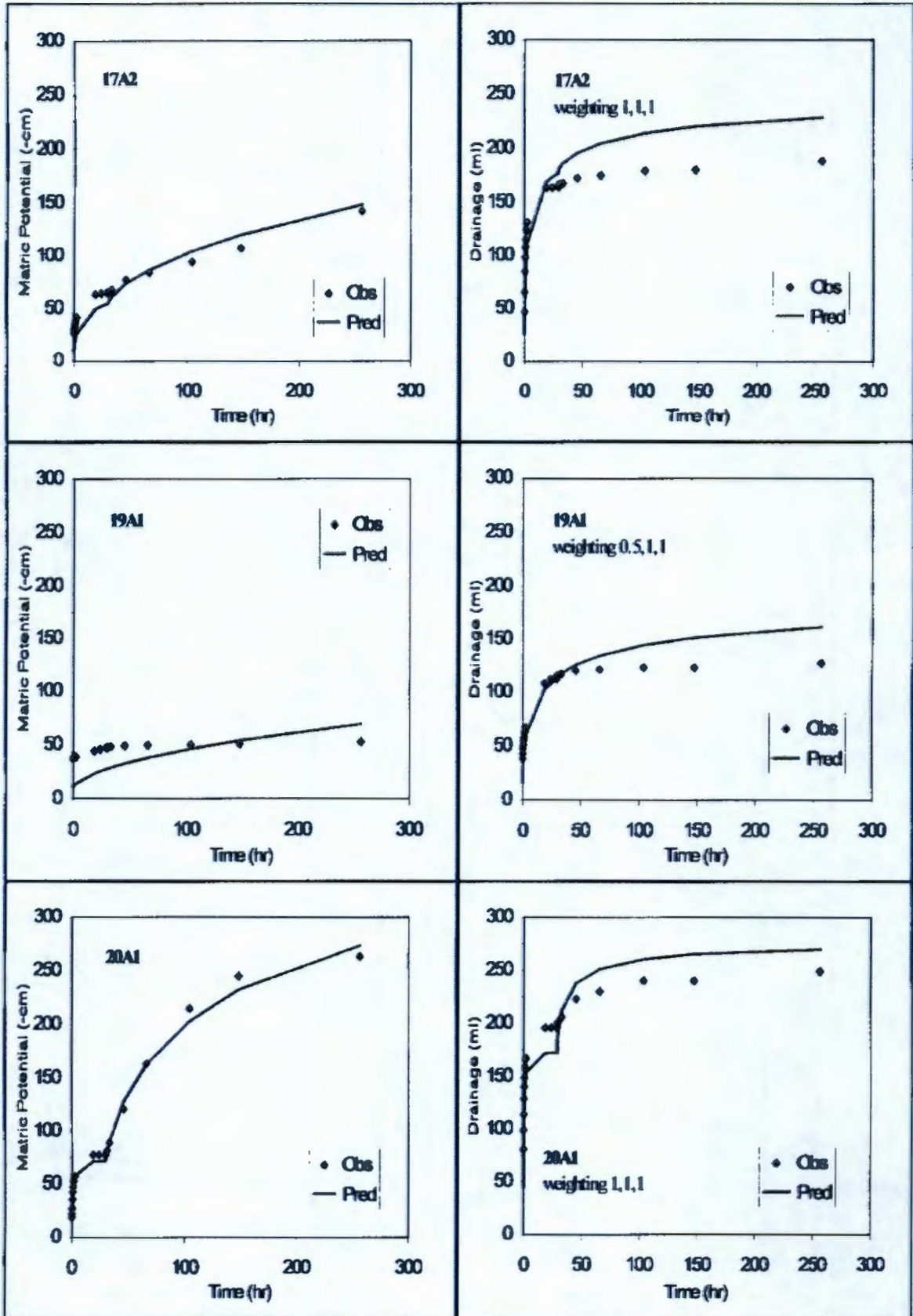
Table 10. Water retention and unsaturated conductivity data for each sample during the steady state tests (nd = no data)

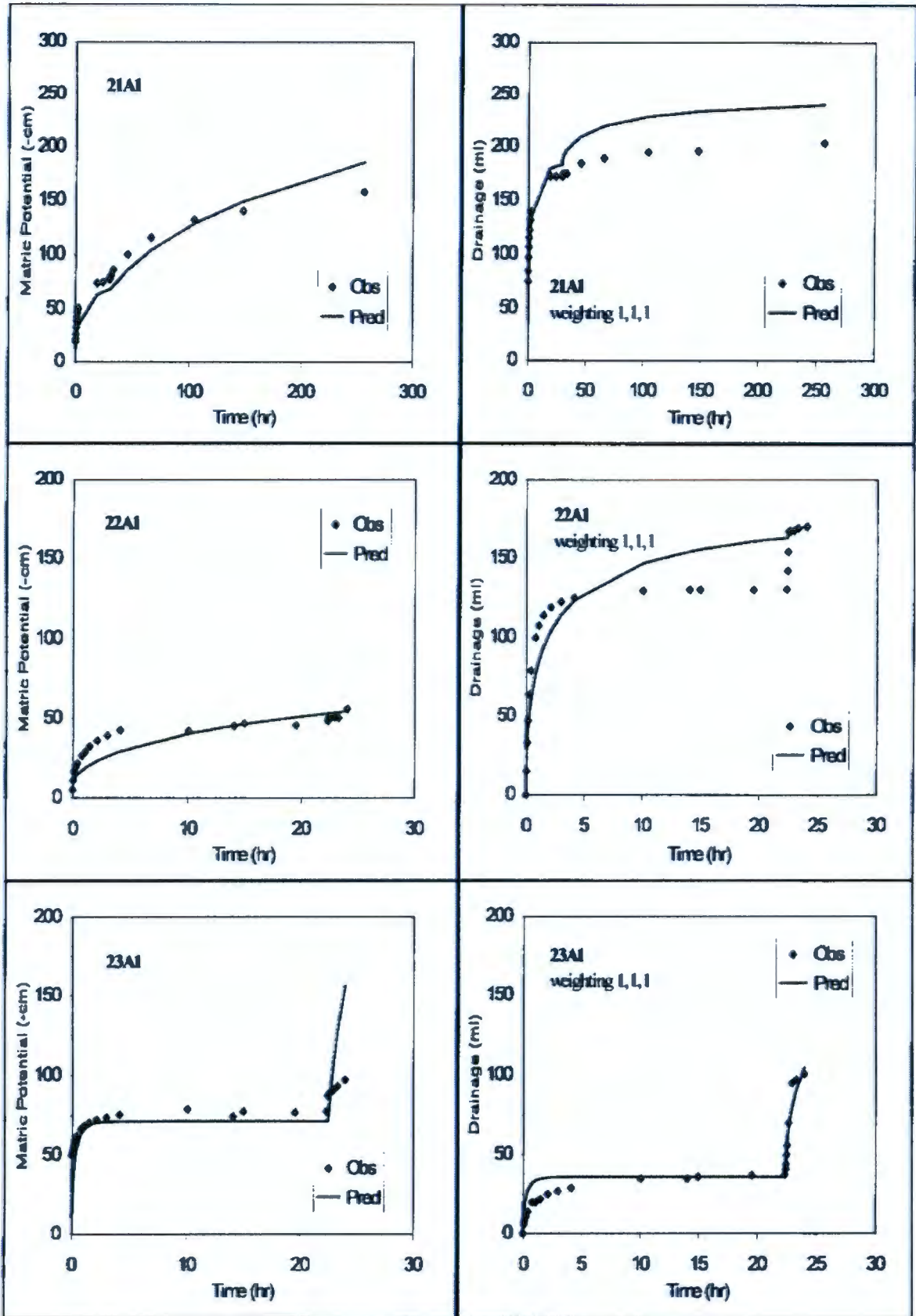
Sample	Matric Potential -cm	Water Content cm ³ /cm ³	Unsaturated Hydraulic Conductivity cm/s
7A	-10.3	0.403	9.1E-04
7A	-13.5	0.405	9.5E-04
7A	-16.5	0.407	9.02E-4
7A	-19.9	0.406	9.0E-04
7A	-41.6	0.227	5.4E-05
10A	-6.1	0.391	1.1E-03
10A	-36.8	0.206	3.4E-05
12A	-8.5	0.336	9.7E-04
12A	-28.2	0.238	1.1E-04
12A	-29.8	0.234	1.1E-04
14A	-23.1	0.245	4.5E-05
15A	-8.8	0.392	2.2E-03
16A	-16.8	nd	2.0E-03
16A	-30.4	nd	2.9E-05
17A	-5.9	0.372	2.1E-04
17A	-23.3	0.249	6.5E-05
17A	-25.3	0.236	4.3E-06
19A	-6.4	0.422	2.3E-03
20A	-8.4	0.377	1.9E-03
21A	-20.8	0.289	6.7E-04
22A	-6.0	0.363	2.2E-03
22A	-22.8	nd	3.9E-04
22A	-25.6	nd	2.3E-04
23A	-20.2	0.374	1.6E-04
24A	-9.9	0.328	5.8E-04
24A	-25.3	nd	4.8E-04
25A	-8.8	0.326	5.1E-04
25A	-26.6	0.227	2.7E-04
27A	-12.7	0.298	2.4E-03
27A	-15.1	0.298	4.3E-04
27A	-19.7	0.285	2.9E-04
29A	-12.7	0.343	4.8E-04
29A	-14.0	0.315	1.0E-04
31A	-12.7	0.383	3.0E-04
31A	-20.3	0.369	3.0E-04
31A	-20.5	0.371	3.0E-04
31A	-28.2	0.370	2.9E-04
32A	-10.1	0.333	1.5E-03
32A	-12.3	nd	7.7E-04
34A	-6.9	0.313	6.3E-04
34A	-15.2	0.197	1.3E-04
35A	-20.3	0.278	1.9E-05

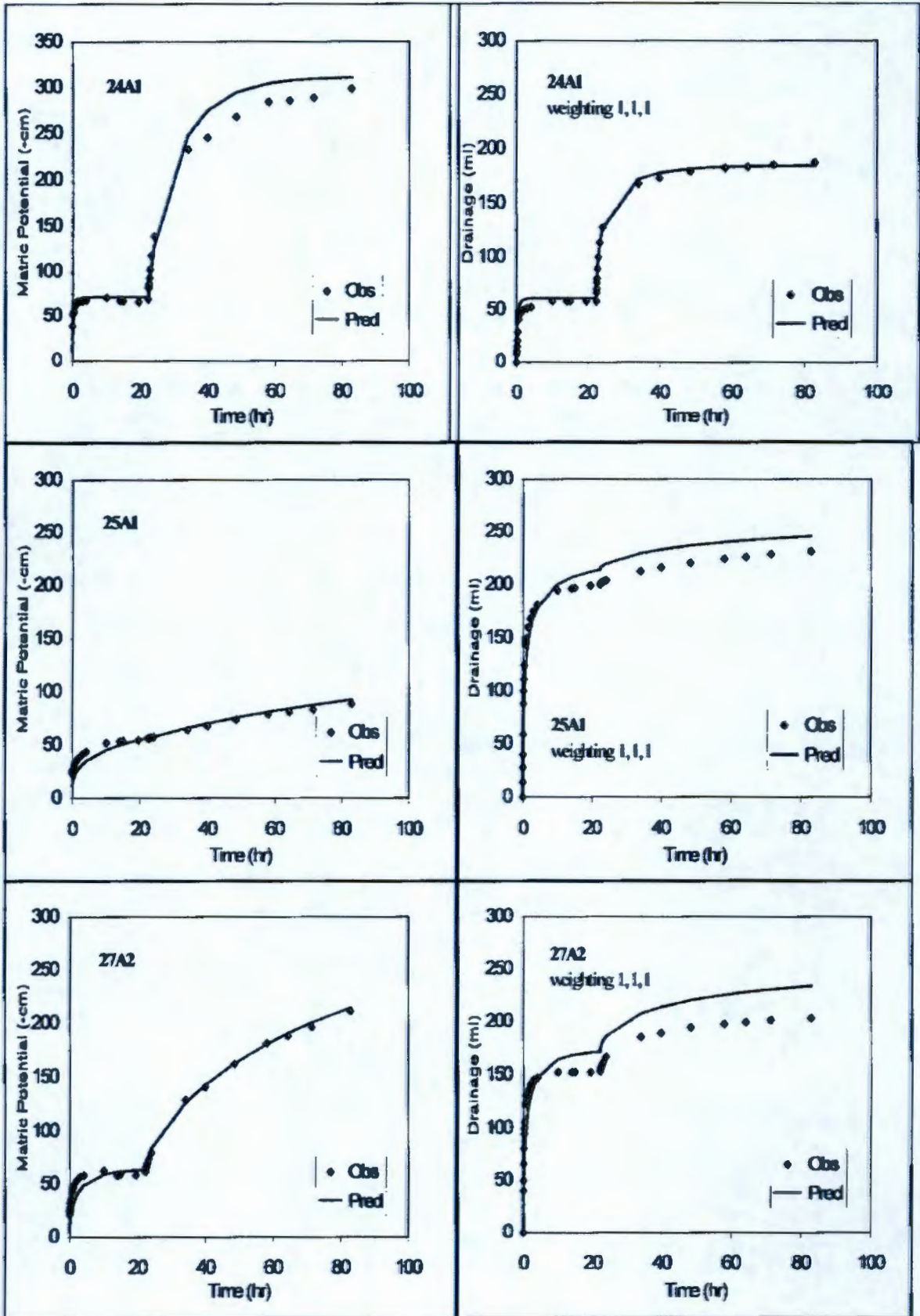
Figure 3. Comparison of predictive model, based on MULSTP-derived parameters, and observed data on matric potential (-cm) and cumulative drainage (mL) for 20 samples (No tension data were available for sample 14A1).

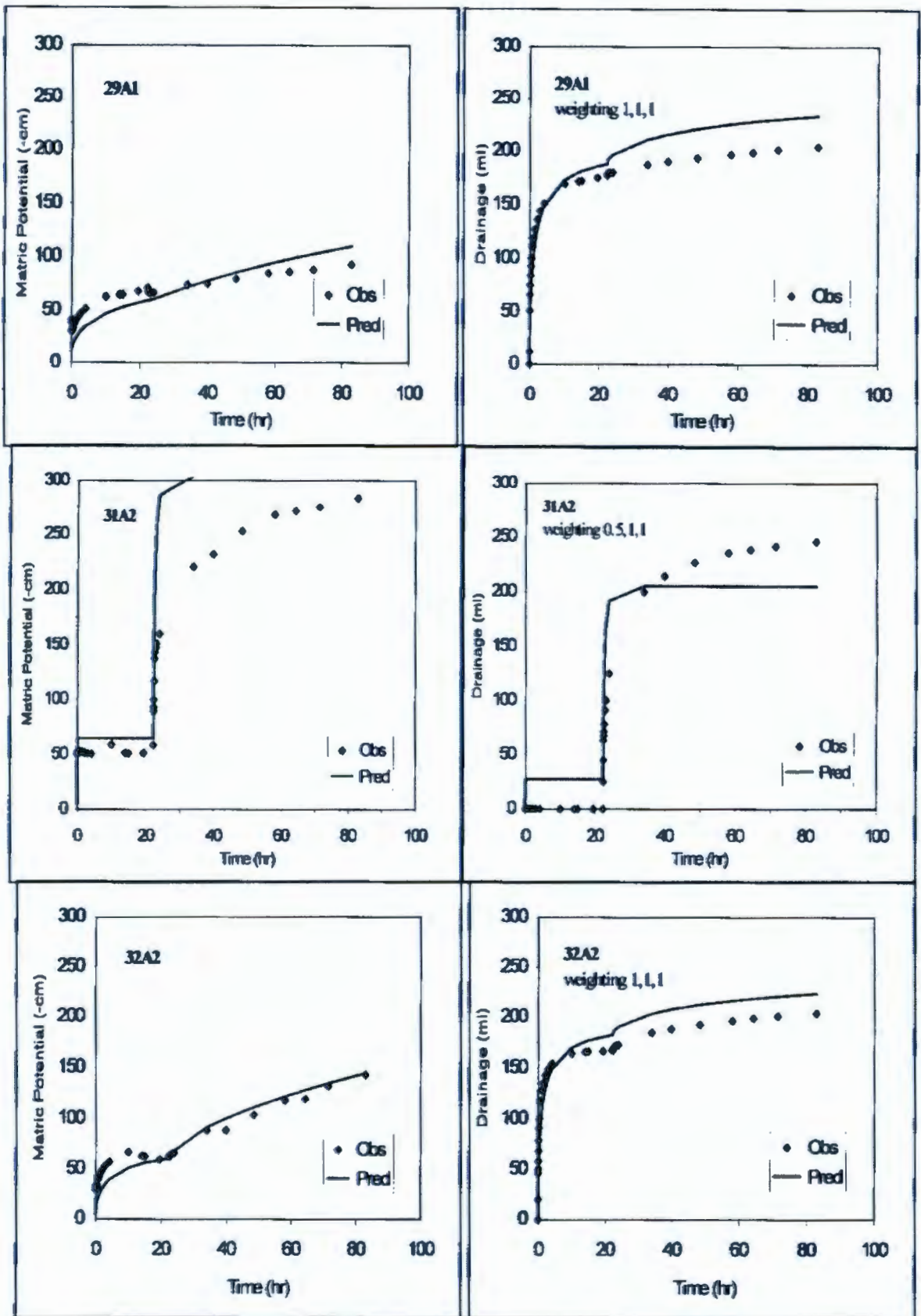


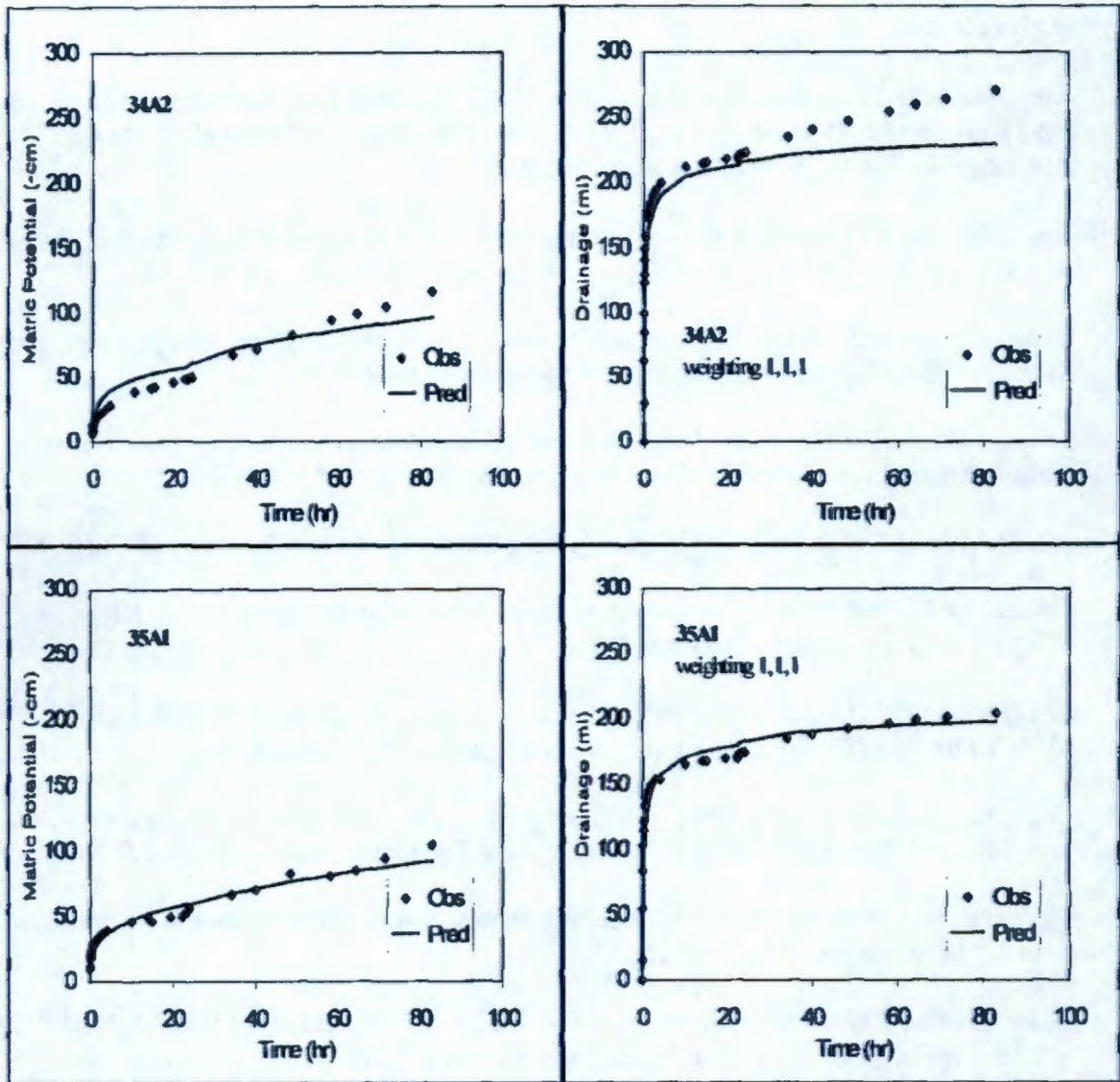












References

- American Society for Testing and Materials. 1985. "Standard Test Method for Particle-size Analysis of Soils. D 422-63 (1972)." 1985 Annual Book of ASTM Standards 04.08:117- 127. American Society for Testing and Materials, PA.
- Blake GR, and KH Hartge. 1986a. "Particle Density." In *Methods of Soil Analysis, Part 1*, ed. A. Klute, pp. 377-382. American Society of Agronomy, Madison, WI.
- Blake GR, and KH Hartge. 1986b. "Bulk Density." In *Methods of Soil Analysis, Part 1*, ed. A. Klute, pp. 363-375. American Society of Agronomy, Madison, WI.
- Eching SO, and JW Hopmans, 1993. "Optimization of hydraulic functions from transient outflow and soil water pressure data," *Soil Sci. Soc. Am. J.* 57:1167-1175.
- Freeze RA and JA Cherry, 1979. *Groundwater*. Prentice-Hall, Inc., Englewood Cliffs, NJ.
- Gardner W.H. 1986. Water Content. In *Methods of Soils Analysis, Part 1*, A. Klute, ed., pp. 493-544, Am. Soc. Agron., Madison, WI.
- Gee GW and JW Bauder, 1986. "Particle-Size Analysis." In *Methods of Soil Analysis, Part 1*, ed. A. Klute, pp. 383-409. American Society of Agronomy, Madison, WI.
- Khaleel R, and EJ Freeman, 1995. "Variability and scaling of hydraulic properties for 200 Area soils, Hanford Site, WHC-EP-0883, Westinghouse Hanford Company, Richland, Washington.
- Khaleel R, and JF Relyea, 1997. "Correcting laboratory-measured moisture retention data for gravels," *Water Resour. Res.* 33:1875-1878.
- Klute A, 1986. "Water Retention: Laboratory Methods," In *Methods of Soil Analysis, Part 1*, ed A. Klute, pp. 635-662. American Society of Agronomy, Madison, Wisconsin.
- Klute A and C Dirksen, 1986. "Hydraulic conductivity and diffusivity: Laboratory methods," In *Methods of Soil Analysis, Part 1*, ed A. Klute, pp. 687-734. American Society of Agronomy, Madison, Wisconsin.
- Kool JB, JC Parker, and MT van Genuchten, 1985a. "Determining soil hydraulic properties from one-step outflow experiments by parameter estimation, I, Theory and numerical studies," *Soil Sci. Soc. Am. J.* 49:1348-1354.
- Kool JB, JC Parker, and MT van Genuchten, 1985b. "Determining soil hydraulic properties from one-step outflow experiments by parameter estimation, I, Experimental studies," *Soil Sci. Soc. Am. J.* 49:1354-1359.

LMHC, 1997. "Statements of work for FY 1998 to 2003 for the Hanford low-level tank waste performance assessment activity," HNF-SD-WM-PAP-062, Rev. 2, Lockheed Martin Hanford Company, Richland, Washington.

Mann FM, RJ Puigh, II, PD Rittmann, NW Kline, JA Voogd, Y Chen, CR Eiholzer, CT Kincaid, BP McGrail, AH Lu, GF Williamson, NR Brown, PE LaMont, 1998. "Hanford Immobilized Low-Activity Tank Waste Performance Assessment," DOE/RL-97-69, U. S. Department of Energy, Richland, Washington.

Reidel SP, and KD Reynolds, 1998. "Characterization plan for the immobilized low-activity waste borehole," Pacific Northwest National Laboratory, Richland, Washington.

Reidel SP, KD Reynolds, and DG Horton, 1998. "Immobilized low-activity waste disposal complex borehole 299-E17-21," PNNL-11957, Pacific Northwest National Laboratory, Richland, Washington.

APPENDIX B

Laboratory Data on Physical and Hydraulic Properties for 100 Area Samples (RETC Input File)

HNF-4769, Rev. 1

15 1 8
 2-1307: mass-based correction : Drying curve
 1 20 24 3 4 0 1 1 8 30 2
 0.0352 0.2309 0.1000 1.6000 0.3750 0.5 1. 1.0
 1 1 1 1 0 0 1

1 0.27E-03

2-1307

100-HR-3 : 43%gr, 46%cs, 11%fs, 0%silt, 0%clay

0.1 0.2309
 7.5 0.2309
 21.0 0.2309
 33.0 0.2200
 52.5 0.2112
 69.0 0.2006
 100.5 0.1809
 202.5 0.1441
 300.0 0.1239
 500.0 0.1042
 500.0 0.1010
 700.0 0.0931
 700.0 0.0870
 1000.0 0.0831
 2010.0 0.0663
 3000.0 0.0575
 5000.0 0.0475
 7000.0 0.0346
 8700.0 0.0304
 14400.0 0.0352
 0.10 2.70E-4
 30.0 5.86E-6
 97.0 9.70E-7
 388.0 2.60E-7

2-1308: mass-based correction : Drying curve
 1 19 23 3 4 0 1 1 8 30 2
 0.0186 0.1176 0.1000 1.6000 0.3750 0.5 1. 1.0
 1 1 1 1 0 0 1

1 0.75E-04

2-1308

100-HR-3 : 58%gr, 22%cs, 9%fs, 11%silt, 0%clay

0.1 0.1176
 7.5 0.1176
 21.0 0.1176
 33.0 0.1176
 52.5 0.1112
 69.0 0.1005
 100.5 0.0858
 202.5 0.0694
 300.0 0.0604
 500.0 0.0520
 500.0 0.0487
 700.0 0.0483
 700.0 0.0428
 1000.0 0.0398
 2000.0 0.0381
 3200.0 0.0329
 5000.0 0.0411
 7000.0 0.0211
 10000.0 0.0186
 0.10 7.50E-5

HNF-4769, Rev. 1

34.0	3.94E-6								
90.0	1.05E-6								
374.0	2.88E-7								
2-1318: mass-based correction : Drying curve									
1	20	24	3	4	0	1	1	8	30
	0.0181	0.1207		0.1000		1.6000		0.3750	
1	1	1	1	0	0	1			
1 0.11E-03									
2-1318									
100-HR-3 : 60%gr, 40%cs, 20%fs, 0%silt, 0%clay									
	0.1	0.1207							
	7.5	0.1207							
	21.0	0.1207							
	33.0	0.1207							
	52.5	0.1207							
	69.0	0.1171							
	100.5	0.1039							
	202.5	0.0859							
	300.0	0.0746							
	500.0	0.0639							
	700.0	0.0588							
	700.0	0.0553							
	1000.0	0.0507							
	1000.0	0.0510							
	2000.0	0.0359							
	3200.0	0.0512							
	5000.0	0.0293							
	7000.0	0.0229							
	10000.0	0.0183							
	15000.0	0.0181							
	0.10	1.10E-4							
	18.0	9.30E-5							
	43.0	4.10E-5							
	138.0	3.80E-6							
2-2663: mass-based correction : Drying curve									
1	21	24	3	4	0	1	1	8	30
	0.0298	0.1301		0.1000		1.6000		0.3750	
1	1	1	1	0	0	1			
1 0.39E-03									
2-2663									
100-BC-5 : 61%gr, 35%cs, 4%fs, 0%silt, 0%clay									
	0.1	0.1301							
	8.0	0.1301							
	11.0	0.1301							
	23.5	0.1301							
	31.5	0.1301							
	53.5	0.1301							
	72.1	0.1301							
	101.0	0.1301							
	203.0	0.1043							
	300.0	0.0877							
	500.0	0.0741							
	700.0	0.0674							
	700.0	0.0633							
	1000.0	0.0602							
	1000.0	0.0594							
	2060.0	0.0482							
	3020.0	0.0426							
	5000.0	0.0370							

HNF-4769, Rev. 1

7000.0	0.0321									
10000.0	0.0297									
15000.0	0.0298									
0.10	3.90E-4									
27.0	1.40E-5									
101.0	1.60E-6									
2-2664: mass-based correction : Drying curve										
1	23	28	3	4	0	1	1	8	30	2
0.0222	0.1214	0.1000	1.6000	0.3750		0.5		1.		1.0
1	1	1	1	0	0	1				

1 0.46E-03

2-2664

100-BC-5 : 73%gr, 19%cs, 8%fs, 0%silt, 0%clay

0.1	0.1214
2.0	0.1214
6.5	0.1214
10.8	0.1214
11.0	0.1214
20.0	0.1214
30.5	0.1214
55.0	0.1111
72.0	0.1047
101.0	0.0911
201.5	0.0700
300.0	0.0593
500.0	0.0504
700.0	0.0458
700.0	0.0512
850.0	0.0442
1000.0	0.0416
1000.0	0.0417
2000.0	0.0301
3000.0	0.0291
5000.0	0.0247
7000.0	0.0233
10000.0	0.0222
0.10	4.60E-4
16.0	8.60E-5
90.0	7.40E-7
100.0	5.70E-7
296.0	5.80E-8

2-2666: mass-based correction : Drying curve										
1	20	25	3	4	0	1	1	8	30	2
0.0365	0.2300	0.1000	1.6000	0.3750		0.5		1.		1.0
1	1	1	1	0	0	1				

1 0.14E-03

2-2666

100-BC-5 : 71%gr, 19%cs, 7%fs, 3%silt, 0%clay

8.0	0.1325
11.0	0.1325
23.5	0.1325
31.5	0.1323
53.5	0.1276
72.1	0.1266
101.0	0.1237
203.0	0.1161
300.0	0.1020
500.0	0.0903
700.0	0.0836

HNF-4769, Rev. 1

700.0 0.0737
 1000.0 0.0753
 1000.0 0.0694
 2060.0 0.0610
 3020.0 0.0544
 5000.0 0.0466
 7000.0 0.0403
 10000.0 0.0358
 15000.0 0.0365
 0.10 1.40E-4
 32.0 3.00E-4
 93.0 3.60E-7
 98.0 4.50E-7
 294.0 2.20E-7

2-2667: mass-based correction : Drying curve

1	22	26	3	4	0	1	1	8	30	2			
0.0241		0.0906		0.1000		1.6000		0.3750			0.5	1.	1.0
1	1	1	1	0	0	1							

1 0.33E-03

2-2667

100-BC-5 : 75%gr, 21%cs, 4%fs, 0%silt, 0%clay

0.1 0.0906
 2.0 0.0906
 6.5 0.0906
 10.8 0.0906
 20.0 0.0906
 30.5 0.0906
 55.0 0.0906
 72.0 0.0906
 101.0 0.0899
 201.5 0.0684
 300.0 0.0597
 500.0 0.0530
 700.0 0.0488
 700.0 0.0563
 850.0 0.0467
 1000.0 0.0452
 1000.0 0.0508
 2000.0 0.0365
 3000.0 0.0353
 5000.0 0.0294
 7000.0 0.0251
 10000.0 0.0241
 0.10 3.30E-4
 19.0 9.66E-5
 96.0 2.39E-7
 305.0 1.97E-7

3-0570: mass-based correction : Drying curve

1	19	25	3	4	0	1	1	8	30	2			
0.0298		0.1500		0.1000		1.6000		0.3750			0.5	1.	1.0
1	1	1	1	0	0	1							

1 0.39E+00

3-0570

100-KR-1 : 60%gr, 33%cs, 7%fs, 0%silt, 0%clay

3.5 0.1195
 7.3 0.1195
 11.0 0.1195
 21.5 0.1195
 35.5 0.1195

49.0	0.1195
74.5	0.1092
99.0	0.1017
200.3	0.0856
300.0	0.0786
500.0	0.0700
700.0	0.0628
850.0	0.0598
1000.0	0.0565
2000.0	0.0429
3000.0	0.0406
5000.0	0.0387
7000.0	0.0327
10000.0	0.0298
0.10	3.90E-1
29.0	6.30E-5
40.0	1.70E-5
56.0	1.80E-6
89.0	4.50E-7
228.0	1.40E-7

3-0577: mass-based correction : Drying curve

1	22	27	3	4	0	1	1	8	30	2			
0.0140	0.1007	0.1000	1.6000	0.3750	0.5	1.	1.0						
1	1	1	1	0	0	1							

1 0.90E-01

3-0577

100-FR-3 : 66%gr, 35%cs, 4%fs, 0%silt, 0%clay

0.1	0.1007
2.5	0.1007
6.5	0.1007
10.0	0.1007
25.0	0.1007
33.5	0.1007
51.0	0.1007
75.0	0.0961
102.0	0.0880
201.5	0.0676
300.0	0.0574
500.0	0.0496
700.0	0.0434
700.0	0.0437
850.0	0.0409
1000.0	0.0379
1000.0	0.0380
2000.0	0.0292
3000.0	0.0268
5000.0	0.0195
7000.0	0.0165
10000.0	0.0140
0.10	9.00E-2
31.0	8.70E-6
59.0	3.10E-6
153.0	8.80E-8
232.0	2.70E-8

3-0686: mass-based correction : Drying curve

1	21	25	3	4	0	1	1	8	30	2			
0.0237	0.1782	0.1000	1.6000	0.3750	0.5	1.	1.0						
1	1	1	1	0	0	1							

1 0.13E-02

3-0686

100-FR-1 : 55%gr, 23%cs, 22%fs, 0%silt, 0%clay

0.1	0.1782
3.5	0.1782
6.0	0.1782
8.0	0.1782
10.0	0.1782
25.0	0.1782
33.5	0.1782
54.5	0.1775
71.5	0.1601
102.0	0.1282
202.5	0.0872
300.0	0.0690
500.0	0.0551
700.0	0.0473
850.0	0.0434
1000.0	0.0387
2000.0	0.0248
3000.0	0.0260
5000.0	0.0215
6300.0	0.0387
10000.0	0.0237
0.10	1.30E-3
23.0	1.60E-4
48.0	3.40E-5
202.0	2.60E-6

3-1702: mass-based correction : Drying curve

1	23	30	3	4	0	1	1	8	30	2			
0.0216		0.0976		0.1000		1.6000		0.3750		0.5	1.	1.0	
1	1	1	1	0	0	1							

1 0.13E-01

3-1702

100-DR-2 :68 %gr,32 %cs,0 0%fs, 0 %silt, %clay

0.1	0.0976
3.0	0.0976
5.0	0.0976
8.0	0.0976
11.5	0.0976
23.5	0.0944
37.0	0.0860
56.0	0.0788
71.5	0.0721
102.5	0.0655
201.0	0.0554
300.0	0.0498
500.0	0.0447
509.9	0.0400
700.0	0.0417
713.8	0.0373
850.0	0.0395
1000.0	0.0380
1019.7	0.0316
3059.1	0.0308
5098.5	0.0262
7137.9	0.0225
10197.0	0.0216
0.10	1.30E-2
30.0	2.30E-6

HNF-4769, Rev. 1

44.0 1.70E-6
 65.0 1.10E-6
 111.0 4.40E-7
 153.0 2.30E-7
 258.0 1.00E-7

4-1086: mass-based correction : Drying curve

1	23	29	3	4	0	1	1	8	30	2			
0.0173		0.1510		0.1000		1.6000		0.3750			0.5	1.	1.0
1	1	1	1	0	0	1							

1 0.11E-01

4-1086

100-K:65 %gr,24 %cs,11 %fs,0 %silt, %clay

0.1	0.1510
4.0	0.1103
12.0	0.1078
20.0	0.1041
31.0	0.1005
52.0	0.0967
70.1	0.0948
100.9	0.0912
213.0	0.0759
300.0	0.0680
500.0	0.0602
510.0	0.0571
690.0	0.0563
714.0	0.0536
1000.0	0.0520
1020.0	0.0520
2039.0	0.0445
3059.0	0.0430
5099.0	0.0398
7138.0	0.0307
9993.0	0.0360
10197.0	0.0334
136538.0	0.0173
0.10	1.10E-2
19.0	1.40E-4
36.0	1.00E-5
88.0	1.40E-6
247.0	4.60E-7
296.0	1.40E-7

4-1090: mass-based correction : Drying curve

1	23	28	3	4	0	1	1	8	30	2			
0.0075		0.1740		0.1000		1.6000		0.3750			0.5	1.	1.0
1	1	1	1	0	0	1							

1 0.21E-03

4-1090

100-K:50 %gr,34 %cs,16 %fs,0 %silt, %clay

0.1	0.1740
4.0	0.1423
12.0	0.1390
20.0	0.1379
31.0	0.1359
52.0	0.1326
70.1	0.1166
100.9	0.1029
213.0	0.0783
300.0	0.0653
500.0	0.0523

510.0 0.0467
 690.0 0.0460
 714.0 0.0452
 1000.0 0.0393
 1020.0 0.0429
 2039.0 0.0287
 3059.0 0.0278
 5099.0 0.0230
 7138.0 0.0156
 8565.0 0.0253
 10197.0 0.0446
 228311.0 0.0075
 0.10 2.10E-4
 61.0 1.40E-5
 120.0 3.60E-6
 231.0 7.60E-7
 320.0 2.90E-7

4-1118: mass-based correction : Drying curve

1	23	29	3	4	0	1	1	8	30	2			
0.0213		0.1760		0.1000		1.6000		0.3750		0.5	1.	1.0	
1	1	1	1	0	0	1							

1 0.86E-03

4-1118

100-K:66 %gr,28 %cs,6 0%fs, 0 %silt, %clay

0.1 0.1760
 5.0 0.1290
 8.0 0.1293
 11.5 0.1272
 27.0 0.1144
 49.0 0.1080
 70.5 0.1017
 104.0 0.0856
 202.0 0.0820
 300.0 0.0763
 500.0 0.0704
 510.0 0.0621
 700.0 0.0663
 714.0 0.0697
 1000.0 0.0626
 1020.0 0.0618
 2039.0 0.0496
 3059.0 0.0497
 5099.0 0.0479
 7138.0 0.0353
 9993.0 0.0365
 16927.0 0.0306
 55982.0 0.0213
 0.10 8.60E-4
 49.0 2.20E-6
 83.0 6.60E-7
 131.0 1.80E-7
 240.0 8.30E-8
 327.0 6.70E-8

4-1120: mass-based correction : Drying curve

1	23	28	3	4	0	1	1	8	30	2			
0.0069		0.1340		0.1000		1.6000		0.3750		0.5	1.	1.0	
1	1	1	1	0	0	1							

1 0.33E-03

4-1120

100-K:63 %gr,20 %cs,17 %fs,0 0%silt, %clay	
0.1	0.1340
5.0	0.1261
8.0	0.1277
11.5	0.1271
27.0	0.1238
49.0	0.1216
70.5	0.1184
104.0	0.0823
202.0	0.0755
300.0	0.0648
500.0	0.0519
510.0	0.0470
700.0	0.0460
714.0	0.0593
1000.0	0.0383
1020.0	0.0383
2039.0	0.0294
3059.0	0.0291
5099.0	0.0280
7138.0	0.0143
9993.0	0.0184
28450.0	0.0131
223824.0	0.0069
0.10	3.30E-4
27.0	4.10E-5
61.0	1.10E-5
88.0	7.40E-6
118.0	4.80E-6

APPENDIX C

Hydraulic Parameters of the Upper Hanford Formation

**Hanford Low-Activity Tank Waste Performance Assessment Activity:
Determination of In Situ Hydraulic Parameters of the Upper Hanford Formation**

AL Ward, RE Clayton and JS Ritter
31 December 1998

Introduction

Under the Hanford Low-Activity Tank Waste Project, the Lockheed Martin Hanford Company (LMHC) is designing and assessing the performance of a disposal facility for radioactive wastes currently stored in single and double shell tanks at the Hanford Site. Part of the performance assessment of such a facility involves the use of numerical models to predict the potential migration and fate of contaminants in through the vadose zone.

A general feature of soils is their spatial heterogeneity, i.e., variation of their hydraulic properties in space. The relation between the matric potential, ψ , and the volumetric water content, θ [the soil water characteristic, $\psi(\theta)$], the hydraulic conductivity tensor, $K(\theta)$, and the diffusivity, $D(\theta)$] are all spatially variable and have been shown to exhibit scale dependence. Thus, vadose flow and transport is a complex, three-dimensional phenomenon, even in soils that appear to be uniform. In addition to the inherent variability, typical field soils may exhibit a number of other structural elements, e.g. lenses, and clastic dikes, that often cause the redirection and concentration of water and solute flux at the local scale. Consequently, a major hindrance to the interpretation and prediction of vadose zone transport is the difficulty in measuring the constitutive properties and the uncertainty over the range of spatial scales required by numerical models. The associated uncertainty in hydraulic properties and its effect of performance of disposal facility is requirement is recognized in the DOE revised interim policy for waste disposal facilities.

The DOE revised interim policy requirement of a reasonable expectation that a disposal facility will comply with the LAW performance objectives implies consideration for uncertainty in model predictions of facility performance. Thus, any model of transport in the vadose zone requires, in the least, knowledge of the average properties of the medium, as well as the magnitude and characteristic length scale of the variations of those properties. Since a major source of uncertainty in model predictions of facility performance will be due to the uncertainty

in hydraulic and transport parameters, there is a need for information on the unsaturated hydrologic properties of the porous media.

The Pacific Northwest National Laboratory (PNNL) is providing geotechnical support to LMHC to assist in the design and performance assessment of the disposal facility. Two related components of the geotechnical support to be provided by PNNL are the determination of *in situ* unsaturated hydraulic parameters for Hanford surface sediments (Task 4b) and the upper Hanford sand sequence (Task 4c) at the proposed location of the disposal facility. In FY 1998, laboratory and field activities for the two tasks were completed and a letter report for Task 4b prepared (Ward et al., 1998). Data analysis and report preparation for Task 4c were deferred until FY-1999. This report represents the completion of Task 4c.

Methods

The experimental site is located approximately 325 m southwest of PUREX plant and about 220 m west of the injection site in the 200E Area used by Sisson and Lu (1984). On completion of the measurements in the surface sediments, a 1.5-m deep trench was excavated and the bottom of the trench instrumented in a manner identical to the surface. Detailed descriptions of the site, experimental design, and instrumentation have presented in the test plan of Ward (1997) and reiterated in the Task 4b letter report (Ward et al., 1998). Briefly, probes were installed along the centerline of the test plot in 25 short rows spaced 0.2 m apart (Figure 1). Each row consisted of 5 TDR probes installed vertically to depths of 0.25, 0.50, 0.75, 1.0, and 1.50 m (Figure 2).

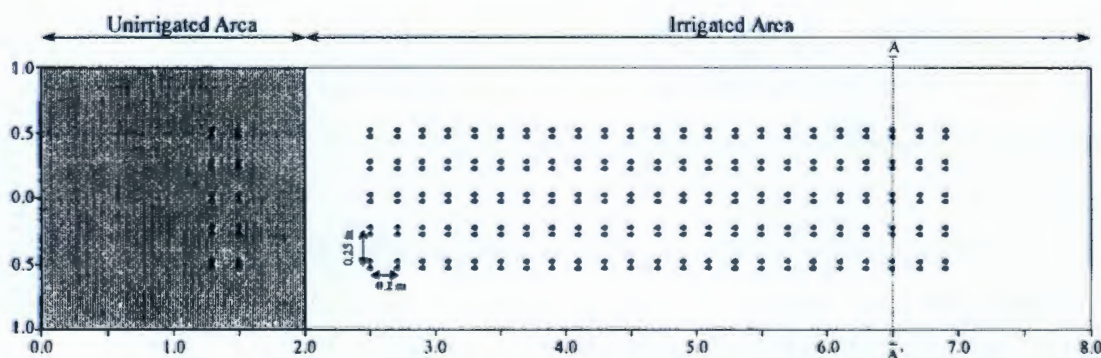


Figure 1. Plan View of Test Plot Showing Instrument Layout. The shaded 2-m section is the unirrigated control.

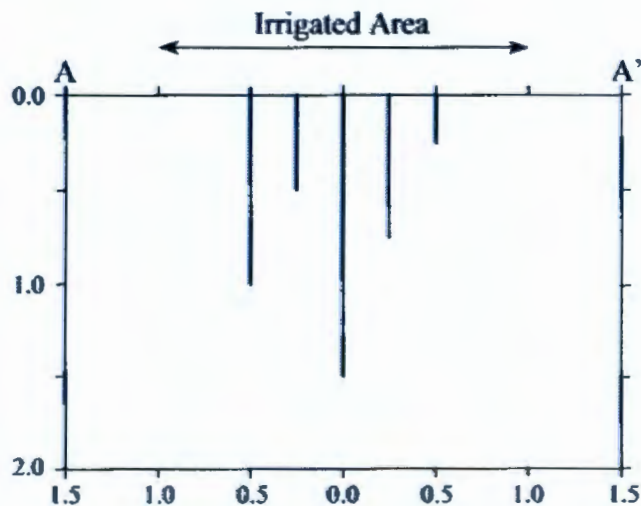


Figure 2. Cross-Sectional View of Test Plot Showing Installation Depths of the Instruments

Six infiltration experiments were conducted over the course of the study. Each experiment was conducted at a different flux density, J_w , to allow determination of $K(\theta_c)$. The values J_w used in the experiment were the same as in the first experiment, i.e., $4.7 \times 10^{-3} \text{ cm s}^{-1}$; $2.5 \times 10^{-3} \text{ cm s}^{-1}$, $1.292 \times 10^{-3} \text{ cm s}^{-1}$, $3.093 \times 10^{-4} \text{ cm s}^{-1}$, $3.54 \times 10^{-5} \text{ cm s}^{-1}$, and $1.35 \times 10^{-5} \text{ cm s}^{-1}$. The maximum application rate during the course of the experiments was determined by the nozzles used on the irrigation system. The lower rates were obtained by increasing the amount of time between each pass by the irrigation system.

Data reduction methods identical to those reported for Task 4b were employed. Briefly, hydraulic parameters for each depth interval were obtained by fitting the van Genuchten (1980) functions to the measured $\psi(\theta)$, and $K(\theta)$ data with the RETC computer program. The RETC program uses non-linear least squares techniques to fit the observed $\theta(\psi)$ and $K(\theta)$ data to closed-form analytical functions (van Genuchten et al., 1991). Unlike in the first experiment, saturated hydraulic conductivity, K_s was measured at fixed intervals along the transect using a tension infiltrometer according to the method of Zhang (1997). The measured K_s provided an additional constraint for the RETC analysis.

Solute breakthrough curves were derived from time domain reflectometry (TDR) measurements of the changes in bulk resistivity, R_t , in response to the application of KCl as a tracer (Ward et al. 1994; Kachanoski and Ward, 1994). The specific mass of tracer applied to the

surface, M_T , was 80 g Cl⁻ per m² of soil surface. At each level of J_w and associated equilibrium water content, θ_e , the specific mass of the tracer present from the surface to depth $z=L$ (L being the length of the TDR probes), as a function of time, $M_L(t)$ [g cm⁻²], was calculated from R_L at each probe location. The probability density function (pdf) of relative solute mass flux, $f_L(t)$, was calculated from the first derivative of $M_L(t)$ with respect to time. This is equivalent to the measured amount of solute, relative to the amount applied, that fluxes past the end of the TDR probe and represents the solute travel-time pdf.

Three methods were compared for determining transport parameters from measured $f_L(t)$. The first and most common approach fitted the solution to the convection-dispersion equation (CDE) to observed $f_L(t)$ to obtain estimates of the mean transport velocity (\bar{v}) and the dispersion coefficient (D). This solution assumes a Dirac delta-function input of solute at the surface and vertical one-dimensional flow. For a semi-infinite soil system, $f_L(t)$ is given by Jury and Roth (1990)

$$f_L(z,t) = \frac{z}{2\sqrt{\pi Dt^3}} \exp\left[-\frac{(z-\bar{v}t)^2}{4Dt}\right] \quad (1)$$

where D [L² T⁻¹] is the dispersion coefficient, \bar{v} [L T⁻¹] is the mean pore water velocity, z [L] is distance positive downward, and t [T] is time. The dispersion can also be expressed as $\lambda \bar{v}$, where λ [L] is the dispersivity of the soil, controlled by the geometry of the transport volume. It is assumed that the TDR probes measure the total amount of solute in the range $0 \leq z \leq L$, regardless of the distribution of the solute along the probes. Then $M_L(t)$ represents the mass of solute, relative to the amount applied, that remains in the region $0 \leq z \leq L$ and is given by

$$M_L(t) = 1 - \int_0^L f_L(L,\tau) d\tau = 1 - C_F \quad (2)$$

where C_F is the flux-averaged, reduced concentration for a step function input of solute, given by (Parker, 1984)

$$C_F = \frac{1}{2} \operatorname{erfc}\left[\frac{L-\bar{v}t}{2\sqrt{Dt}}\right] + \frac{1}{2} \exp\left[\frac{\bar{v}L}{D}\right] \operatorname{erfc}\left[\frac{L+\bar{v}t}{2\sqrt{Dt}}\right] \quad (3)$$

A similar development for the convective lognormal transfer function (CLT) model gives the following relationship (Jury, 1983)

$$M_{i,T}(t) = \frac{1}{2} \operatorname{erfc} \left[\frac{\ln(t) - \mu}{\sqrt{2}} \right] \quad (4)$$

in which μ [] is the mean of log transform of the travel time, $\ln(t)$, σ is the standard deviation of $\ln(t)$. Fitting of Eq. [4] to observed data to obtain μ and σ constitutes the second approach. The third and final approach makes use of time moment analysis to obtain the transport parameters from $M_{i,T}(t)$. The mean or expected travel time, $E_{i,T}$, is given by (Kachanoski et al, 1992)

$$E_{i,T} = \frac{\int_0^T [-dM_{i,T}(t)/dt] t dt}{A_{i,T}} \quad (5)$$

while the variance of the solute travel time, $\operatorname{Var}_{i,T}(t)$, is given and by

$$\operatorname{Var}_{i,T}(t) = \frac{\int_0^T [-dM_{i,T}(t)/dt] (t - E_{i,T})^2 dt}{A_{i,T}} \quad (6)$$

where

$$A_{i,T} = \int_0^T [-dM_{i,T}(t)/dt] dt \quad (7)$$

and represents the area under the breakthrough curve.

Differences between the three approaches lie in the assumptions made about the transport process. The CDE is essentially the far-field limit for solute transport. It assumes that v is the same at every location and differences in arrival time at an observation plane are due to random diffusion/dispersion processes. Thus, travel time of a solute particle to a depth $z = L$ is assumed to be uncorrelated to its travel time in the next depth increment. In contrast, the CLT does not require any particular assumption about the underlying transport process, except that it is linear and stationary. Information on the transport process is implicit in the measured transfer function. At any particular location, v is constant with depth, but it varies in the horizontal plane. Thus, solute spreading at the field scale is attributed to the horizontal spatial variability in vertical transport velocity. Since the vertical solute velocity at any given location is constant with depth,

the horizontal spatial pattern of travel times to an observation plane at $z = L$ is correlated with the spatial pattern of travel time in the next depth increment. The CLT can be used for all transport regimes and is not restricted to near- or far-field limits. However, because of the assumption of linearity and stationarity, this form of the CLT is not applicable to contaminants that exhibit nonlinear interactions with soil components, or to situations of transient water flow. In addition, it provides an integral description of transport from the surface to depth L and there are no provisions for either predicting transport to depths shallower or deeper than the measurement depth. The method of moment is a direct method and makes no assumption about the transport process. Moments can be used to determine parameters of any stable, linear process that can be represented by a transfer function. The n^{th} moment of $f_i(t)$ is given by

$$M_n = \int_0^{\infty} f_i(t) t^n dt \quad (8)$$

The mean travel time of the system is equal to the first moment, M_1 ; the second moment M_2 is a measure of the dispersion; while the third moment, M_3 , is related to the skewness. The main problem with ordinary moments is that higher moments are unreliable due to magnification of small errors in the tail. Nevertheless, for a particular flow model, specific relations exist between the moments and the model parameters.

In each approach, the dispersivity was calculated from the fitted parameters. The dispersivity for the CDE, λ_{CDE} , was calculated as

$$\lambda_{\text{CDE}} = \frac{D}{v} \quad (9)$$

An equivalent dispersivity for the CLT, λ_{CLT} was calculated as

$$\lambda_{\text{CLT}} = \frac{L}{2} [\exp(\sigma^2) - 1] \quad (10)$$

while from moment analysis method, λ_{MOM} was calculated as

$$\lambda_{\text{MOM}} = \frac{L}{2} \frac{\text{Var}_{i,L}}{E_{i,L}^2} \quad (11)$$

Results

Saturated Hydraulic Conductivity

Figure 3 shows the mean K_s measured at 40-cm intervals along the surface and 1.5-m deep transects. The three high values at the proximal end of the two transects were likely due to poor surface contact and treatment as outliers can be statistically justified (Acton, 1966). Overall, the results show an unexpected similarity in K_s at the two depths. At the surface, measured K_s (minus the outlier at $x = 1.6$ m) was 0.0013 ± 0.0006 cm s^{-1} , while at $z = 1.5$ m, K_s was 0.0008 ± 0.0003 cm s^{-1} . An analysis of variance was performed to test the null hypothesis of no difference between K_s measured in the two transects (Snedecor and Cochran, 1980). The value of F was significant at the 1% level ($F^{**} = 7.82 < F[0.99;1,24]=8.25$). Thus, measured K_s are from two different populations or soil types.

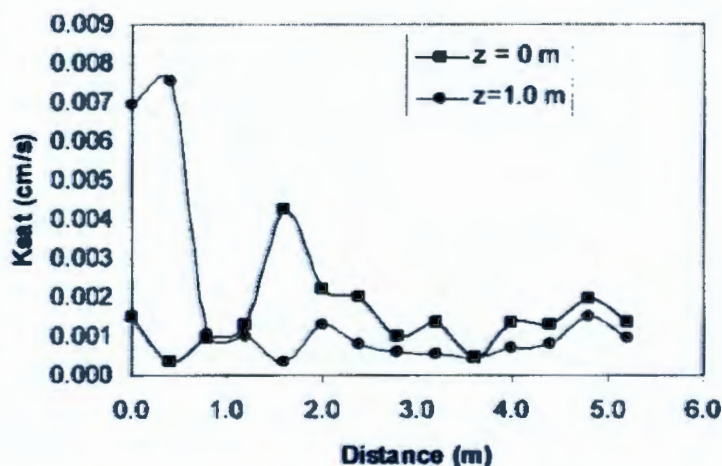


Figure 3. Mean saturated hydraulic conductivity measured along the surface and 1.5-m deep transects. Measurements were made using a tension infiltrometer at a head of -2 cm. Values at $x = 0$ and 0.4 m ($z = 0$ m) and $x = 1.6$ m ($z = 1.5$ m) were treated as outliers in calculating the mean and variance of K_s .

Spatial Variation in Water Flux Density

An added advantage of using the TDR system for infiltration measurements is its ability to measure soil water storage, W , as a function of time, t . For a given probe length, $W(t)$ is given

simply by $\theta(t) \cong L$, where $\theta(t)$ is the water content averaged over the length of the probe. During the time before the wetting front first reaches a depth L , the derivative of cumulative W with respect to time should be equal to the water flux at the soil surface, assuming no plant water uptake or evaporation (Parkin et al., 1992). Thus, spatial variation in water flux density, from which the variation in infiltration rates can be inferred, can be determined from early time measurements of $W(t)$.

Figure 4 shows the $W(t)$ ($L = 0.25$ m; $x = 0$ m) and the linear relationship fitted at early time. The rate of application at the soil surface was 2.5×10^{-6} cm s^{-1} . The calculated flux is 3.95×10^{-5} cm s^{-1} , an indication of the variability in the hydraulic conductivity.

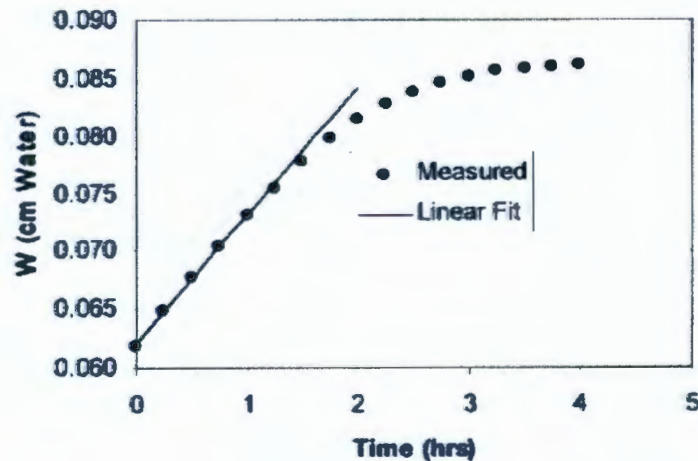


Figure 4. Cumulative storage versus time with a 25-cm probe at $x = 0$ m. The solid line shows a linear fit used to determine water flux density.

Figure 5 shows the distribution of flux along the transect based on measurements at the 25-cm depth. This result shows that even under a constant flux of water at the surface, the actual infiltration rate can be quite variable. The local-scale average (an average of the 24 measurements) is 2.38×10^{-6} cm s^{-1} , while the field-scale average (valued fitted to the average $W(t)$ curve) is 2.61×10^{-6} cm s^{-1} . Similar increases in flow and transport properties from the local scale to the field scale have been made by other researchers (e.g. Kachanoski et al., 1990). The increase from the local scale to field scale is related to the scale dependence of the lateral

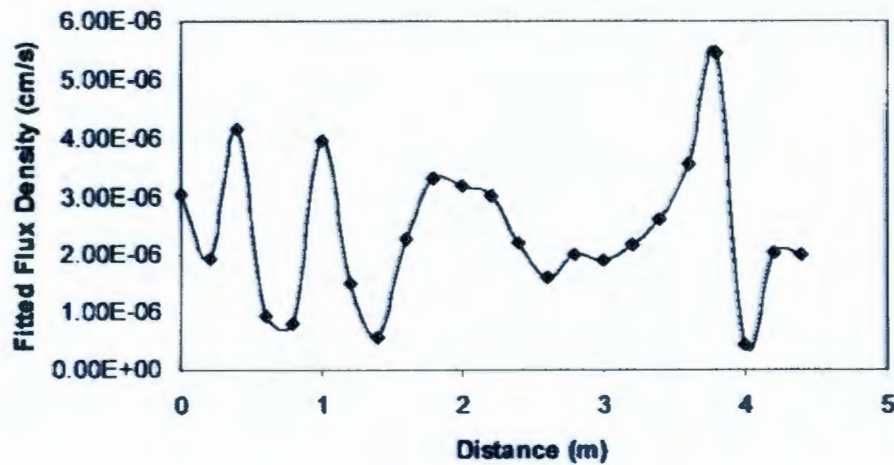


Figure 5. Spatial variation in measured surface flux density. Measurements were made with a 25-cm probe.

variations in water flux density. In this case, most of the variation can probably be explained by the distribution of sagebrush root channels (many of which were present) and micro-topography.

Water Retention Properties

Figure 6 shows the field-averaged moisture characteristic and the fitted van Genuchten relationship for the plot. Figures 7 through 11 show the plots of the individual depths. These data represent mostly imbibition data, collected as the profile was wetted to steady state at each flux of interest. There are some desorption data, mostly obtained between wetting cycles as maintenance was performed on the system. There was generally very little drainage during these periods and the data are not obvious from the plots.

As seen from the data presented, there are not many measurements at matric suctions greater than around 500 cm. The profile remained relatively wet following the first experiment, except very near the surface. In addition, most of the joints between the transducer and tensiometer failed at suctions greater than 400 to 500 cm.

Figure 6 shows that the data can be treated as essentially one population, suggesting some degree of homogeneity. To determine whether there was any advantage to be gained from treating the data otherwise, the measurements were separated out by depth interval and the

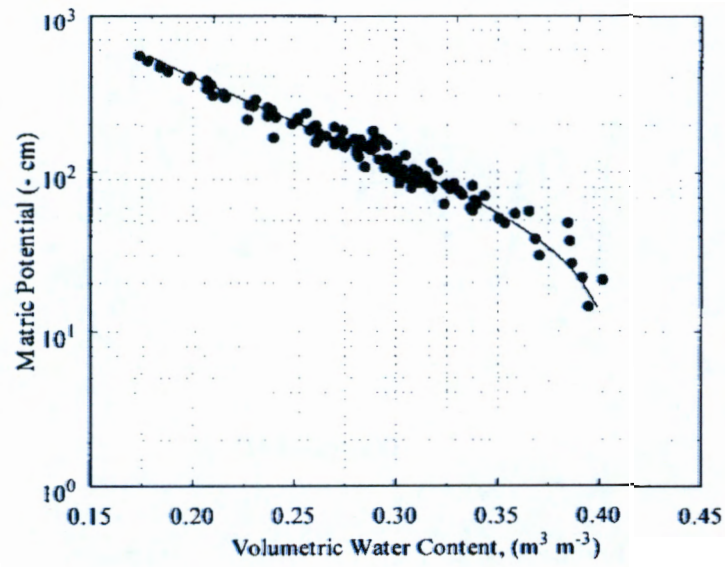


Figure 6. Fitted and observed field-averaged moisture characteristic function. This plot includes measurements from all depth intervals.

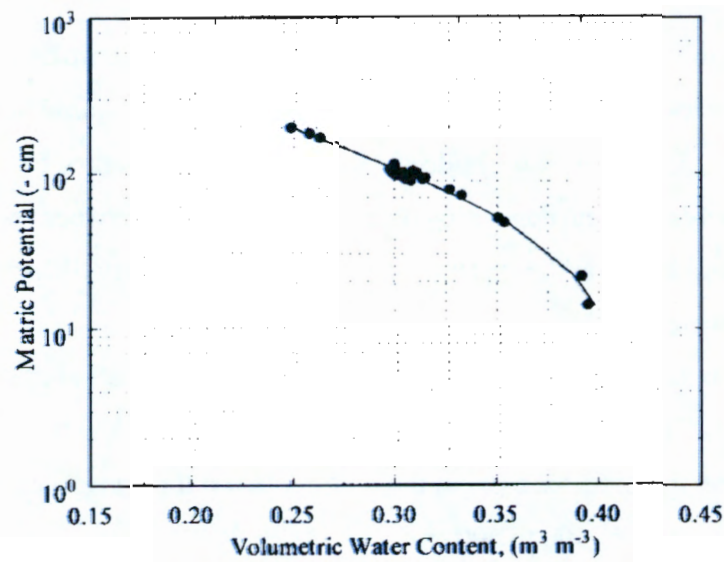


Figure 7. Fitted and observed field-averaged moisture characteristic function for the 0-25 cm depth.

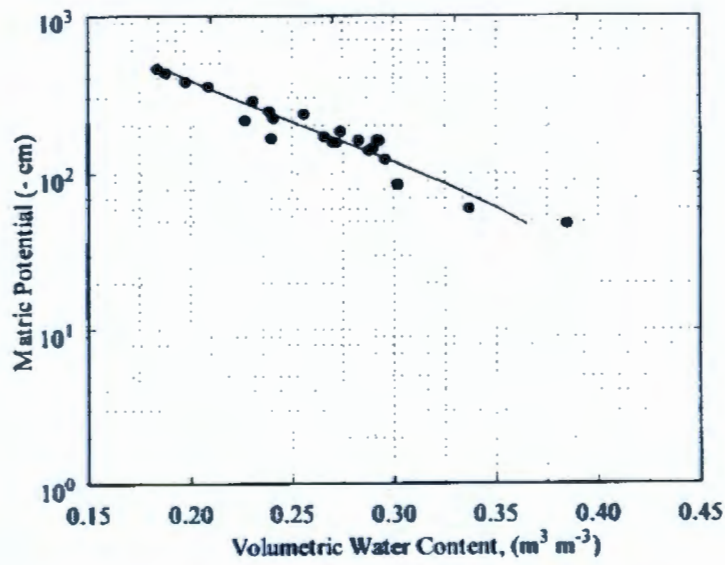


Figure 8. Fitted and observed field-averaged moisture characteristic function for the 25-50 cm depth.

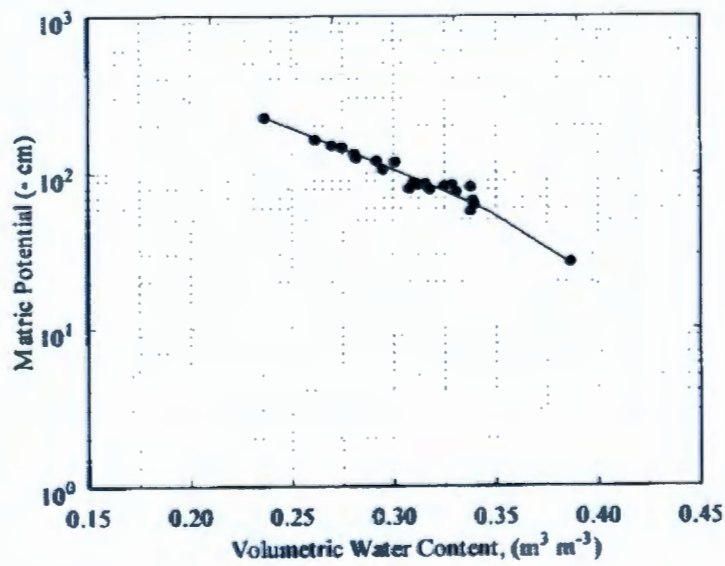


Figure 9. Fitted and observed field-averaged moisture characteristic function for the 50-75 cm depth.

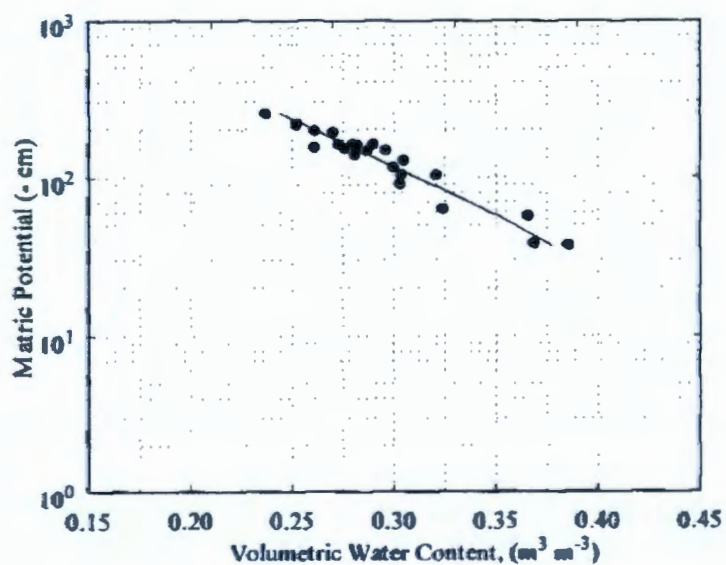


Figure 10. Fitted and observed field-averaged moisture characteristic function for the 75-100 cm depth.

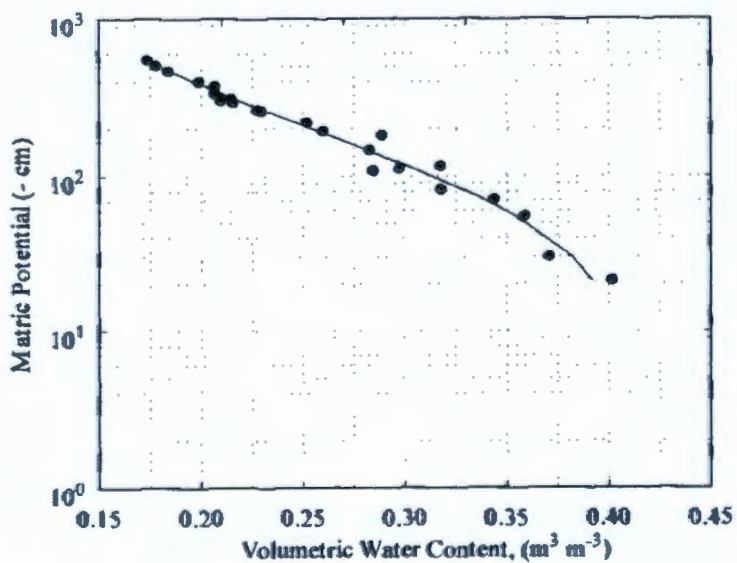


Figure 11. Fitted and observed field-averaged moisture characteristic function for the 100-125 cm depth.

Table 1. A comparison of Fitted Moisture Retention Parameters.

Sample	Depth (m)	Fitted Parameters				Measured K_s (cm s^{-1})
		θ_r	θ_s	α (cm^{-1})	n	
1 ^(a)	1.5	0.0187	0.4131	0.148	1.309	5.73×10^{-4}
2	1.5	0.0336	0.3367	0.0211	1.536	5.73×10^{-4}
299-E24-95 ^(b)	1.83	0.000	0.3550	0.0061	1.538	1.40×10^{-4}
Task 4b ^(c)	0-0.25	0.007	0.3566	0.1554	1.724	Not measured
	0.25-0.50	0.007	0.3863	0.0741	1.595	Not measured
	0.50-0.75	0.029	0.4215	0.0381	2.468	Not measured
	0.75-1.0	0.035	0.4083	0.0355	2.036	Not measured
	1.0-1.5	0.024	0.3980	0.0290	2.497	Not measured
Task 4c ^(d)	0-0.25	0.00	0.3172	0.0015	2.024	8.37×10^{-4}
	0.25-0.50	0.00	0.4163	0.0162	1.400	Not measured
	0.50-0.75	0.00	0.4164	0.0139	1.419	Not measured
	0.75-1.0	0.00	0.4403	0.0256	1.303	Not measured
	1.0-1.25	0.00	0.4089	0.0127	1.433	Not measured
	Plot Avg.	0.00	0.4117	0.015	1.390	Not measured

(a) Khaleel and Freeman (1995), from the former Grout Site, on the east side of the 200E Area.

(b) Khaleel et al., (1995), one of 15 repacked, 5.1-cm diameter cores.

(c) Surface sediments values are plot averages for each depth interval with 24 samples.

(d) This experiment, values are plot averages for each depth interval with 24 samples.

parameters fitted for each depth. The van Genuchten parameters θ_r , α , n , and θ_s were all fitted and are summarized in Table 1. Table 1 also compares these results with those from the surface sediments and from a set of independent measurements conducted on cores.

The results from this study (Task 4c) compare reasonably well with the previous results, falling within the range of values observed on samples 1 and 2 from the former Grout Site (Khaleel and Freeman, 1995). However, the fitted parameters suggest soil of a somewhat finer texture than expected for this site. As further verification of the field-measured properties, soil samples were taken from the pit on completion of the infiltration experiments and an analysis of particle sizes performed in the laboratory. Results of the analysis show a mean distribution 70.6% sand, 17.7% silt and 11.6% clay. The high silt and clay content may explain the low values of n and α observed in this study.

Solute Transport Parameters

Figure 12 shows the TDR-measured relative mass flux, $M(t)$, at $L=0.25$ m. The variability in transport, even at such a shallow depth is clear. This behavior is consistent with the variability in water flux density and K_s , observed at the surface.

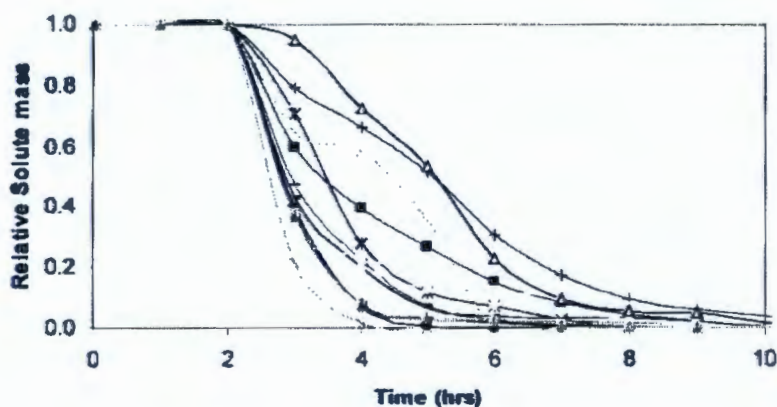


Figure 12. Spatial variability in TDR-measured relative solute mass flux at a depth of 0.25 m. Twenty four measurements were obtained along a 5 m transect at 0.20 m intervals.

Figure 13 shows an example of the observed data, and the fitted results obtained with the CDE and CLT transport models. In both cases, the models diverge from the observed data at late time ($t \geq 5$ hrs), leading to a higher predicted dispersion coefficient and travel-time variance. Although the discrepancy is not large, it suggests that these models may not be the most appropriate for predicting field-scale solute transport.

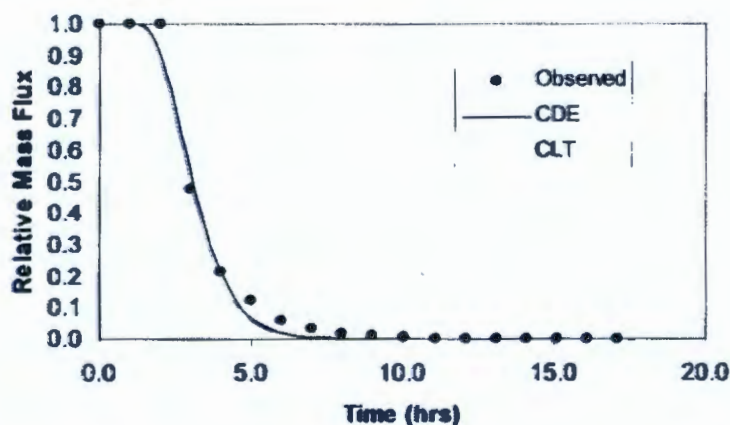


Figure 13. Example of $M_L(t)$ and the least squares fit of the convective dispersion equation (CDE) and convective lognormal transfer function (CLT) models.

Figure 14 shows an example of the solute travel time probability density function obtained by taking the first derivative of an $M(t)$ curve. Theoretically, the area under $f_L(t)$ should equal exactly 1.0, provided all of the solute mass applied can be accounted for. In most cases, the value was less than 1.0, suggesting that either some of the solute may have moved beyond the measurement depth without being detected (preferential flow); moved laterally; or experienced some other delay in vertical transport. The long tails observed in Figure 12 support the hypothesis of delayed vertical movement. The results of the transport analysis are summarized in Table 2.

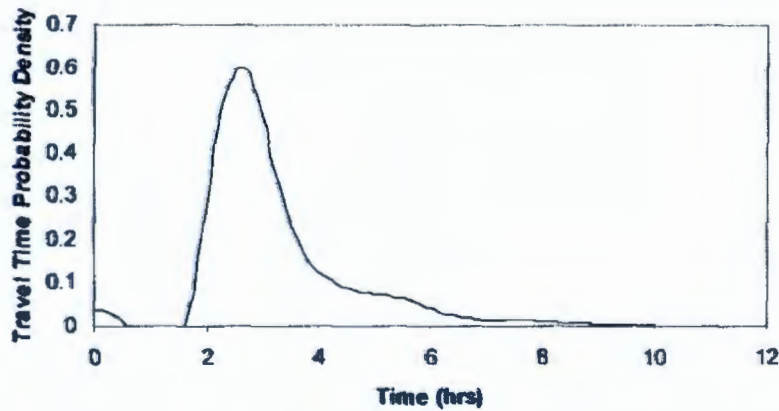


Figure 14. Solute travel time probability density function obtained by taking the first time derivative of the relative mass flux shown on Figure 13.

Table 2. Parameter estimates for the upper Hanford Formation from field transport experiments. D and v are the dispersion coefficient and pore water velocity of the convective dispersion equation (CDE); μ_p and σ_p are the population mean and variance of the convective lognormal transfer function (CLT); M_1 and M_2 are the expected travel time and travel time variance obtained by moment analysis; and λ_{CDE} , λ_{CLT} and λ_{MOM} are the dispersivities obtained by the three techniques.

L	θ_c	CDE				CLT			MOM		
		D	v	λ_{CDE}	t_L	μ_p	σ_p	λ_{CLT}	M_1	M_2	λ_{MOM}
m	m^3/m^3	cm^2/h	cm	cm	h	h	h^2	cm	h	h^2	cm
0.25	0.331	10.79	8.14	1.32	3.07	3.23	0.106	1.39	3.43	1.98	2.03
0.50	0.312	11.74	8.64	1.36	5.78	5.95	0.056	1.44	6.03	3.88	2.67
0.75	0.294	42.40	9.18	4.62	8.17	8.29	0.12	4.79	8.44	9.59	5.05
1.00	0.283	66.61	9.54	6.98	10.48	10.75	0.137	7.32	10.85	16.88	7.17
1.25	0.283	66.04	9.54	6.92	13.10	13.78	0.112	7.44	13.95	24.32	7.81

Generally the CDE and CLT models predict the same average transport velocity, but differ in their predicted dispersion or degree of solute spread. A useful comparison of the CDE and CLT

has been given in terms of the existence or absence of correlated travel times with depth (Jury, 1982). For uncorrelated flow, the CDE predicts a linear increase in travel time variance with depth. For correlated flow, the CLT predicts an increase in travel time variance as the square of the distance. By comparing the results of the analysis, conclusions can be made on the appropriateness of different transport models.

The CDE, CLT and moment analysis shows reasonably good agreement in the transport parameters. All three methods predict essentially the same mean travel times to the depths of interest. Travel time was linear with depth, except for a small decrease (increase in v) that corresponded to a decrease in θ_c . This is probably due to increasing coarseness of the soil with depth.

The change in travel time variance with depth show that M_2 at the 0.50-m depth was 2 times that at the 25-cm depth, while M_2 at 100 cm was 4 times that at 50 cm. The 2x increase from 25 cm to 50 cm does not meet the criterion for correlated flow required by the CLT model but satisfies the 2x increase required for uncorrelated flow described by the CDE (Jury, 1982). In general, a 4x increase in variance requires constant velocity with depth, which does not exist initially, but becomes more so at greater depth. A CDE approach would be appropriate for modeling transport in this soil.

Table 2 also shows generally good agreement in the dispersivities obtained with the two models. However, λ_{MOM} was almost double the α_{CDE} and α_{CLT} , particularly at the smaller depths. The higher λ_{MOM} values reflect the larger travel time variance used in their derivation. Nevertheless, the range $1.32 \geq \lambda \geq 2.67$ cm observed in the shallow depths is comparable to the $0.01 \geq \lambda \geq 2.0$ cm reported for unconsolidated cores by Freeze and Cherry (1979). Another point worth noting is the increase in λ with depth down to 0.75 m, after which it essentially becomes constant. This result is consistent with the concept of a scale-dependent dispersivity and suggests for vertical transport in this soil, the scale over which λ becomes constant may be smaller than predicted from literature values obtained from horizontal transport in the saturated zone. With respect to upscaling and the extrapolation of data from one site to the next, these observations suggest a need for site-specific transport measurements at a range of scales and concomitant measurements of $\psi(\theta)$ in the same transport volume.

Summary and Conclusions

Field-measured hydraulic properties have been shown to be more representative of natural flow and transport processes but are generally difficult to measure. In this study, it was shown that vertically-installed time domain reflectometry (TDR) probes, when combined with a sprinkler-imposed constant flux system, can be used to measure the spatially variable hydraulic properties. The infiltration rate, when combined with the measured equilibrium water content and matric potential, provide direct measurements of the moisture characteristic function, $\psi(\theta)$, and the unsaturated hydraulic conductivity function, $K(\theta)$ at the field scale.

A series of infiltration tests were conducted at the site of the proposed LLTWDS during the summer of 1998. Measurements of K_s were made using a tension infiltrometer. The spatial distribution of K_s and water flux density determined from water storage measurements appear to be related to micro-topography and root channels.

Saturated water content and the other van Genuchten parameters, α , n , and θ_r were fitted with the program RETC. The goodness of fit was generally good with coefficients of determination (r^2) all exceeding 0.95.

The fitted mean saturated water content ranged from $0.3172 \text{ m}^3 \text{ m}^{-3}$ to $0.440 \text{ m}^3 \text{ m}^{-3}$, increasing slightly with depth. Neither the fitted α nor n showed any dependence on depth. Both parameters were less variable than those observed for the surface sediments.

Solute transport parameters were also obtained from field measurements using KCl as a tracer. Analysis of the data using the traditional CDE and the less common CLT models, as well as with moment analysis, showed reasonably good agreement in the transport parameters. The three methods predicted the same mean travel times. Fitted dispersivities also showed good agreement between methods and are within the range observed on unconsolidated cores. Dispersivity also increased with depth down to 0.75 m, after which it essentially became constant. This result suggests a scale-dependent dispersivity, which in this soil appears to be somewhat smaller than predicted from measurements in the saturated zone.

This test has resulted in a data set that can be used in the development of a catalogue of hydraulic and transport properties, one that will be amenable to geostatistical analysis and will facilitate the testing of upscaling theories. Comparisons of the data from this study with those from previous studies show remarkable similarity.

References

- Acton, F. S. 1966. Analysis of straight-line data. Dover Publications Inc. New York., pp 224-229.
- Freeze, R. A., and J. A. Cherry. 1979. Groundwater. Prentice Hall, NJ.
- Jury, W.A., 1982. Simulation of solute transport using a transfer function. *Water Resour. Res.* 38:363-368.
- Kachanoski, R.G., C. Hamlin, and I. J. van Wesenbeeck. 1990. Spatial variability of water and solute flux in a layered soil. *In* Roth, K., H. Fluhler, H., W. A. Jury, and J. C. Parker (Eds.) *Field-scale water and Solute Flux in Soils*, . Birkhauser Verlag, Basel.

Kachanoski, R. G., A. L. Ward, and I. J. van Wesenbeeck, 1994. Measurement of Transport Properties at the Field Scale. Transactions of the 15th World Congress of Soil Science. Vol. 2a:106- 126.

Khaleel, R, and E. J. Freeman, 1995. Variability and scaling of hydraulic properties for 200 Area soils, Hanford Site. WHC-EP-0883, Westinghouse Hanford Company, Richland, Washington.

Khaleel, R., J. F. Relyea, and J. L. Conca. 1995. Evaluation of van Genuchten-Maulem relationships to estimate unsaturated hydraulic conductivity at low water contents. *Water Res. Resour.* 31:2659-2668.

Parkin, G.W., D. E. Elrick, and R. G. Kachanoski. 1992. Cumulative storage of water under constant flux infiltration: Analytical solution. *Water Resour. Res.* 28:2811-2818.

Snedecor, G.W., and W.G. Cochran. 1980. Statistical methods. Iowa State University Press, Iowa, 507 pp.

van Genuchten, M. Th., 1980. A closed form equation for predicting the hydraulic conductivity of unsaturated soils. *Soil Sci. Soc. Am. J.* 44: 892-989.

van Genuchten, M. Th., F. J. Liej, and S.R. Yates. 1991. The RETC code for quantifying the hydraulic functions of unsaturated soils. EPA/6000/2-91/065. 93 pp. R.S. Kerr Environ. Res. Lab., U.S. Environmental Protection Agency, Ada, OK.

Ward, A.L., R.E. Clayton and J.C. Ritter. 1997. Fabrication and Testing of an Integrated Soil Water Content-Matric Potential Probe. A letter report for activity SIW03490 submitted to the Lockheed Martin Hanford Company, September 1997.

Ward, A.L., R.E. Clayton and J.C. Ritter. 1998. Hanford Low-Activity Tank Waste Performance Assessment Activity: Determination of In Situ Hydraulic Parameters of Hanford Sediments A letter report for activity Task 4b submitted to the Lockheed Martin Hanford Company, September 1998.

Zhang, R., 1997. Infiltration models for the disc infiltrometer. *Soil Sci. Soc. Am. J.* 61:1597-1603

APPENDIX D

**Physical and Hydraulic Measurements of FY1998 Clastic Dike
Samples**

Physical and Hydraulic Measurements of FY 1998 Clastic Dike Samples

MJ Fayer and JS Ritter
19 March 1999

Introduction

Pacific Northwest National Laboratory (PNNL) assists the Lockheed Martin Hanford Company (LMHC) in designing and assessing the performance of disposal facilities for radioactive wastes stored in single and double shell tanks at the Hanford Site. To predict contaminant migration from these facilities requires estimates of the physical and hydraulic properties of sediments within the vadose zone beneath and around the disposal facility. An unusual feature of the Hanford Site is the presence of vertical sediment structures known as clastic dikes in all of the major lithologies of the unsaturated zone. Fecht et al. (1998)¹ discussed dike structure and etiology and summarized some of the measurements that have been made.

Because clastic dikes could impact the performance of the ILAW disposal site, a work plan was prepared that provides details on the measurement and analysis of clastic dikes (Khaleel 1998)². As part of the work plan, a PNNL task was initiated, entitled "Hydraulic Property Lab Tests for ILAW Samples." One objective of this task is to provide the measured data for clastic dike samples. Samples were obtained in fiscal year 1998 for characterization. The objective of this letter report is to document the physical and hydraulic properties of the clastic dike samples.

Properties

Physical and hydraulic properties are required for the clastic dike samples and the samples of the surrounding matrix. Multiple measurements of these properties are required to give some estimate of the degree of variability within each geologic material. The properties are:

Particle Size Distribution. Particle size distribution (PSD) refers to the fractions of the various particle-size classes (e.g., the fraction of particles with diameters between 1 and 2 mm).

Particle Density (ρ_p). Particle density is the mass of the sediment or construction material particles per unit volume of the same sediment or material. This property is used to relate the bulk density to the porosity.

Bulk Density (ρ_b). Bulk density is the mass of oven-dry material per unit bulk volume. The unit bulk volume is the combined volume of material, water, and air prior to oven drying.

Porosity (ϕ). Porosity is the volume of voids per unit bulk volume.

¹ Fecht, KR, KA Lindsey, BN Bjornstad, DG Horton, GV Last, and SP Reidel. "An atlas of clastic injection dikes of the Pasco Basin and Vicinity," BHI-1103 Draft A, Bechtel Hanford Inc., May 1998.

² Khaleel R, January 1998. "Work plan for measurement and analysis of hydraulic properties for clastic dikes and the ILAW Borehole No. 1 sediment samples," Fluor Daniel Northwest, Inc., P.O. Box 1050, Richland, Washington.

Water Retention. Water retention refers to the retention of water by the sediment at various matric potentials. Mathematical functions are fit to the retention data and the resulting parameters are used directly in computer models for predicting water and contaminant movement. Numerous functions are available, but the van Genuchten function is most commonly used:

$$\theta = \theta_r + (\theta_s - \theta_r) \left[1 + (\alpha h)^n \right]^{-m}$$

where θ_s = saturated water content (cm^3/cm^3)
 θ_r = residual water content (cm^3/cm^3)
 h = matric potential (-cm)
 α, n, m = empirical fitting parameters (α units are $1/\text{cm}$; n and m are dimensionless)

Typically, m is approximated as $m = 1 - 1/n$

Saturated Hydraulic Conductivity (K_s). Saturated hydraulic conductivity is the proportionality constant in the Darcy equation that relates the flux density to a unit potential gradient.

Unsaturated Hydraulic Conductivity [$K = f(\theta, \psi)$]. Unsaturated hydraulic conductivity is the proportionality factor in the Richards equation that relates the flux density to a unit potential gradient at a specific water content. Because the water content varies in the unsaturated zone, the unsaturated conductivity varies also.

Mathematical functions are used to represent the unsaturated conductivity data; these functions are typically estimated using the water retention functions and saturated conductivity. When measured unsaturated conductivity values are available, the conductivity and retention data can be fit to optimize both the retention and conductivity functions. Several functions are available, but the Mualem conductivity function is most commonly used (in conjunction with the van Genuchten retention function, assuming $m = 1 - 1/n$):

$$K = K_s \frac{\left\{ 1 - (\alpha h)^{n-1} \left[1 + (\alpha h)^n \right]^{-m} \right\}^2}{\left[1 + (\alpha h)^n \right]^{2m}}$$

The K_s value and the pore interaction term (ℓ) are the only requirements for this model. The parameter ℓ is typically assigned a value of 0.5.

Clastic Dike Samples

In March 1998, grab samples were collected from clastic dikes near the towns of Touchet and Lowden, WA (sites identified by Fecht et al. as No. 64 Touchet Road and No. 76 West Lowden). These samples were processed only for particle density and size distribution because of their small size and disturbed nature.

In September 1998, core samples were collected from a clastic dike and surrounding matrix at the Goose Egg site described by Fecht et al. (1998); this site is 6.3 km south-southwest of the ILAW Disposal Site. Two-foot long core liners were constructed from 3.0 in. ID PVC. One end of each liner was sharpened and placed on selected spots, either on a dike or the matrix. A sledge hammer was used to sink the liner into the sediment. The liners did not penetrate very easily and we could see broken, loose material on the top of the sample. The liners were brought back into the laboratory and sectioned into 6-in. lengths, starting with the sharpened end, which was deepest and least affected by the disturbance at the top of the liner. A total of seven undisturbed sections of these lined cores were identified as suitable for testing. All cores were taken from near surface (< 1 m) deposits within 10 m of Army Loop Road. Table 1 lists the sample numbers, depths, and diameters.

Methods

The core samples were tested with the multistep and steady-state methods, then sectioned for the tests of particle size distribution, particle density, and water retention using pressure plates and vapor adsorption. The cores were prepared for the multistep and steady-state tests according to the procedures described by Fayer et al. (1998)³.

Procedures

Table 2 lists the procedures used to analyze the samples. Additional details for each procedure are discussed below. These additional details are almost exactly the same as those used by Fayer et al.

Particle Density. Two replicates of the particle density test were performed using the pycnometer method (Blake and Hartge 1986a). The Touchet and Lowden sample size was 10 g. For the Goose Egg samples, the entire core was homogenized following the bulk density test. Of this loose material, 8 to 28 g was used for the particle density test. The only deviation was for sample 4A. Because it was so heterogeneous, sample 4A was sub-sampled in three distinctly different regions. Each subsample was tested for particle density.

³ Fayer MJ, AL Ward, JS Ritter, and RE Clayton, 1998. "Physical and hydraulic measurements of FY 1998 borehole cores," Letter Report to Mr. Fred Mann, Fluor Daniel Northwest, September 10, 1998.

Table 1. Clastic dike samples analyzed in fiscal year 1998.

Sample ID	Description of Sample	Core Internal Diameter in.	Location of Clastic Dike
1h	infill	na	Touchet
2h	infill	na	Touchet
3h	infill	na	Touchet
4h	infill	na	Touchet
5h	silt/clay skin	na	Touchet
6h	silt/clay skin	na	Touchet
7h	infill	na	Lowden
8h	matrix	na	Touchet
1	matrix, some dike/sand bands	3.0	Goose Egg Hill Site
2A	matrix	3.0	Goose Egg Hill Site
2B	matrix	3.0	Goose Egg Hill Site
3A	dike/matrix mix	3.0	Goose Egg Hill Site
3B	dike/matrix mix	3.0	Goose Egg Hill Site
4A	mostly dike	3.0	Goose Egg Hill Site
4B	mostly matrix, some dike	3.0	Goose Egg Hill Site

Table 2. Procedures for measuring physical and hydraulic properties.

Number	Title	Comment
PNL-MA-567, SA-2	Sieve Procedure	For materials > 50 μm effective diameter
PNL-MA-567, SA-3	Particle-Size Analysis	Hydrometer method for materials < 50 μm effective diameter
PNL-MA-567, SA-4	Constant Head Hydraulic Conductivity (HC)	Laboratory measurement for materials with $\text{HC} > 10^{-6}$ cm/s
PNL-MA-567, SA-5	Falling Head--Saturated Hydraulic Conductivity (HC)	Laboratory measurement for materials with $\text{HC} < 10^{-6}$ cm/s
PNL-MA-567, SA-6	Water Retention Procedure	Laboratory method for core or bulk sample (saturation to air dry)
PNL-MA-567, SA-7	Water Content	Necessary for constant head hydraulic conductivity
PNL-MA-567, SA-8	Clod Density/Bulk Density	Necessary for constant head hydraulic Conductivity
PNL-MA-567, SA-9	Determining Particle Density	Necessary for constant head hydraulic conductivity
Klute (1986)	Water Retention: Laboratory Methods	Pressure plate and vapor adsorption methods
Klute and Dirksen (1986)	Hydraulic Conductivity and Diffusivity: Laboratory Methods	Steady-state flux control method for unsaturated conductivity
Eching and Hopmans (1993)	Unsaturated Hydraulic Properties	Multistep outflow method for unsaturated conductivity and water retention estimation

Particle Size Distribution. The PSD test was performed using the methods ASTM 1985 and Gee and Bauder (1986). The Touchet and Lowden sample size was 40 g. For the Goose Egg samples, the entire core was homogenized following the bulk density test. Of this loose material, 80 g was used for the particle size distribution test. The only deviation was for sample 4A. Because it was so heterogeneous, sample 4A was sub-sampled in three distinctly different regions (as mentioned previously). Each subsample was tested for particle density.

Bulk Density. A single measurement of bulk density was made for each intact Goose Egg core. Following the conductivity test, the sediment in the core was oven dried and weighed. Dividing this weight by the volume of the core yielded the bulk density, as per the method of Blake and Hartge (1986b).

Porosity. A single estimate of porosity was made using the bulk density of intact Goose Egg cores and the average particle density. The formula used was $\phi = 1 - \rho_b / \rho_s$ (Freeze and Cherry 1979).

Water Retention. Water retention data for the Goose Egg samples were measured using the pressure-plate extraction and vapor equilibrium methods described by Klute (1986). The tests were conducted on the subsample created after the bulk density core was homogenized. For sample 4A, separate tests were conducted for the three subsamples mentioned previously. Additional retention measurements were obtained during the unsaturated conductivity tests.

Saturated Hydraulic Conductivity. Saturated hydraulic conductivity for the Goose Egg cores was measured on the intact cores prior to the unsaturated conductivity tests using the method of Klute and Dirksen (1986). The measurement of saturated conductivity was conducted several times to verify that a steady value of conductivity was achieved.

Unsaturated Hydraulic Conductivity. The multistep and steady state methods were used to measure unsaturated conductivity of the Goose Egg cores. Both methods were performed on the same core using the same sensor locations. The multistep method, which is an improvement of the one-step method of Kool et al. (1985 a,b), provides $\theta-\psi$ pairs and cumulative outflow. These data were used in conjunction with the SFOPT program (a modified version of the MULSTP program of Eching and Hopmans 1993) to determine the optimal set of hydraulic parameters.

Because several tests must be performed on the same core, the following test sequence was established: saturated conductivity, multistep unsaturated conductivity, and steady state unsaturated conductivity. Following the saturated conductivity test, the cores were re-wetted to saturation and analyzed using the multistep method. After equilibrating the cores with zero pressure at the lower plate, three pressure increments were used that were equivalent to head values of 10.9, 71, and 315 cm. Following the multistep test, the cores were rewetted and tested using the steady-state method.

Results

When opened for the bulk density measurements, several cores had noticeable layering. The most dramatic layering occurred in sample 4A, in which it appeared that most of the sample was fine-textured dike material. Three sections of this core were sub-sampled for individual tests of particle density and size distribution, and water retention. These samples are referred to as 4A1, 4A2, and 4A3 in Tables 3, 4, 6, and 7.

Table 3 shows that particle density varies between 2.65 and 2.73 g/cm³ for the various infill, clay skin, and matrix materials. There appears to be no distinction between infill, skin and matrix in the two locations studied. The particle densities of the three subsamples of 4A are identical.

Table 4 shows the results for both the sieve and hydrometer methods. In all samples, the gravel content was less than 1%. Figure 1 shows all of the data combined to highlight the degree of variability in particle size distribution. Included in Figure 1 are the distributions for dune sand from the southern edge of the ILAW site and sandy gravel from the Grout spoils pile. The clay skins and dike material have the finest particle size distribution. The infill material has a predominance of sand particles between 100 and 200 μm diameter, as does dune sand. Almost all of the infill material particles sizes are less than 500 μm , whereas about 20% of the dune sand particles are greater than 500 μm . The particle size distributions of the subsamples within 4A showed sand contents varying from 42 to 90%. These differences help to explain the water retention differences discussed below.

Table 5 shows that the bulk density ranged from 1.46 to 1.57 g/cm³. Table 5 also shows the porosity data, which ranged from 0.424 to 0.464. These ranges are smaller than the variations observed by Fayer et al. for the FY 1998 ILAW borehole samples.

Table 6 shows the pressure plate data for four pressures. As expected, samples that had dike material had higher water contents at any given pressure. Within 4A, water content varied between 0.04 and 0.155 cm³/cm³ at a matric potential of -530 cm, and 0.024 and 0.089 cm³/cm³ at a matric potential of -4080 cm. These differences are large and will make it challenging to represent the properties of the entire core with the properties measured at discrete locations.

Table 7 shows that the vapor adsorption data covered a range of matric potential from -11,600 cm to as dry as -1,460,000 cm. The associated water contents ranged from 0.08 to 0.004 g/g. Most of the measurements are in the very low potential range. There are very few measurements in the range from -10,000 to -100,000 cm.

Table 8 shows the saturated hydraulic conductivity values for the Goose Egg Hill cores range from 1.8×10^{-4} to 5.4×10^{-3} cm/s. The matrix samples generally had the highest values. The results in Table 8 are consistent with other measurements. For the matrix at their dike sites, Fecht et al. measured K_s values that mostly ranged from 1 to 4×10^{-3} cm/s. The one sample that was different had a K_s value of 2×10^{-5} cm/s. This particular sample was measured with a different technique (i.e., the unsaturated flow apparatus, or UFA). For samples with various amounts of dike material and clays skins, Fecht et al. measured K_s values ranging from 5×10^{-5}

to 9×10^{-4} cm/s. The values in Table 8 fall within this range. Most of the values also fall within the lower portion of the range of values reported by Fayer et al. for the FY 1998 ILAW borehole samples. The lowest value in Table 8 (1.8×10^{-4}) is only slightly lower than the lowest ILAW borehole value (2.6×10^{-4}).

Table 9 shows the parameter estimates and fitting statistics determined using the SFOPT program with data from the multistep test. The parameter α varied from 0.0092 to 0.0839, a factor of about 10, and the parameter n ranged from 1.33 to 2.49. These ranges seemed small given the presence of fine-grained zones in some samples, but the statistics indicated reasonable fits to the data.

Some additional fitting tests were performed. To demonstrate the impact of the location of the tensiometer, sample 2A was refitted using the upper rather than lower tensiometer data. Of all the samples, sample 2A had the greatest differences in tension (about 40 cm) between the two tensiometer locations. The refitting reduced α by half (to 0.0342 cm^{-1}) and increased n by 33% (to 2.63). The R^2 was actually improved (from 0.747 to 0.894) and the mass error was reduced (from 1.51 to 0.59%). Outflow data represent the response of the entire sample, whereas the matric potential data are derived from a sample volume that could almost be considered a point. An assumption of the fitting process is that the material is homogeneous. With clastic dikes, the samples are not homogeneous, so point measurements are more likely to deviate from the expected values. The results from refitting sample 2A using the upper tensiometer data illustrate the parameter differences that could be encountered by using tension measurements elsewhere in the column. The matric potential sets from the other samples were much closer in value, so the differences in fitting results (between using the upper versus lower tensiometer data) should not be so large.

An additional fitting exercise was performed to demonstrate the impact of weighting the data. In this exercise, the matric potential and water retention weights were progressively reduced from 1.0 to 0.0 for sample 2A using the upper and lower tensiometer data. Figure 2 shows the sensitivity of the parameter estimates to the weighting used. Because tension is a point measurement, we may want to consider reducing the weight given to such data. One solution may be to weight the tension data according to the fraction of the sample volume that it measures.

The same fitting exercise using variable weighting was also performed for sample 3A using just the lower tensiometer data. The results were similar for most weights. The only exception was a weight of 0.0, which caused the program to terminate without a solution. In this case, the outflow data were not sufficient to allow the program to find an optimal solution.

Table 10 shows the $\theta\text{-}\psi\text{-}K$ triplets that were generated using the steady state method. All of the measurements are at matric potentials above -54 cm. Even so, unsaturated conductivity values were 1 to 2 orders of magnitude less than the saturated values. Because the potentials were so high, the water contents were also relatively high.

Summary

Samples were collected from clastic dike sites in the Columbia Basin in September 1998 and analyzed for physical and hydraulic properties. Eight disturbed samples were obtained from two sites in the towns of Touchet and Lowden, Washington. Seven undisturbed cores were obtained from a site near Goose Egg Hill, which is located 6.3 km SW of the ILAW site. Testing included particle density, particle size distribution, bulk density, water retention, and saturated and unsaturated conductivity. Saturated conductivity values were similar to values reported by Fecht et al. for other clastic dike samples. The samples exhibited some variability but not as much as reported by Fayer et al. for the ILAW borehole samples. The impacts of tensiometer location and data weighting were demonstrated.

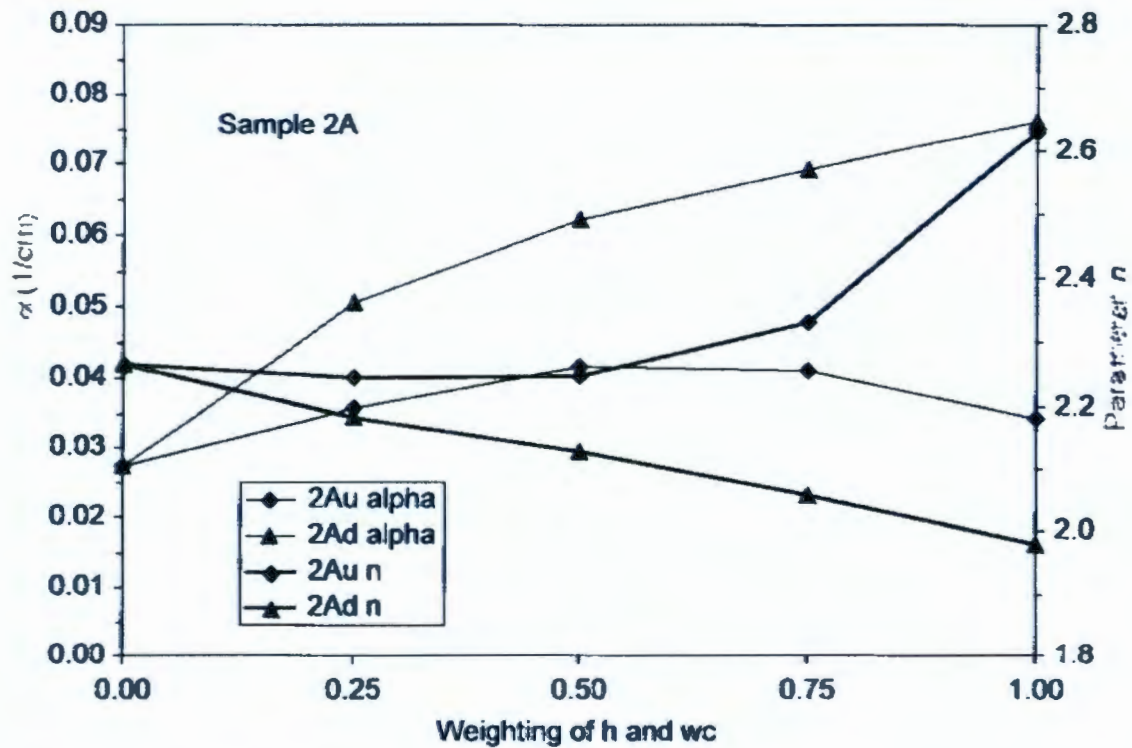


Figure 2. Effect of data weighting on prediction of parameters α and n .

Table 3. Particle density

Sample	Particle Density rep 1 (g/cm^3)	Particle Density rep 2 (g/cm^3)	Average Particle Density, g/cm^3
1h	2.668	na	2.67
2h	2.677	na	2.68
3h	2.708	na	2.71
4h	2.698	na	2.70
5h	2.695	na	2.70
6h	2.651	na	2.65
7h	2.719	na	2.72
8h	2.681	na	2.68
1	2.729	2.734	2.73
2A	2.707	2.709	2.71
2B	2.713	2.709	2.71
3A	2.720	2.720	2.72
3B	2.722	2.722	2.72
4A1	2.717	2.730	2.72
4A2	2.720	2.727	2.72
4A3	2.720	2.727	2.72
4B	2.713	2.733	2.72

Table 4. Particle size distribution

Sample 1h		Sample 2h		Sample 3h		Sample 4h	
Particle Diameter (μm)	% Less Than Diameter	Particle Diameter (μm)	% Less Than Diameter	Particle Diameter (μm)	% Less Than Diameter	Particle Diameter (μm)	% Less Than Diameter
2000	100.0	2000	100.0	2000	100.0	2000	100.0
1000	100.0	1000	100.0	1000	100.0	1000	100.0
500	100.0	500	99.9	500	100.0	500	100.0
250	99.9	250	99.9	250	92.3	250	99.9
106	87.5	106	98.3	106	44.7	106	85.6
75	66.5	75	91.7	75	34.7	75	60.6
53	40.3	53	58.2	53	22.8	53	34.0
52.2	37.5	49.0	60.0	54.1	17.5	52.7	30.0
31.0	25.0	30.8	27.5	31.6	12.5	31.1	20.0
17.3	17.5	17.4	15.0	17.4	10.0	17.3	12.5
10.0	15.0	10.1	12.5	10.1	7.5	10.1	10.0
7.1	12.5	7.2	10.0	7.1	7.5	7.1	10.0
5.8	12.5	5.8	10.0	5.9	5.0	5.8	10.0
5.1	12.5	5.1	10.0	5.1	5.0	5.0	10.0
1.5	7.5	1.5	7.5	1.5	5.0	1.5	7.5

Sample 5h		Sample 6h		Sample 7h		Sample 8h	
Particle Diameter (μm)	% Less Than Diameter	Particle Diameter (μm)	% Less Than Diameter	Particle Diameter (μm)	% Less Than Diameter	Particle Diameter (μm)	% Less Than Diameter
2000	99.9	2000	100.0	2000	99.8	2000	100.0
1000	99.9	1000	100.0	1000	98.3	1000	99.9
500	99.9	500	100.0	500	90.3	500	99.7
250	99.9	250	100.0	250	42.3	250	99.4
106	98.0	106	99.7	106	18.0	106	93.7
75	94.3	75	99.4	75	15.7	75	81.4
53	84.9	53	97.8	53	13.3	53	48.7
46.6	75.0	44.2	95.0	54.5	12.5	50.6	47.5
27.9	62.5	26.4	85.0	31.5	12.5	31.1	22.5
15.9	47.5	15.3	67.5	17.4	7.5	17.5	10.0
9.6	32.5	9.2	52.5	10.1	7.5	10.2	7.5
6.8	27.5	6.7	42.5	7.1	6.2	7.2	7.5
5.6	25.0	5.5	37.5	5.8	5.0	5.9	7.5
4.9	22.5	4.8	35.0	5.1	5.0	5.1	7.5
1.5	10.0	1.4	17.5	1.5	5.0	1.5	5.0

Table 4. (cont.) Particle size distribution

Sample 1		Sample 2A		Sample 2B		Sample 3A	
Particle Diameter (μm)	% Less Than Diameter	Particle Diameter (μm)	% Less Than Diameter	Particle Diameter (μm)	% Less Than Diameter	Particle Diameter (μm)	% Less Than Diameter
2000	99.7	2000	100.0	2000	100.0	2000	100.0
1000	98.3	1000	100.0	1000	100.0	1000	100.0
500	93.2	500	99.9	500	99.9	500	99.6
250	83.5	250	95.7	250	96.1	250	89.8
106	38.9	106	17.5	106	12.0	106	35.1
75	30.8	75	7.3	75	5.9	75	18.4
53	25.6	53	4.5	53	4.2	53	10.5
51.3	24.8	56.7	5.6	56.6	6.0	55.1	11.3
30.7	17.9	32.9	4.8	32.8	5.0	32.6	5.6
17.2	13.8	18.0	4.4	18.0	4.0	18.0	4.4
10.1	10.6	10.4	4.0	10.4	3.5	10.4	4.0
7.2	8.8	7.4	3.8	7.4	3.5	7.4	3.5
5.9	8.8	6.0	3.8	6.0	3.5	6.0	3.1
5.1	8.5	5.2	3.5	5.2	2.8	5.2	2.8
1.5	4.8	1.5	3.5	1.5	2.5	1.5	2.5

Sample 3B		Sample 4A1		Sample 4A2		Sample 4A3	
Particle Diameter (μm)	% Less Than Diameter	Particle Diameter (μm)	% Less Than Diameter	Particle Diameter (μm)	% Less Than Diameter	Particle Diameter (μm)	% Less Than Diameter
2000	99.7	2000	100.0	2000	99.9	2000	99.8
1000	99.4	1000	99.9	1000	99.8	1000	99.6
500	98.6	500	99.8	500	99.7	500	99.4
250	90.4	250	93.6	250	98.2	250	97.1
106	44.4	106	13.9	106	71.5	106	60.3
75	25.6	75	9.6	75	63.0	75	50.6
53	18.8	53	7.4	53	56.1	53	42.8
53.2	18.8	56.0	7.5	45.2	47.0	46.9	41.3
31.8	11.3	32.4	6.9	28.3	34.1	28.7	31.3
17.7	7.5	17.9	5.6	16.2	25.7	16.5	22.5
10.3	6.5	10.3	4.8	9.6	21.3	9.8	16.5
7.3	5.0	7.3	4.0	nd	nd	7.0	15.0
6.0	5.0	6.0	3.8	5.7	13.8	5.8	12.5
5.2	4.8	5.2	3.8	5.0	13.8	5.0	12.3
1.5	3.5	1.5	3.1	1.5	7.5	1.5	7.5

Table 4. (cont.) Particle size distribution

Sample 4B	
Particle Diameter (µm)	% Less Than Diameter
2000	100.0
1000	99.8
500	99.1
250	64.8
106	8.1
75	6.0
53	4.9
56.3	6.3
32.8	4.4
18.0	3.8
10.4	3.1
7.4	3.1
6.0	2.8
5.2	2.8
1.5	2.5

Figure 1. Summary of particle size distributions for all samples, along with dune sand from the ILAW site and sandy gravel taken from the Grout Spoils pile.

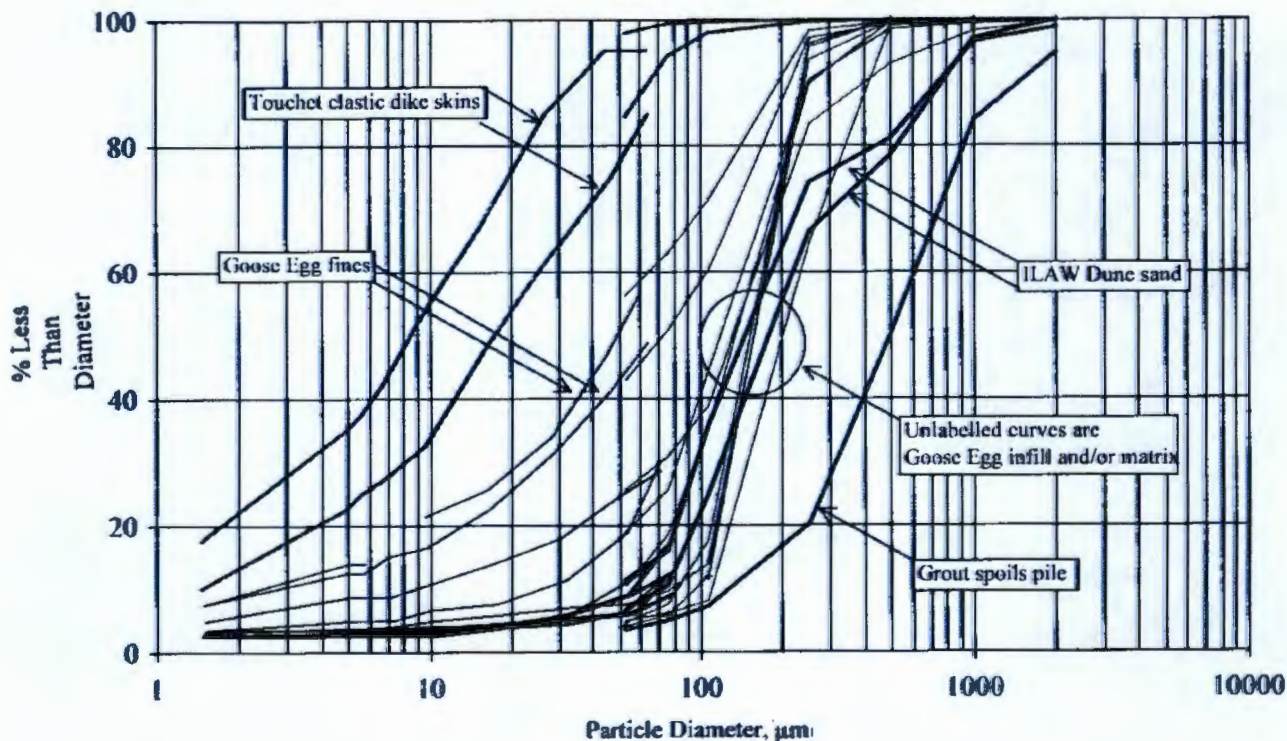


Table 5. Core volume, bulk density, and porosity data for the core samples.

Sample	Core Volume (cm ³)	Bulk Density (g/cm ³)	Porosity (cm ³ /cm ³)
1	693	1.57	0.424
2A	684	1.50	0.446
2B	693	1.51	0.443
3A	689	1.46	0.464
3B	698	1.52	0.443
4A	698	1.49	0.454
4B	684	1.57	0.425

Table 6. Water retention data from the pressure plate technique for the core samples.

1		2A		2B		3A	
Matric Potential -cm	Water Content g/g						
530	0.1001	530	0.0233	530	0.0339	530	0.0363
1010	0.1088	1010	0.0210	1010	0.0311	1010	0.0322
2040	0.0701	2040	0.0216	2040	0.0243	2040	0.0288
4080	0.0549	4080	0.0099	4080	0.0209	4080	0.0219

3B		4A1		4A2		4A3	
Matric Potential -cm	Water Content g/g						
530	0.0678	530	0.0401	530	0.155	530	0.133
1010	0.0740	1010	0.0363	1010	0.149	1010	0.116
2040	0.0585	2040	0.0302	2040	0.125	2040	0.0901
4080	0.0450	4080	0.0242	4080	0.0887	4080	0.0722

4B	
Matric Potential -cm	Water Content g/g
530	0.0298
1010	0.0258
2040	0.0212
4080	0.0162

Table 7. Water retention data from the vapor adsorption technique for the core samples (measurements at potentials above -10,000 cm are uncertain and should be used with caution).

1		2A		2B		3A	
Matric Potential -cm	Water Content g/g						
28182	0.033	258592	0.018	11648	0.022	121667	0.012
693204	0.012	262464	0.0073	22040	0.017	516971	0.007
1433126	0.009	533191	0.0071	286323	0.008	1018703	0.006
		891172	0.0059	1446643	0.004	1444671	0.005
		1442563	0.0045				

3B		4A1		4A2		4A3	
Matric Potential -cm	Water Content g/g						
98149	0.016	361735	0.010	36699	0.041	19639	0.041
209007	0.011	1233979	0.005	56058	0.036	25367	0.039
326217	0.008	1367281	0.005	992535	0.015	1050295	0.012
1392767	0.005	1459642	0.004	1103810	0.014	1431458	0.010
1450243	0.005			1424506	0.013		

4B	
Matric Potential -cm	Water Content g/g
1395754	0.004
1466263	0.004
1428052	0.004

Table 8. Saturated hydraulic conductivity of the core samples.

Sample	Saturated Hydraulic Conductivity (cm/s)			Average Saturated Hydraulic Conductivity (cm/s)	Method
	Rep 1	Rep 2	Rep 3		
1	5.97E-04	5.97E-04	5.97E-04	5.97E-04	Constant head
2A	4.77E-03	4.97E-03	4.37E-03	4.70E-03	Constant head
2B	3.38E-03	3.06E-03	2.98E-03	3.14E-03	Constant head
3A	3.29E-03	3.58E-03	3.37E-03	3.41E-03	Constant head
3B	1.14E-03	1.14E-03	1.14E-03	1.14E-03	Constant head
4A	1.67E-04	1.96E-04	1.89E-04	1.84E-04	Constant head
4B	5.56E-03	5.40E-03	5.32E-03	5.43E-03	Constant head

Table 9. Parameters and statistics for the van Genuchten function fitted to data from the multistep method using SFOPT (θ_s and K_s were held constant at their measured values; θ_r was estimated for a ψ value of -15,300 cm from the pressure plate and vapor adsorption data; $m=1-1/n$; $f=0.5$; matric potential values were from the lower tensiometer; all data were weighted by a factor of 1.0)

Sample	θ_s (cm ³ /cm ³)	θ_r (cm ³ /cm ³)	α (1/cm)	n (-)	R^2	Mass Balance Error, %
1	0.424	0.063	0.0839	1.33	0.878	2.37
2A	0.446	0.019	0.0762	1.98	0.747	1.51
2B	0.443	0.023	0.0741	1.84	0.815	1.47
3A	0.424	0.025	0.0143	2.49	0.985	0.67
3B	0.448	0.050	0.0593	1.54	0.860	1.48
4A	0.454	0.030	0.0092	1.97	0.968	0.79
4B	0.425	0.021	0.0823	2.09	0.836	1.60

Table 10. Water retention and unsaturated conductivity data for each sample during the steady state tests (nd = no data). Matric potential and water content values represent the average of sensors at two depths (approx. 4 and 11 cm) in the sample.

Sample	Matric Potential -cm	Water Content cm^3/cm^3	Unsaturated Hydraulic Conductivity cm/s
1	15.5	0.267	5.4E-5
1	40.2	0.250	2.9E-6
2a	25.6	0.259	2.0E-03
2a	45.3	0.156	1.3E-4
2b	33.9	0.354	1.0E-4
2b	34.2	0.352	1.0E-4
2b	52.6	0.331	3.7E-5
3a	33.3	0.220	2.7E-4
3a	53.9	0.207	8.1E-5
3a	53.3	nd	3.9E-5
3b	13.6	nd	1.5E-5
3b	48.0	0.293	1.4E-5
4a	19.5	0.365	8.9E-6
4a	22.2	nd	9.3E-6
4b	17.5	0.249	4.9E-5
4b	35.6	0.196	2.9E-5

References

- American Society for Testing and Materials. 1985. "Standard Test Method for Particle-size Analysis of Soils. D 422-63 (1972)." 1985 Annual Book of ASTM Standards 04.08:117- 127. American Society for Testing and Materials, PA.
- Blake GR, and KH Hartge. 1986a. "Particle Density." In *Methods of Soil Analysis, Part 1*, ed. A. Klute, pp. 377-382. American Society of Agronomy, Madison, WI.
- Blake GR, and KH Hartge. 1986b. "Bulk Density." In *Methods of Soil Analysis, Part 1*, ed. A. Klute, pp. 363-375. American Society of Agronomy, Madison, WI.
- Eching SO, and JW Hopmans, 1993. "Optimization of hydraulic functions from transient outflow and soil water pressure data," *Soil Sci. Soc. Am. J.* 57:1167-1175.
- Freeze RA and JA Cherry, 1979. *Groundwater*. Prentice-Hall, Inc., Englewood Cliffs, NJ.
- Gee GW and JW Bauder, 1986. "Particle-Size Analysis." In *Methods of Soil Analysis, Part 1*, ed. A. Klute, pp. 383-409. American Society of Agronomy, Madison, WI.
- Khaleel R, and EJ Freeman, 1995. "Variability and scaling of hydraulic properties for 200 Area soils, Hanford Site, WHC-EP-0883, Westinghouse Hanford Company, Richland, Washington.
- Klute A, 1986. "Water Retention: Laboratory Methods," In *Methods of Soil Analysis, Part 1*, ed A. Klute, pp. 635-662. American Society of Agronomy, Madison, Wisconsin.
- Klute A and C Dirksen, 1986. "Hydraulic conductivity and diffusivity: Laboratory methods," In *Methods of Soil Analysis, Part 1*, ed A. Klute, pp. 687-734. American Society of Agronomy, Madison, Wisconsin.
- Kool JB, JC Parker, and MT van Genuchten, 1985a. "Determining soil hydraulic properties from one-step outflow experiments by parameter estimation, I, Theory and numerical studies," *Soil Sci. Soc. Am. J.* 49:1348-1354.
- Kool JB, JC Parker, and MT van Genuchten, 1985b. "Determining soil hydraulic properties from one-step outflow experiments by parameter estimation, I, Experimental studies," *Soil Sci. Soc. Am. J.* 49:1354-1359.

APPENDIX E

Quality Assurance/Quality Control (QA/QC) Considerations

Quality Assurance/Quality Control (QA/QC) Considerations

This data package is based on data reported in appendices A through D or taken from peer-reviewed, open literature. Data reported in appendices A, C, and D were collected by Pacific Northwest National Laboratories (PNNL), following applicable PNNL QA/QC procedures. Data reported in appendix B were collected by Westinghouse Hanford Company Geotechnical Engineering Laboratory (GEL), following applicable GEL QA/QC procedures.

For analysis of data collected in the laboratory and field and those based on literature, a peer review procedure was established and followed. The peer review members were selected based on their experience and knowledge of specific subject areas. The internal peer review was provided per Fluor Daniel Northwest (FDNW) internal procedures. PNNL provided the Hanford technical review for the data package. A review of the data package was also provided by the Hanford Site Vadose Zone/Groundwater Integration Project. Finally, an external peer reviewer (i.e., Professor L. W. Gelhar, Massachusetts Institute of Technology, Cambridge, MA) has reviewed the data package.